DSE - A320 Alternative Fuel

Design the next generation sustainable A320 operating on Liquified Natural Gas for the year 2030.

B. Cont	4135849	K. Kaur	4175018
M.M. Doole	4160436	L. Klespe	4192117
C.L.V. Driessen	4012631	C.H.J. Ng	4193474
M. Hoekstra	4139372	E.M. Rezunenko	4160371
P.B. Jahn	4160630	N.C.M. van Zon	4134184

Final Report

Design Synthesis Excercise

TU Delft Delft University of Technology

Faculty of Aerospace Engineering

July 1, 2014

Table of Contents

Chapter 1

Introduction

The objective of this project is to design the next generation sustainable A320, capable of using alternative fuels for the year 2030. The current A320-200 is taken as a baseline, given that the specified requirements are that the new design should have similar or better performance characteristics to the current single aisle aircraft. The goal of the task is to bring forward a design that will have significant reductions in greenhouse gas emissions and be compliant with noise regulations, as well as reducing specific fuel consumption to be attractive for airlines.

The report is divided into four parts. The first parts begins with understanding the sustainability issues present. From this the project aims are formulated. Last of all, candidate fuels are given and the best is chosen.

The conceptual design phase begins with design options followed by a tradeoff, mission and direct operating cost analysis. The design options showcase 8 innovative designs that were developed.

The third part is the preliminary design phase. The standard ATA 100 numbering system as published by the Air Transport Association is used for system classification. The following systems have been designed and are presented in this part.

- **ATA25 - Equipment & furnishings** is discussed in chapter 11 on fuselage design.
- **ATA26 - Fire protection** is discussed in chapter 12 on engine design.
- **ATA28 - Fuel system** covers both the kerosene and LNG systems (see chapters 10 and 9).
- **ATA32 - Landing gear** covers the position of the main and nose gears in chapter 15
- **ATA48 - In-flight fuel dispensing** is discussed in chapter 10 on the fuel system.
- **ATA49 - Auxiliary power unit** is discussed in chapter 12 on engine design.
- **ATA53 - Fuselage** configuration and covered in chapter 11 on fuselage design.
- **ATA55 - Stabilizers** involves the empennage, vertical and horizontal tail sizing (see chapter 15 on stability and control.
- **ATA57 - Wing** planform definition is presented in chapter 15 on wing design.
- **ATA70 - Powerplant** is discussed in chapter 12 on engine design.

Finally, the last part of this report thoroughly looks into operations, certification, noise mitigation and performance aspects of the aircraft. The part ends with a detailed comparison of the baseline A320-200 and the new A320LNG.

Chapter 2

Sustainability

Sustainability is one of the growing fields of interest in today's economy. As the worlds population increases, the importance of developing renewable and clean energy sources increases. This section will give a definition of global warming and an understanding of the importance of a sustainable design.

2-1 Global Warming

Global warming, in general terms, can be described by two parameters: the radiative forcing and global warming potential. Radiative forcing is defined as *'The global, annual mean radiative imbalance to the Earth's climate system caused by human activities. The parameter is given in W/m^2 and is used to give an indication of the contribution of each pollutant to the global warming process and make a comparison between different future aviation-scenarios. A positive radiative forcing leads to global warming'* [91].

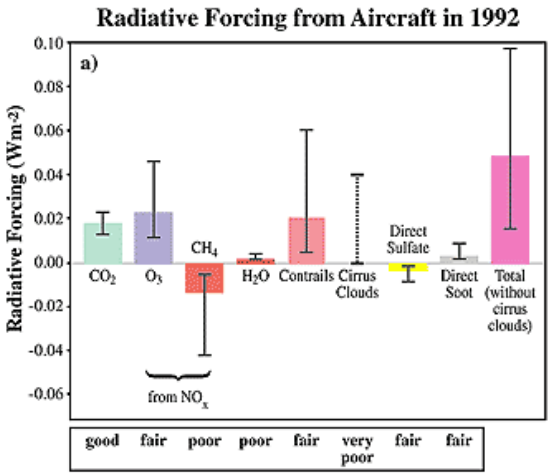

Figure 2-1: Contribution of aircraft emissions to radiative forcing in 1992

The global warming potential of a pollutant describes its ability to trap heat in the atmosphere, taking into account the residence time of each gas [108]. The official definition is the following: *'The ratio of global warming, or radiative forcing, direct and indirect, from one unit mass of a greenhouse gas to that of one unit mass of carbon dioxide (CO_2) cumulated over a period of time'* [108].

Figure 2-2 shows the calculation process of global warming potential for aviation. Figure 2-3 shows the overall contribution of aviation to the global warming process.

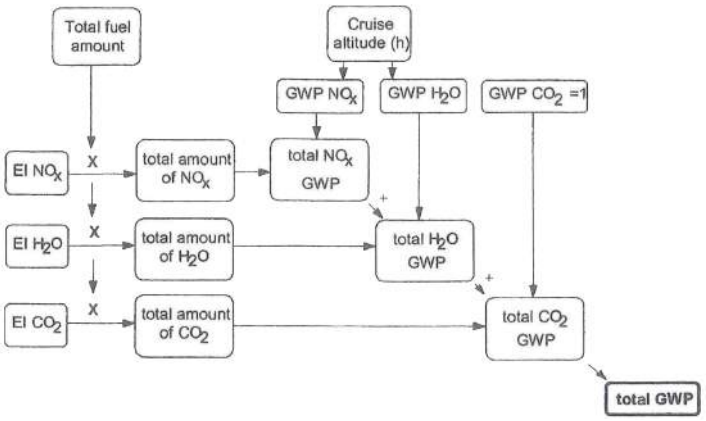

Figure 2-2: Calculation of Global Warming Potential

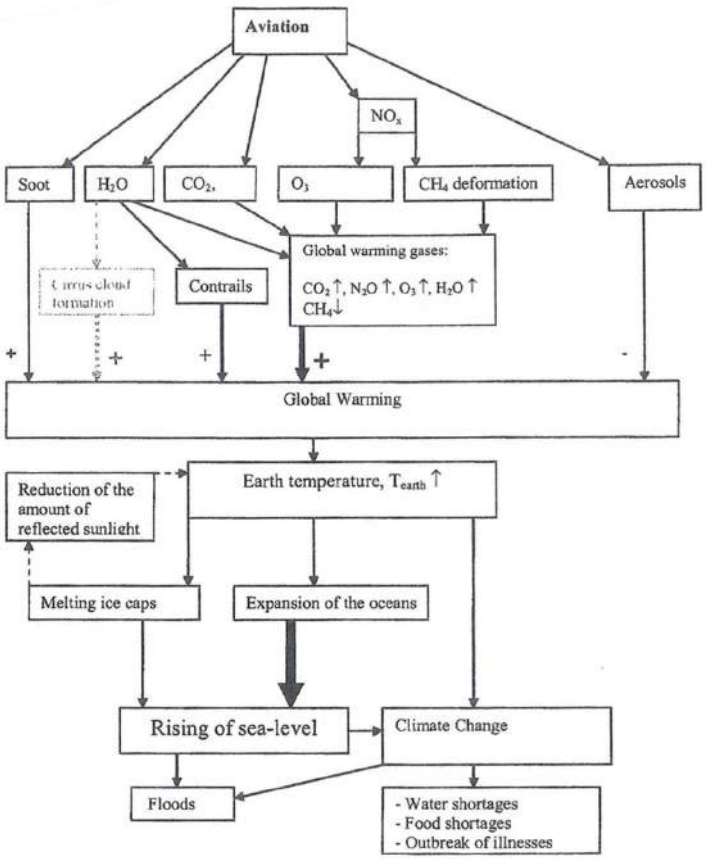

Figure 2-3: Contribution of Aviation to the Global Warming Process

2-2 Externalities

The aviation industry is currently running on kerosene. This form of energy extraction has proven to work on a wide-scale, however the resultant negative externalities of this fuel have become more well known in recent decades. In this case the externalities refers to the cost on

society by greenhouse effects induced by the combustion process. These costs are not taken on by the airliners and hence the cost of jet fuel to society is actually higher than priced.

Carbon Dioxide - CO_2

It is well known that CO_2 emissions are a factor in climate change [62]. The contribution of the aviation industry to global CO_2 levels in transportation is significant. Furthermore the effects of carbon dioxide are long lasting as can be seen in figure 2-4.

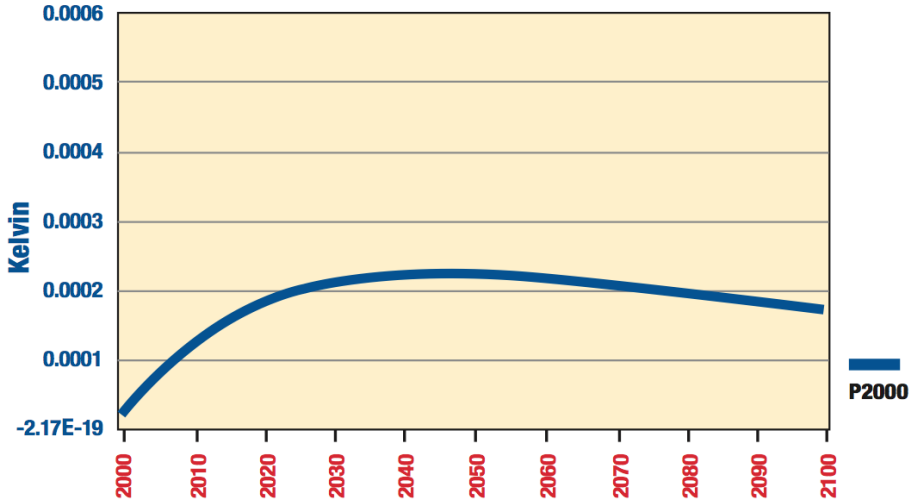

Figure 2-4: Temperature response for single year CO_2 emissions [62]

Figure 2-4 shows the global temperature change over time due to the aviation emissions in one single year. The ICAO report states the following on the graph: "*50% of an increase in concentrations will be removed within about 30 years, a further 30% being removed within a few centuries, and that the residual 20% remains in the atmosphere for many thousands of years. Thus, a simplistic concept of a simple 100 to 150 year lifetime is incorrect, and at worse dramatically underestimates impacts.*" The decay of CO_2 is consequently a slow process and the continual yearly emissions add up.

LNG has different properties and life cycle compared to oil and this results in differences in emissions. When comparing the life cycles of fuel and LNG, it was found that less CO_2 is expelled during the natural gas process and liquefaction than during the kerosene process. In addition for the same amount of heat, burning natural gas produces about 30% less carbon dioxide than kerosene combustion.

Consequently, the end-use emission of CO_2 per equivalent energy from LNG is smaller than that of kerosene as can be seen in figure 2-5.

Mono-Nitrogen Oxides - NO_x

Nitric oxide NO and nitrogen dioxide NO_2 are both air pollutants that are produced by oxidation during combustion at high temperatures. The ratio of NO and NO_2 in the air is

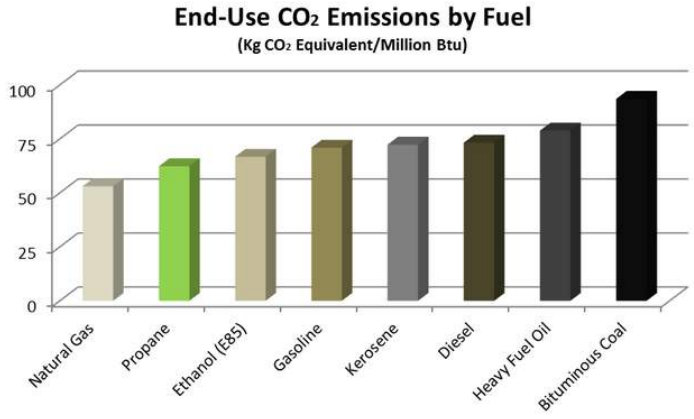

Figure 2-5: Global CO_2 emissions for different fuels [30]

determined by the intensity of sunshine and the concentration of ozone. Their adverse atmospheric effects contribute to production of acid rain and ozone. While the effect of increased O_3 concentration due to NO_x emissions is local, it is still considered to be a greenhouse gas and contributes to global warming. It has also been argued that the presence of NO_x has a cooling effect by reducing ambient concentrations of methane, however this has not yet been quantified. The aviation industry's contribution to the emission of NO is around 2% and of NO_2 and mean ozone 1%. Most of this emission, estimated around 95%, occurs during the cruise phase [73]. Overall LNG has approximately 66% less NO_x emissions compared to kerosene [35].

Sulfur Oxides - SO_2

Sulfur oxides are an invisible, highly reacting toxic gas formed mostly during combustion of elemental sulfur. It is a major air pollutant as it contributes to the occurrence of acid rain and the forming of atmospheric particles. These particles can highly impact health when inhaled, leading to respiratory illnesses. The largest contribution of SO_2 comes fossil fuel combustion, which makes up around 73% of the total emission [10]. This means that the combustion of jet fuel contributes to the formation of this toxic gas. Quality natural gasses usually have very low concentrations of sulfur, which leads to very small emissions of SO_2 which can be assumed to be negligible. This means that LNG has almost zero emissions of SO_2 [9].

Water Vapour

Water vapour is formed during the combustion of fuel and has been found to be one of the most abundant and significant greenhouse gas, as it traps heat when formed in the air. Furthermore the heating effect of water vapour increases with altitude as it needs more time to disappear. In the troposphere it is estimated to have a lifetime in the order of days, whereas in the stratosphere it can take months [97].

It was found that the combustion of LNG, for the same amount of energy as kerosene, produces 1.39 times the amount of water vapour compared to kerosene. [97]

Chapter 3

Objectives

This chapter sets the requirements and targets the next generation A320 has to meet. It then presents why alternative fuel is a necessary change for the aviation industry, due to financial and sustainability issues.

3-1 Requirements and Project Targets

Important requirements for this next generation A320 are given and have to be met. This serves to ensure the new aircraft meets the demand of airlines. They are listed as the following and are respect to the A320-200:

1. Can take-off and land at all current A320 airport destinations
2. Has the same minimum speed stall characteristics
3. Seats the same amount of passengers

The Advisory Council for Aeronautics Research in Europe (ACARE) was launched at the Paris Airshow in June 2011, compromising of about 40 members, with the aim to set common goals for CO_2, NO_x and noise reduction for the aviation industry. One of the targets within the *Flightpath 2050 vision* aimed to reduce CO_2 emissions per passenger kilometre by 75%, NO_x emissions by 90% and perceived noise by 65%, all relative to the year 2000. In light of these goals a set of targets has been established for the design of an aircraft competing with the A320.

Based on ACARE, targets relative to the current Airbus A320-200 have been set for the next generation A320 taking into the achievable shorter time span, which are:

- 50% CO_2 reduction
- 65% NO_x reduction
- 80% SO_x reduction
- 25% noise reduction
- No increase in the effect of water vapour on Global Warming Potential (GWP)

Chapter 4

Fuel Candidates

To meet the objectives in chapter 3 a new energy source and related technology development are required. It is therefore important to determine the choice of alternative fuel.

4-1 Alternative Fuel Options

Given the stringent weight and volume constraints that are key for any aircraft design, it is best to compare the specific volume and mass of various alternative fuels. These values are plotted in figure 4-1. Ideally, the best fuel for aviation would be in the top-right corner of the graph, with the highest energy content per unit mass and unit volume. Unfortunately such a fuel does not exist and hence a trade-off must be made. The blue curve plotted on the figure corresponds to potential fuels suitable for aircraft. Two candidate fuels stand out:

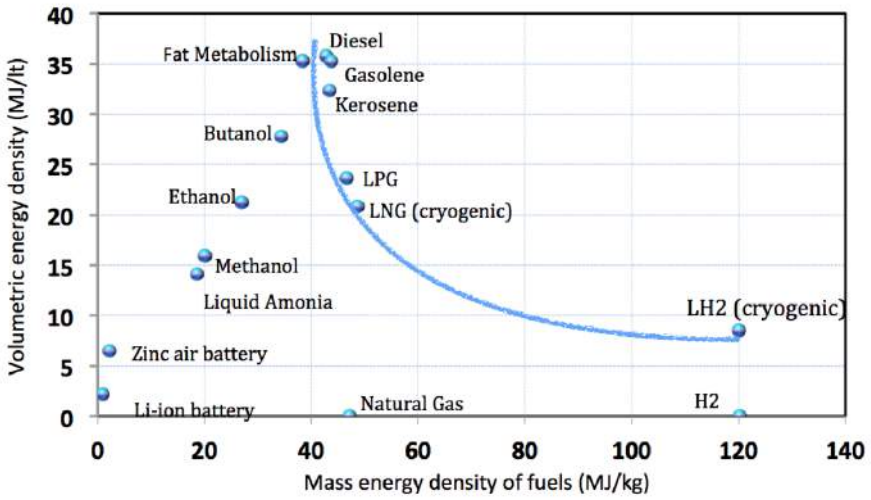

Figure 4-1: Specific volume and mass of alternative fuels [54]

- **Liquid Hydrogen.** One major advantage of liquid hydrogen (LH_2) is its high mass energy density. For the same energy content, the mass is reduced by approximately 2/3 compared to kerosene. However, the infrastructure of LH_2 is still in its infant stages. Significant technological developments and investments are required to be able to meet the aviation industry's fuel demand. A disadvantage is the volume required. Compared to kerosene, this is 4 times higher for the same energy density.
- **Liquefied Natural Gas.** Another fuel option is liquefied natural gas (LNG). Similar to LH_2, the fuel system has to be upgraded to handle cryogenic fuel. The infrastructure

is more readily available for LNG than LH_2, as it is already used in the transport sector. Therefore, it is more likely to be available and to be able to cope with the aviation fuel demand by 2030.

Liquid natural gas is therefore proposed as the candidate fuel, as it is a promising source of usable fuel by 2030 that can meet the emission goals.

4-2 Challenges with Liquefied Natural Gas

In the current A320, kerosene is stored inside the wings. This is done to maximize payload-carrying space within the fuselage. Due to the cryogenic nature of LNG, the fuel must be stored at very low temperatures of -161° C below its boiling point at a pressure of 1 bar. As a consequence, specially designed cylindrical tanks must be developed. A major design challenge of LNG is therefore the placement of the pressurized cryogenic tanks.

A 50/50 configuration is proposed to reduce the volume necessary for LNG tanks. In this configuration, 50 percent of the fuel capacity is LNG, and the remaining half is kerosene. This drastically reduces the required LNG tank size and hence provides drag whilst still providing weight improvements. Moreover, a 50/50 configuration provides a seamless transition towards LNG given that not all airports will have the capability to fuel LNG aircraft (completely). Whether this meets the emission goals though must be investigated.

4-3 Jet Fuel Price Forecast

The prediction of jet fuel prices is based on the 2012 Annual Energy Outlook report by EIA [7]. The results can be seen in figure 4-2, which also displays the expected growth of natural gas. The adjustment to the pricing of LNG, by taking into account liquefaction and storage, can be seen in section 4-4.

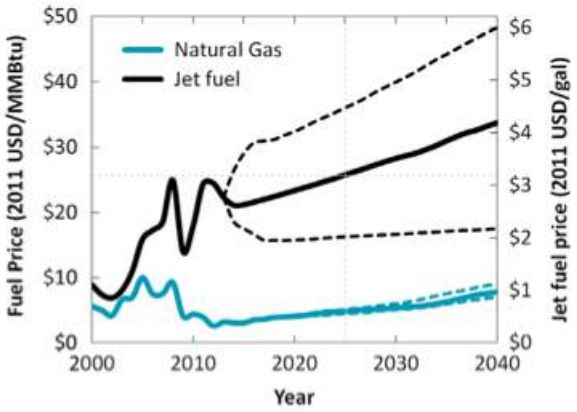

Figure 4-2: Jet fuel vs natural gas price forecast [101]

For the further cost analysis, the nominal forecast case will be considered. By 2025 the price of fuel is expected to be \$3.2/gal.

4-4 LNG Price Forecast Comparison

From figure 4-2 natural gas is expected to be around $6/MMBtu in the year 2025, read off the left vertical axis. The following additional costs arise in determining the LNG costs, taken from the Progress in Aerospace Sciences journal [101]. The major price variation will be found in the liquefaction procedure as the costs associated vary the most due to the scale of the industry. A conservative estimation will be taken here.

- Liquefaction: $6/MMBtu
- Transportation: $0.3/MMBtu
- Storage: $0.82/MMBtu

This adds up a total cost of $7.12/MMBtu to convert natural gas to LNG, and hence the forecast price of LNG in 2025 will be $13.12/MMBtu. Equated to the same energy density per dollar, LNG is found to be approximately half the price of kerosene:

- **Jet fuel**: 40.22 MJ/$
- **LNG**: 80.38 MJ/$

Chapter 5

Mission Analysis

This chapter focuses on the Airbus A320 flight mission. The chapter will first investigate the current operation of the global A320 fleet to determine how the aircraft is actually flown and thus establish the needs of the market. Subsequently different flight configurations are analysed from a sustainability point of view for the A320LNG design.

To determine how the Airbus A320 is being used today, a database of 16500+ Airbus A320 routes [88] from airlines around the world is used to determine the average stage length for a typical flight.

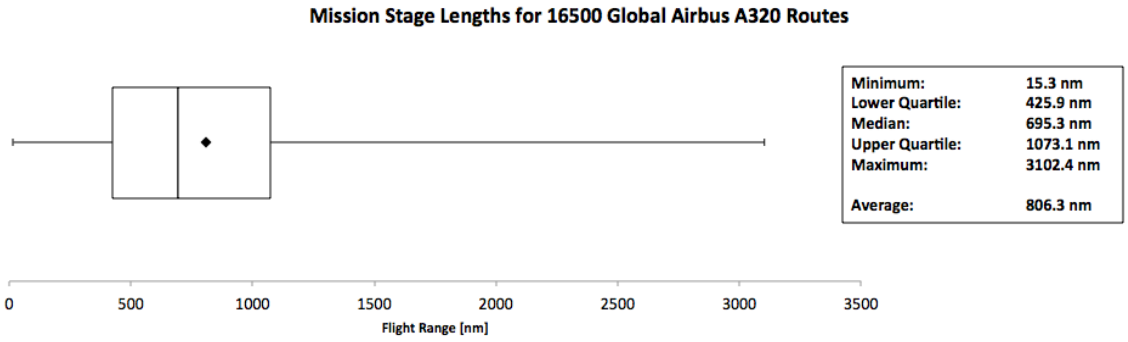

Figure 5-1: Average Stage Length for 16500+ Airbus A320 Routes

As can be deduced from figure 5-1 the Airbus A320 is, on average, used for flights of approximately 800 nautical miles range. It can also be concluded that 75 percent of flights around the world are less than 1073.1 nautical miles. This distance is only one third of the published maximum range of the Airbus single-aisle aircraft.

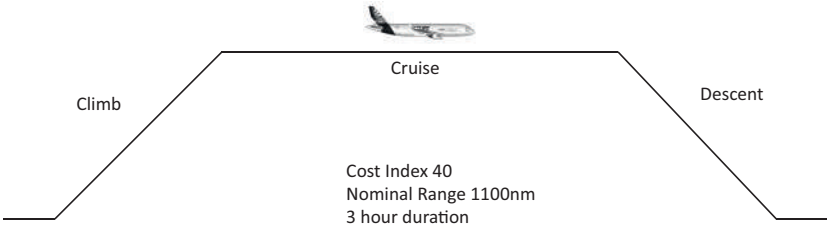

Figure 5-2: Flight from Amsterdam to Reykjavik

An 1100 nm flight from Amsterdam to Reykjavik is taken as a case study (see figure 5-2). The Airbus aircraft flight computers determine the climb, cruise and descent speeds based on the cost index selected by the airline [110]. The cost index is an input parameter for the flight computers that trade fuel economy for flight time. A low CI value results in minimum fuel burn but a more lengthy flight and a high CI value results in minimum flight time at the

expense of an increased fuel burn (typical values range from 0 to 999). Most airlines operating the A320 use a CI value of 40, which is also recommended by Airbus [110]. Based on these values the following fuel values are computed, shown in table 5-1.

Table 5-1: A320 Flight from Amsterdam to Reykjavik

Phase	Fuel Used [kg]	Time	Distance [nm]
Climb	1897 (25%)	23.7 minutes	165
Cruise	5599 (73%)	2 hours 22 minutes	836
Descent	112 (2%)	14.9 minutes	90
Total	7608	3 hours	1091

Hence it can be confirmed that the total fuel required for this mission is less than 50 percent of the total fuel capacity of the A320 and hybrid operation is permissible, as well as feasible with a 50/50 configuration. In such a configuration the airline is able to fly such a 1100 nm flight on either kerosene or LNG, or a combination of both. Combining the use of both fuels provides a flexibility advantage and as kerosene prices rise a cost advantage.

The use of either LNG or kerosene is investigated so that the targets stated in chapter 3 can best be met. This is done by optimising the the three stage lengths; short, medium and long.

Short Range For a short duration flight (< 1.5h) two flight options will be possible. The first one will be to perform the flight completely on LNG if the weather allows it to fly at lower altitudes (under the the tropopause) to minimise the water vapour effect. Moreover, a major part of this flight range is climb and descent, where LNG is far more sustainable. The second option will be adopted if the weather does not allow a lower altitude, than LNG and kerosene will be combined as explained in the next paragraph. Figure 5-3 indicates the complete usage of LNG for all stages of the mission profile.

Mid and Long Range A mid range flight equates to the nominal mission range of around 1100 nm which is around 3 hours. Although the majority of predicted A320 flights are shorter than 1100 nm, it is desirable to be capable of fulfilling the current spectrum of A320 flights in an economic manner. Therefore this section also include the advised flight profile for missions lasting longer than 5 hours which was decided to be performed in the same way as for mid-range. The second option has combined use of kerosene and LNG. Take-off and climb to 9000 m are achieved with LNG. The cruise phase is then performed on kerosene, whereby higher altitudes can be flown. Lastly, descent and landing are again done on LNG. Figure 5-4 gives a graphical representation of this mission profile.

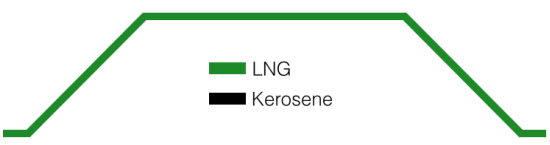

Figure 5-3: Complete LNG fuel distribution

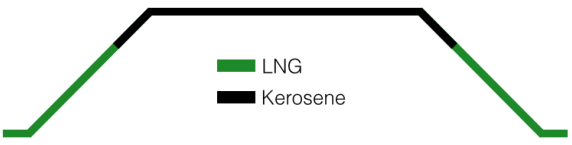

Figure 5-4: Combined fuel distribution

Chapter 6

Design Options

This chapter presents the final eight design options, each derived from a combination of the design elements discussed in the previous chapter, that were traded off to get the final design.

Design 1: Low Wing Configuration with Tanks on Fuselage

Figure 6-1: Sketch of Design Concept 1

Figure 6-2: Sketch of Design Concept 2

The first concept (figure 6-1) represents the current Airbus A320 configuration with the LNG fuel tank integrated onto the top of the fuselage. This tank runs along the entire fuselage and is covered in a fairing. This design contains a fuel tank on top of the fuselage and a heavy empennage. The development costs are low as only slight modifications to the current aircraft are necessary. Maintenance is relatively easy as the engines and fuel lines are easily accessible. Safety issues arise as the fuel lines feeding the engines have to run inside the fuselage.

Design 2: Wing Pods

Design 2 (figure 6-2) includes externally mounted wing pods, which reduces costs for maintenance and increases safety. The fuel system is positioned near the engines. Material is used to connect the pods and wings, this increases the weight of the aircraft.

Design 3: LNG in Cargo Compartments

In this concept, the fuselage length is increased to accommodate LNG fuel tanks in the cargo bays. The cargo bay size has to be increased to accommodate LNG without comprising original cargo space. Kerosene can be stored in the outer and inner tank. The centre tank can be used for storage in the case when only kerosene is used. To shorten the length of fuel pipes, LNG is stored at the back of the forward cargo compartment and the front of the aft cargo compartment. It is decided that the same quantity of LNG is stored in the front cargo and aft cargo compartments so there is no significant shift in the centre of gravity.

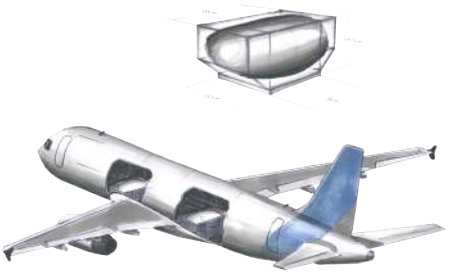

Figure 6-3: Sketch of Design Concept 3

Figure 6-4: Sketch of Design Concept 4

Design 4: C-tail Configuration and Wing-Podded Tanks

This design option focuses on more sustainable aviation with the use of open rotor engines. This is achieved in exchange with increased noise emissions. The engines are installed on the tail to reduce effect of noise to passengers and to increase passenger safety in the case of engine failure. The kerosene is kept in the inner tanks of the wing. Two open rotor engines are mounted on the tail and fuel pods are placed under each wing. This option offers good accessibility for maintenance, the engines and the pods can be disassembled easily for inspection and repair.

Design 5: T-tail Configuration with Fuselage Tanks

Figure 6-5: Sketch of Design Concept 5

Figure 6-6: Sketch of Design Concept 6

This design (figure 6-5) includes a top-mounted LNG tank, low wing and T-tail configuration. The tanks on the top are covered with a fairing. The aircraft is powered by two open rotor engines mounted to the back of the fuselage. The fuselage of the aircraft needs to be redesigned in order to carry the weight of the tank and fuel. The wings need to be made heavier than original as there is no more bending relief for the wings. The high mounted engines limit accessibility from the ground and this complicates maintenance procedures. One risk of using T-tail is deep stall.

Design 6: High Wing Configuration with Wing-Mounted Engines

The design (figure 6-6) shows a number of similarities with concept 1. However, a high wing configuration is used instead of low wing. This is done to integrate the tank fairing with the centre wing box/fuselage. The high wing configuration grants enough ground clearance to mount the open rotor engines under the wing. This placement causes a very turbulent air stream at the location of the current tail. Therefore, a canard configuration is chosen after performance and safety considerations. The integration of fuel tank fairing and centre wing box reduces additional drag. The canard configuration improves stall performance of the aircraft. Passenger comfort is directly effected by the noise emissions because the engine is positioned next to the fuselage.

Design 7: Propulsive Fuselage

Figure 6-7: Sketch of Design Concept 7

Figure 6-8: Sketch of Design Concept 8

This design aims for minimisation of structural caused drag for engine fuselage integration. This is achieved by not using pylons or alike components. In order to provide sufficient thrust, one counter rotating propeller around the fuselage with two compressors and turbines are utilised. This propulsion system is located outside the pressurised section, behind the bulkhead with double function as a firewall.

The LNG tank is located above the engines, enabling a simpler heat exchange. The APU is placed aft tank so the LNG can also be used for the APU. The propulsion and LNG fuel system is located behind the firewall/bulkhead. The kerosene has to be pumped to the rear of the aircraft.

Design 8: Boxed Wing Configuration With Empennage Mounted Engines

The next design is a box wing with open rotor engines mounted at the rear of the aircraft under the tail. The fuel tanks are located at the rear of the aircraft and integrated on top of the fuselage. The vertical struts cause the overall weight of the aircraft to increase. Due to its unconventional design configuration the cost required for R&D is higher. In terms of maintenance, the fuel tanks are less accessible compared to wing podded tanks. Refuelling time is relatively high compared to wing podded tanks due inaccessibility. The aft positioned engines and tanks causes the centre of gravity to shift backwards resulting in a decrease in static stability of the aircraft.

Chapter 7

Trade-Off

This chapter outlines the criteria that were used to trade-off the design options. Eleven criteria were used which were weighted based on their relative importance to the design goals. The first criterion used is the weight of the aircraft. This criterion is then weighted based on four primary factors. The second criterion is R&D costs. The costs related to R&D are important since it impacts the time frame of the design process and also negatively affects the implementation of the design process. The next criterion is the turnaround time which has an impact on the airline operational costs. The fourth criterion is the center of gravity range, which is important for the stability of the aircraft. The next criterion is safety. The main factor governing this criteria are the location of the fuel tanks. The sixth criterion in the trade-off table is maintenance. The driving factors for this being the engine location and tank position.

Next two criteria are lift over drag (L/D) ratio and engine performance which, impacts the aerodynamic efficiency of the design. The ninth criterion is the family concept which is based on the ease of future modifications. The next criterion is the certification of the aircraft. This is based on the ease of implementing the design without any objections from the certification authorities. The final criterion is sustainability which is further subdivided into emissions and the noise produced by the designs. The robustness of the final trade-off table is checked by carrying out a sensitivity analysis and then the final design is choice is stated.

7-1 Final trade-off table

In this section the final trade-off table is presented. All criteria taken into account, as mentioned in the introduction, are given a specific weight. As can be seen in table 7-1 design option 4 has the highest score, this is the final design concept.

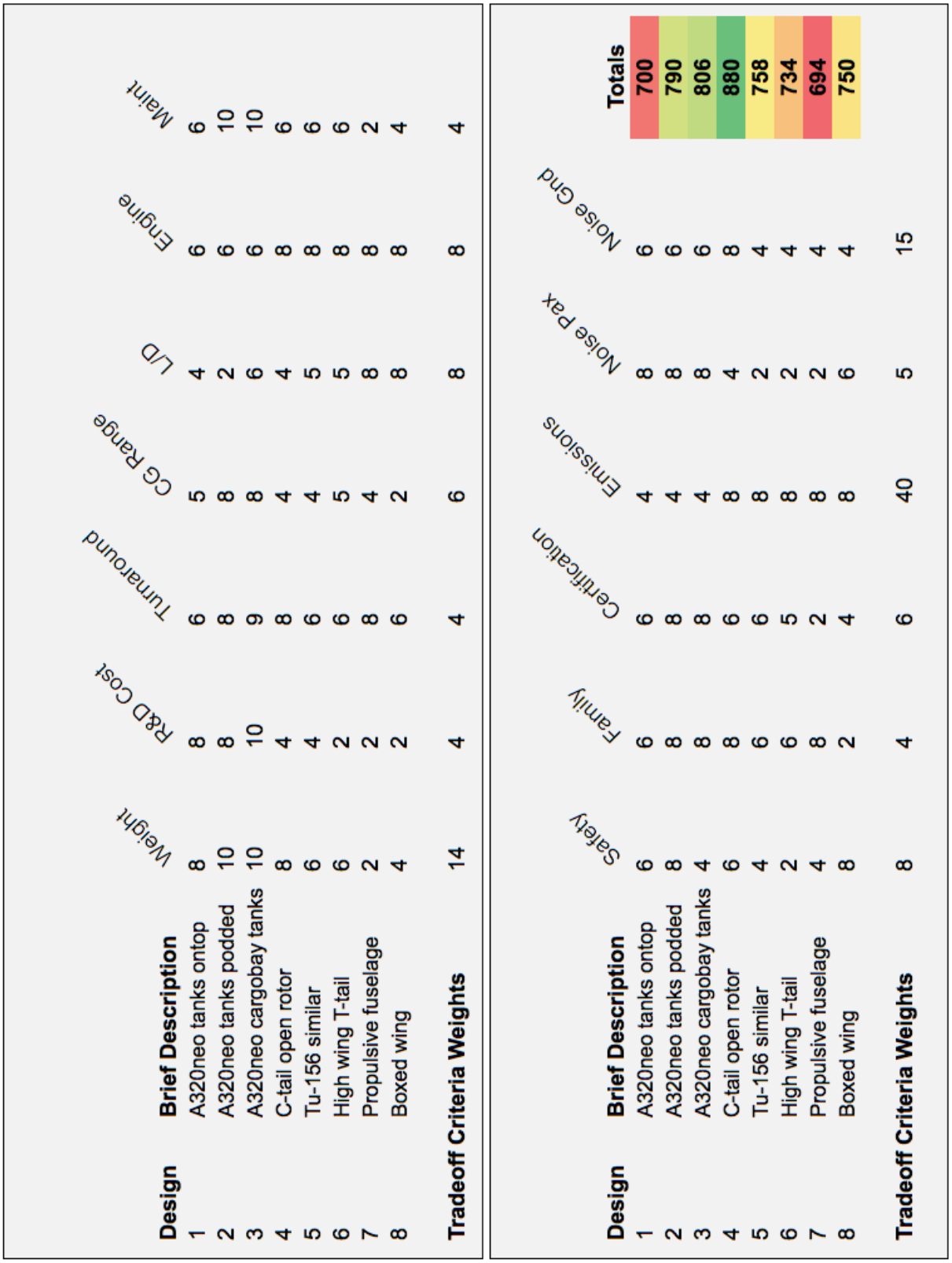

Design	Brief Description	Weight	Safety	R&D Cost	Family	Turnaround	Certification	CG Range	Emissions	L/D	Noise Pax	Engine	Noise Gnd	Maint	Totals
1	A320neo tanks ontop	8	6	8	6	6	6	5	4	4	8	6	6	6	700
2	A320neo tanks podded	10	8	8	8	8	8	8	4	2	8	6	6	10	790
3	A320neo cargobay tanks	10	4	10	8	9	8	8	4	6	8	6	6	10	806
4	C-tail open rotor	8	6	4	8	8	6	4	8	4	4	8	8	6	880
5	Tu-156 similar	6	4	4	6	6	6	4	8	5	2	8	4	6	758
6	High wing T-tail	6	2	2	6	6	5	5	8	5	2	8	4	6	734
7	Propulsive fuselage	2	4	2	8	8	2	4	8	8	2	8	4	2	694
8	Boxed wing	4	8	2	2	6	4	2	8	8	6	8	4	4	750
Tradeoff Criteria Weights		14	8	4	4	4	6	6	40	8	5	8	15	4	

Figure 7-1: Final Tradeoff Table

7-2 Sensitivity analysis

In order to determine how sensitive the trade-off is to changes in weight assigned to the different criteria a sensitivity analysis is done. In the trade-off, the weight given to the sustainability criteria are equal to the weight given to the design criteria. For the sensitivity analysis, this ratio is adjusted to see the affects. First of all, the design criteria are given a weight twice as large. Design option 4 is still leading in this case. However, the difference with design option 3 is now negligible (0.16 percent difference in overall score). Design option 3 is third with a difference in score of 2.77 percent. Secondly, the sustainability criteria are given a weight twice as large. This leads again to design option 4 as the primary choice followed by design option 8 with a 12.88 percent difference in score. Design option 5 is third. This shows that design option 4 is superior when considering sustainability.

Next, all criteria in which design option 4 has a low score (lower than 5) are given a weight twice as high as the current weight. In this case, again design option 4 ends first and again the difference with number two, which is design option 3, is negligible (0.21 percent in score). The fact that if the weight of the non-sustainability criteria is multiplied by 2 and design option 4 is still choice number one and that if all lower scores of option 4 are given a weight twice as high and it again is number one shows that design number 4 is the right final design concept.

7-3 Final Design Concept

After carrying out the trade-off and the sensitivity analysis the fourth design option scored the highest and hence it was selected to be the final design choice. The chosen design is a C-tail configuration with open rotors fitted on the rear of the fuselage. This configuration shifts the center of gravity aft. Therefore, the fuel tanks are podded underneath the wings such that the center of gravity will not go too much aft. The kerosene fuel tanks remain located in the wings. The fuel will have to be transported from the wings to the engines by pipelines which will be running through the fuselage. The design is presented in figure 7-2.

7-4 Innovation

The final configuration features many innovative features that will lead Airbus into the future. The open rotors will provide significant fuel and emission reductions and is a novelty within the industry. Furthermore the LNG technology is groundbreaking and will become a great technology knowledge base for future cryogenic transport solutions. Finally the design will feature the latest in composite materials and advanced aerodynamic wing design.

Figure 7-2: Final Design Option

Chapter 8

Direct Operating Cost Analysis

A breakdown of the direct operating cost (DOC) for a typical Airbus A320 mission will be made. There are several costs included in the DOC (see figure 8-1) and these are defined as costs directly related to the flying of the aircraft. Indirect costs such as sales, marketing, administration and customer support are not included.

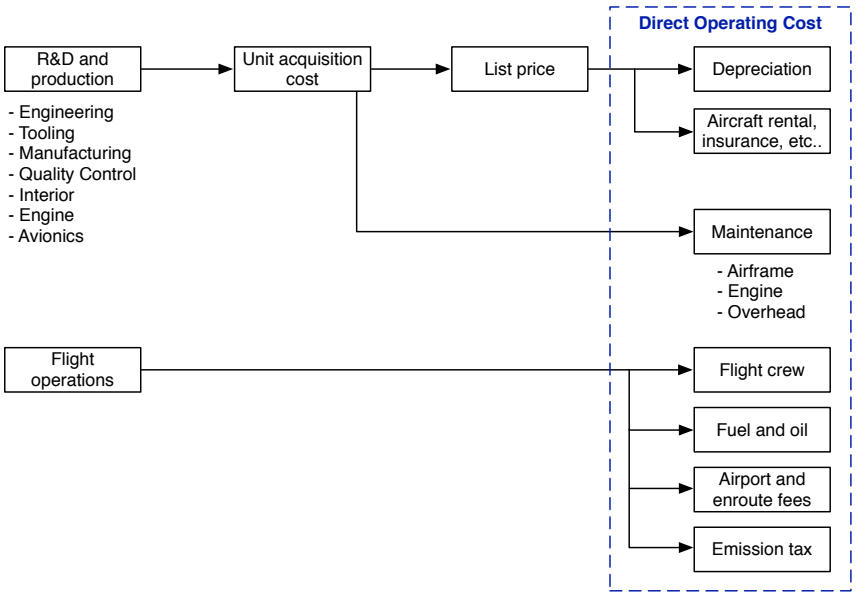

Figure 8-1: Direct Operating Cost

The unit acquisition cost is calculated based on a model developed on empirical formulas [28] and concludes that the A320LNG will be 8% more expensive than the A320neo. Airbus list prices indicate that the A320neo is 9.5% more expensive than the A320-200 [13].

Direct Operating Cost Breakdown

Baseline values for direct operating cost are taken from IATA reports [85, 63] and the respective changes for the A320LNG aircraft are calculated. The composition is shown in figure 8-2. Following is a motivation behind the assumptions made to calculate the DOC for the A320LNG. The changes compared to the current A320-200 are shown in figure 8-3 and motivated below.

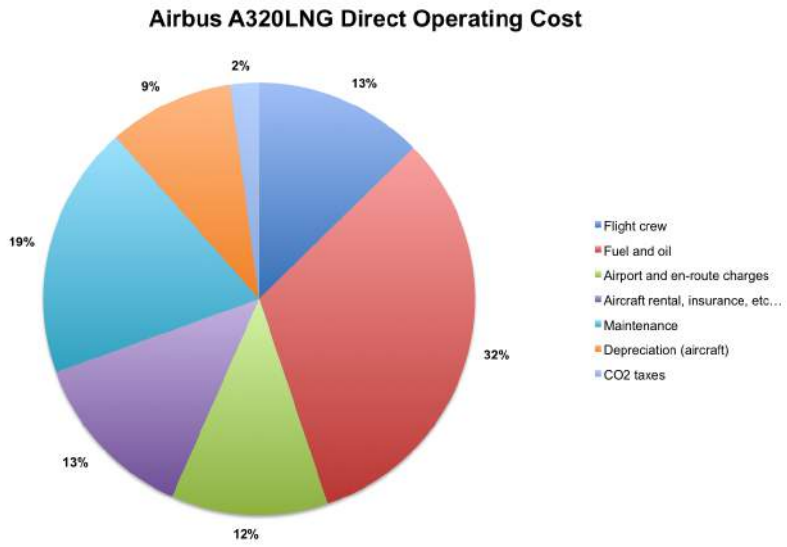

Figure 8-2: A320LNG DOC Composition

Table 8-1: A320neo to A320LNG DOC Breakdown

Change	**Explanation**
Flight crew	No change
Fuel and oil	Decreases based on the difference in energy content per dollar and hybrid operation
Airport and enroute charges	Airport fees increases to compensate on investment in LNG infrastructure
Aircraft rental and insurance	Aircraft rental and insurance increases based on increased acquisition cost
Maintenance	Maintenance increases based on new technologies and parts
Depreciation (aircraft)	Depreciation increases based on increased acquisition cost
Emission taxes	Emission taxes are based on CO_2 emissions due to kerosene and LNG and a tax is 25 USD/ton

Case Study: Return on Investment for Qatar Airways

Qatar Airways is taken as a case study for the implementation of a LNG powered Airbus A320 aircraft. From their timetables all the flight routes flown with the A320 family were extracted together with the frequency of flights per week. Subsequently the distances and flight times were calculated and the estimated kerosene required (block fuel) was computed. From this conclusions were made on the Qatar Airways A320 usage, summarized in table 8-3.

Direct operating cost projections are made for Qatar Airways with the following assumptions.

- Current Airbus A320 fleet starts going out-of-service in 2025 with no A320-200's left in the Qatar Airways fleet by 2036.

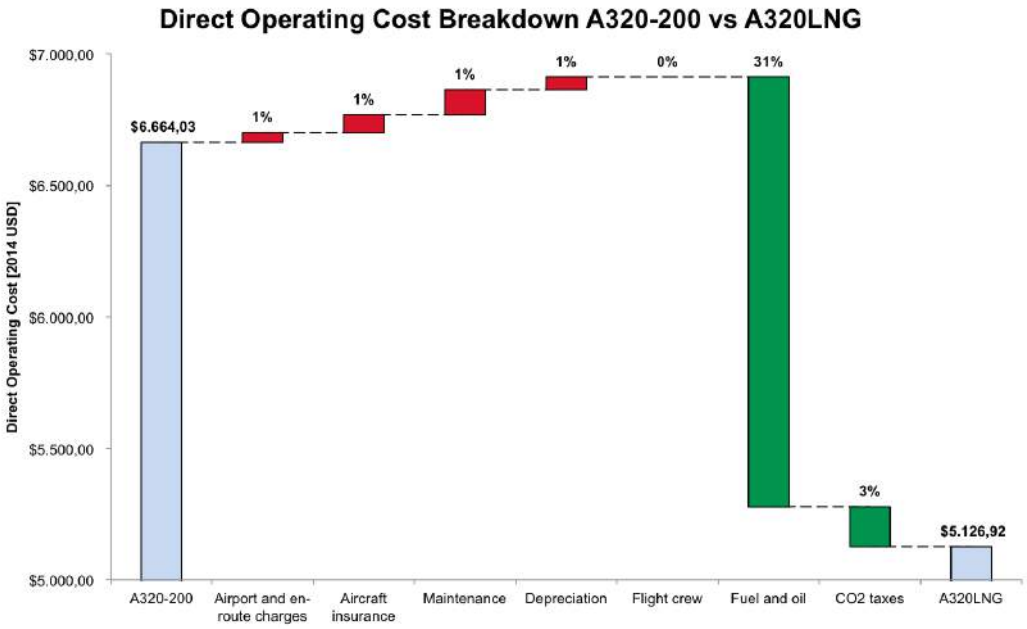

Figure 8-3: A320-200 to A320LNG Direct Operating Cost Breakdown. Total decrease in DOC is estimated to be 25%.

Table 8-2: Qatar Airways A320 Fleet

Aircraft	Amount
Airbus A319LR	2
Airbus A320-200	32
Airbus A321-200	12
Airbus A320neo	50 on order (30 options)

Table 8-3: Results from QR A320 Route Network Analysis

Qatar Airways A320 Fleet	Averaged across A320 Fleet
Distance [nm] per week per aircraft	31499 nm
Flight cycles per week per aircraft	34.13 flight cycles
Flight hours per week per aircraft	87 hours 24 minutes

- First A320neo aircraft delivered in 2020, last one in 2034. Total of 65 orders (15 options turned to orders). A320neo fleet remains in service until at least 2050.
- First A320LNG aircraft delivered in 2029, followed by 7-11 deliveries per year in accordance with an increasing air travel demand of 6-7% per year.

Based on these results an estimation of annual DOC savings can be made if Qatar Airways were to transition to A320LNG aircraft. Concluding this case study the A320LNG is expected to provide lucrative benefits for the gulf carrier.

$$\text{Annual DOC Savings} = \$480.73 \times 87,4 \text{ hrs} \times 46 \text{ aircraft} \times 52 \text{ weeks} = \$100,515,854 \quad (8\text{-}1)$$

Case Study: Effect of Changing Cruise Speed on DOC

The direct operating cost, as presented in figure 8-1, can be split up into two parts:

- **Fuel related costs:** based purely on fuel burn and therefore is a combination of specific fuel consumption and the time the engines are running.
- **Time related costs:** consider the additional costs for every extra minute the flight takes. For example flight crew and maintenance costs will increase.

The trade-off between these costs is referred to as the cost index, a parameter that varies per airline based on their best operating economics. An analysis is done for the A320LNG to determine the best cruise speed for minimum total cost. The model is based on a mission from Amsterdam to Istanbul. Fuel costs are based on the fuel consumption of the open rotor engine used and time costs are based on models in literature [13]. Fuel costs reach a minimum at the maximum range cruise (MRC) mach number, after which they increase. The minimum total direct operating cost is found to be at a minimum cost cruise (MCC) mach number of 0.73. Similar results are found for other flight routes and ranges. Another comparison is done on the same mission to Istanbul. This model compares a current A320-200 flying Mach 0.78 with an A320LNG cruising at Mach 0.73. The same cost model assumptions are used, results are presented in figure 8-5. Concluding this case study the most economic cruise speed for the A320LNG is Mach 0.73 and at this speed it will be cheaper to operate than an A320-200.

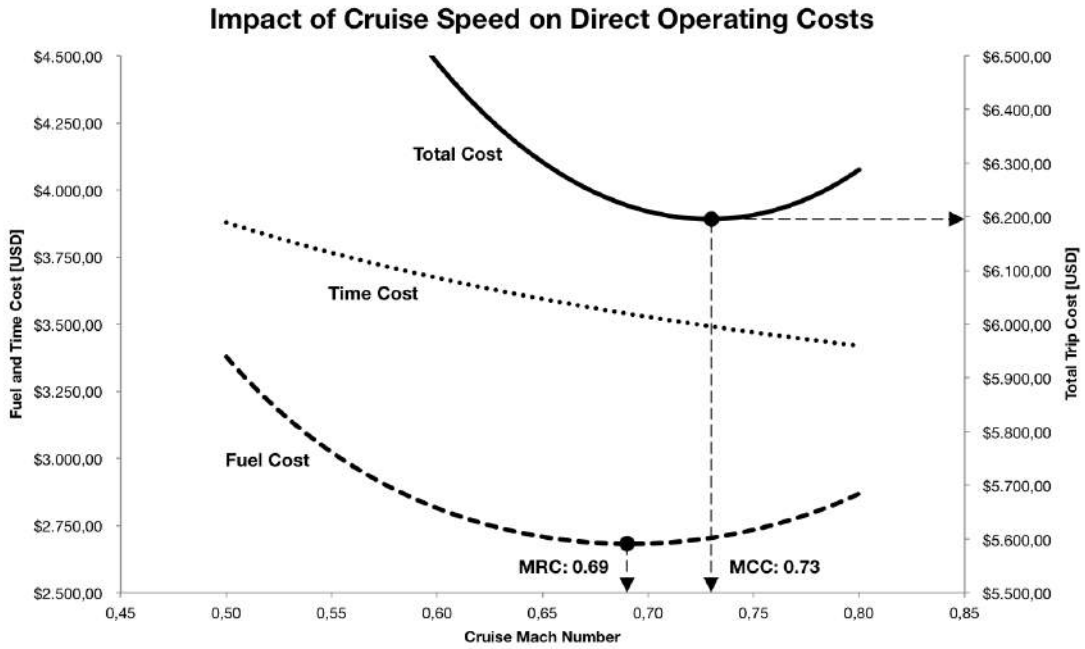

Figure 8-4: Effect of Cruise Speed on DOC

Subsequently a study is preformed on the impact on direct operating cost if the cruise speed were to decrease from M0.78 to M0.73. The analysis compares an A320-200 flying Mach 0.78 with an A320LNG flying Mach 0.73 for the same flight route. Furthermore the computations are based on the costs presented in figure 8-2. Results are presented in figure 8-5.

Concluding this case study the most economic cruise speed for the A320LNG is Mach 0.73 and at this speed it will be cheaper to operate than an A320-200.

Direct Operating Cost Analysis A320 vs A320LNG	**Case Study Mission: Amsterdam (AMS) to Istanbul (IST)** *Comparison of A320 at M0.78 and A320LNG at M0.73*					
Distance	1196	nm				
Cruise flight level	FL330					
OAT at cruise (ISA)	321,45	K				
Cost Index	50			10		
Cruise mach number	0,786			0,731		
Cruise speed	549,09	kts		510,67	kts	
Cruise average fuel burn	1047	kg/h/eng		878,92	kg/h/eng	
SFC open rotor vs turbofan				14%	reduction	
	Time	**Dist (nm)**	**Fuel (kgs)**	**Time**	**Dist (nm)**	**Fuel (kgs)**
Engine start-up	0:06:00	0	0	0:06:00	0	0
Taxi to runway	0:10:00	0	100	0:10:00	0	0
Takeoff	0:03:00	0	150	0:03:00	0	129
Climb to FL330	0:24:12	170	2043	0:22:45	154,5	1716,99
Cruise 1	1:42:10	935,00	3565,68	1:50:23	939,50	2993,27
Descent from FL370	0:14:45	91	197	0:18:00	102	126,85
Landing	0:03:00	0	50	0:03:00	0	43
Taxi to gate	0:10:00	0	100	0:10:00	0	0
Shutdown	0:02:00	0	0	0:02:00	0	0
	2:55:07	**1196**	**6205,68**	**3:05:08**	**1196**	**5009,11**
Time difference	10,02	mins		5,72%	change	
Fuel difference	1196,58	kgs		19,28%	change	
Direct Operating Costs	**USD**	**USD**	**Comments**			
Cost Index	50	10				
Flight crew	2287	2418	Increase due to longer flight time			
Fuel and oil	7746	4691	Decrease due to less fuel burn			
Airport and en-route charges	2013	2122	No change (fees are not time dependent)			
Aircraft rental, insurance, etc…	2135	2326	No change (fees on monthly basis)			
Maintenance	3141	3618	Increase due to longer flight time			
Depreciation (aircraft)	1555	1695	No change (on yearly basis)			
CO2 taxes	572	312	Decrease due to less fuel burn			
Total for entire flight (USD)	**19450**	**17181**	**-11,7% total change in DOC**			
	$	**-2.269,03**	**absolute change in DOC (USD)**			
	$	**-3.312.778,66**	**annual savings on this sector (4 flights a day)**			

Figure 8-5: Comparison of A320-200 at M0.78 with A320LNG at M0.73

Chapter 9

ATA28/48 - Fuel Tank

In this chapter the fuel tank design will be discussed. First of all, the tank and insulation material will be discussed. Next, the steps to come to the final design will be presented as well as forces, fairing and pylon design, the venting and refuelling system and de-icing procedures. Finally, the tank layout is presented and the verification and validation procedures are discussed.

9-1 Requirements

The design on the fuel tank is based on several requirements as shown below. The requirement which most influences the design is A320LNG-REQ-ATA28-01 since this determines the maximum pressure for which the tank has to be designed.

- **A320LNG-REQ-ATA28-01:** The tank shall be able to withstand the maximum pressure due to a 72 hour normal heat flux at the tank's maximum fuel capacity without venting or exceeding the maximum operating pressure. The ambient temperature during the 72 hours period shall be 25 degrees Celsius. NPFA 4.3.5 [19]
- **A320LNG-REQ-ATA28-02:** All tank materials which are in contact with the LNG shall be able to withstand the cryogenic temperatures of -162 degrees Celsius at a pressure of 1 bar. NPFA 57 4.3.1.1 [19]
- **A320LNG-REQ-ATA28-03:** The occurrence of icing on the tank shall be prevented.
- **A320LNG-REQ-ATA28-04:** A strike with a bird at take-off or landing speed shall not cause catastrophic flight conditions.
- **A320LNG-REQ-ATA28-05:** Containers shall be equipped with a device that provides an indication of when the container is filled to the maximum allowable liquid level. NFPA 57 4.3.2 [19]
- **A320LNG-REQ-ATA28-06:** The container shall be equipped with shut-off valves that allow for its complete isolation from the rest of the vehicular fuel system. NFPA 57 4.3.4 [19]
- **A320LNG-REQ-ATA28-07:** All safety relief devices on vehicular fuel containers that discharge to the atmosphere shall vent outside of the vehicle. NPFA 4.4.3 [19]
- **A320LNG-REQ-ATA28-08:** Each tank shall have a LNG volume capacity of $7.5m^3$.
- **A320LNG-REQ-ATA28-09:** To calculate the stresses in the walls of the LNG tank, a safety factor of 1.5 shall be used.
- **A320LNG-REQ-ATA28-10:** Minimum allowable thickness of the walls of the tanks is 0.002m due to manufacturing constraints.

9-2 Materials

The tank consists of an inner and outer wall with insulation in between. Both the tank wall material and the insulation material have to be decided on which will be done in this section.

Tank material

For the tank material different kinds of metal are considered: stainless steel, titanium and aluminium alloy. In table 9-1 the properties of several considered materials are shown. In order to determine which material to use, the yield stress and the density are considered. The yield stress is taken into account because this determines the thickness required of the tank. The density is taken into account because this determines the weight of the tank. Other considerations include cost, manufacturability, corrosion and properties at cryogenic conditions.
NASA states that successful application of composites for cryogenic fuel tanks can result in a weight reduction up to 30 percent and a cost reduction of 25 percent [83]. Due to the potential reduction in weight and cost, composites can be a good alternative to metals for the design of a cryogenic fuel tank. However, due to the lack of detailed research, composites are not chosen for this study.
The final choice is Aluminium 7075-T6 because it has all the aforementioned advantages of aluminium and has a high yield strength of 503 MPa. This metal is also used in the inner tank of the space shuttle to separate the liquid oxygen and liquid nitrogen [17]. Although aluminium has a lower yield stress than titanium, it has a lower density. The high price of titanium and the fact that it is harder to manufacture makes aluminium favourable. Thermal conductivity is not taken into account because it is assumed that the insulation material provides all insulation.

Table 9-1: Material properties [1, 78, 22, 16, 2]

Material	**Density** g/cm^3	**Heat conductivity** W/mK	**Melting point** $[°C]$	**Yield stress [MPa]**
Titanium Ti-6Al-4V	4.42	7.2	1649	828
Stainless steel 316	8.00	16.3	1370 - 1400	205
Stainless steel 305	7.99	16.2	1399 - 1454	241
Aluminium 7075-T6	2.81	130	477 - 635	503

Insulation material

LNG is stored at cryogenic temperatures, hence heat exchange should be minimized if possible. This is achieved by having insulation material between the inner and outer wall. The required insulation material needs to have low thermal conductivity and low density. There are several options available: multilayer insulation, insulation foams and aero-gels.
All the properties of different insulation materials under consideration are shown in table 9-2. Multilayer insulation is not used because of the high vacuum required. It is decided not to use

foams because of possible cracking due to thermal cycling [92]. Furthermore, aerogels have the advantage of a low conductivity. This allows the insulation to be thinner which is beneficial since this reduces the size of the fuel tanks, ultimately reducing the drag. A choice is made between Cabot P100 and Cryogel-Z. Cryogel-Z is chosen because it is specially developed for cryogenic applications. It has good flexibility and compression resistance. Cryogel-Z is also able to withstand thermal shocks. It is environmentally friendly and it can be disposed safely. It also has a high fire resistance. It is very durable since it has good bounce-back properties meaning that in case of compression it returns to its original position after compression [8].

Table 9-2: Insulation properties [92] [87] [40] [29] [33] [18]

	Density g/cm^3	**Heat conductivity** $W/(m \cdot K)$
AUSPERL Perlite	49.6	0.0405
Rigid polyurethane foam	60	0.025
Foamglas HLB800	120	0.024
Cabot P100	120-180	0.011
Cryogel-Z	130	0.01125

Radiation properties

Important radiation properties to consider are the emissivity and reflectivity. Emissivity depends on material and temperature of its surface. Polished and shiny surfaces have lower emissivity than rough surfaces. However, in case of the fuel tank, wear and the accumulation of dirt affects the surface roughness. Large variations in temperature can also result in a change in emissivity over time. In this case, the surface temperature is assumed to not change much over time. The emissivity of the aluminium surface is conservatively estimated to be 0.5 to account for degradation over time[66]. The reflectivity of the material represents the fraction of light which is reflected. A high reflectivity is beneficial since this reduces the heat transfer into the tank. For aluminium reflectivity of 0.5 is used [37].

9-3 Structural Design

For the structural design, a cylindrical tank with spherical caps is used. This shape is used because it is a simple model and good for high pressures. (proportionate to boil-off rate). It is also the most beneficial for stress distribution. In a cylindrical tank, the average stress is lower and thus the required wall thickness is lower, this results in a lighter tank. For aerodynamic considerations, it is considered to build a fairing around part of the fuel tank in which the systems are placed.

9-3-1 Sizing of Fuel tank

The main requirement for the structural design is A320LNG-REQ-ATA28-01 (see appendix 9-3-2), which states that the fuel tank shall be able to withstand the pressure built up after 72 hours of heat transfer with all valves closed.
An iterative process is used to come to the final tank frontal area, length and weight. The

modelling language Modelica is used to build a software tool which is able to simulate the physical conditions inside the tank after 72 hours of heat transfer. Section 9-3-2 shows the modelling assumptions used to make code for heating of the tank at ground conditions.

9-3-2 Assumptions Fuel Tank

Several assumptions are made while designing the fuel tank. The assumptions and their impact are:

- Assumption: The tank is assumed to be thin walled when calculating the stresses in the tank
  Effect: Higher orders of the thickness are neglected as thickness compared to other dimensions is very small. Therfore, the effect will be negligible on the calculated stresses.
- Assumption: The LNG consists of 100% methane.
  Effect: This assumption is made because the software program FluidProp does not contain a mixture for LNG. The effect is that the calculated pressure will be a little higher than the actual pressure because the methane has a higher density, hence it introduces some conservatism in the design.
- Assumption: To calculate the heat transfer due to the forced convection around cylindrical bodies (see A320LNG-REQ-ATA28-01 in section A.), the velocity is assumed to be equal to a typical wind velocity of 15 m/s. *Effect:* If the wind velocity is lower, more heat transfer will occur making pressure increase at a slightly higher rate.
- Assumption: Outside temperature is 25 degrees Celsius.
  Effect: This is taken as a conservative estimate resulting in a safer design since this results in a maximum possible heat transfer.
- Assumption: The temperature of the inner tank material is equal to the temperature of the LNG.
  Effect: Since the inner tank has a high thermal conductivity this assumption introduces negligible error.
- Assumption: All heat received by the tank surface is transferred to the insulation material.
  Effect: The effect is negligible since the thickness of the outer wall is small compared to the insulation material and its thermal conductivity is very high.
- Assumption: Heat transfer due to radiation from the Earth and atmosphere is ignored when calculating pressure and boil-off within the tank.
  Effect: The effect is negligible as maximum heat emitted by the Earth and its atmosphere is much less than that of sun. Moreover, wing shielding of the fuel tank from the sun is not taken into account. Therefore, the effect of neglecting the radiation from the Earth and atmosphere is further depleted.
- Assumption: The insulation is sectioned into two parts. The outer part has a temperature equal to the surface temperature and the inner part has a temperature equal to the temperature of the outside of the inner shell.
  Effect: In reality the insulation has a temperature gradient. However, because the walls are thin the effect is negligible.
- Assumption: When calculating the drag force of the LNG tanks, the angle of attack of the tanks with respect to the airflow is assumed to be zero degrees.

Effect: In reality the LNG tanks might have an angle of attack increasing the drag a little bit.

- Assumption: The strength of the radiation from the sun is changed over time based on values obtained at a measuring station, this value is multiplied such that the maximum radiation is around $1400 W/m^2$ which is the maximum solar radiation value on earth [95].
  Effect: Since the maximum value is taken equal to the maximum solar radiation reaching the earth, a worst case scenario is assumed and it introduces some conservatism into the design.

The equations used in the program can be found in appendix C. Given the initial conditions of the system, the tool calculates the changes in pressure, vapour mass, LNG mass and the temperature of the LNG, insulation and tank wall. The initial condition is defined as the point at which the temperature of LNG is 111K and the initial pressure is 1 bar. All values of the parameters used are given in table 9-3.

Table 9-3: Values of parameters used in Modelica

Parameter	**Value**	**Unit**
Thermal conductivity of metal	120	$W/(mK)$
Thermal conductivity of insulating material	0.01125	$W/(mK)$
Velocity of air	15	m/s
Reflectivity	0.5	–
Emissivity	0.5	–

The required volume of LNG in each tank is $7.5 m^3$. To account for LNG boil off, the total volume of the tank is taken as $8.5 m^3$. This volume is taken because it is found to provide sufficient room for pressure build up inside the tank. Initially, several different radii are chosen, between 0.55 m and 0.8 m, which results in different lengths of the fuel tank as calculated by equation 9-1.

$$l = \left(\frac{V_{tank} - \frac{4}{3}\pi {r_i}^3}{\pi {r_i}^2} \right) \tag{9-1}$$

where V_{tank} is the volume of the tank, r_i is the radius of the inner skin, l is the length of the cylindrical section of the tank.

The fuel tank is designed for pressure after 72h as stated in the requirement 9-1. As shown in the figure 9-1, after pressure 6.9bar the pressure increases tremendously. This is because total mass of LNG and total volume is fixed (therefore the process is isochoric process) and after 6.9 bar, the LNG curve leaves the saturation belt on the liquid side of the T-s diagram. Therefore it is not feasible to design a tank that can withstand the pressure higher than 6.9 bar. Through an iterative process, it was found that 2mm is the minimum thickness of the inner shell that can withstand this pressure. In order to calculate the required thickness of the insulation material, the simulation tool is run several times until the minimum insulation thickness is found for which the tank pressure is 6.9 bar after 72 hours.

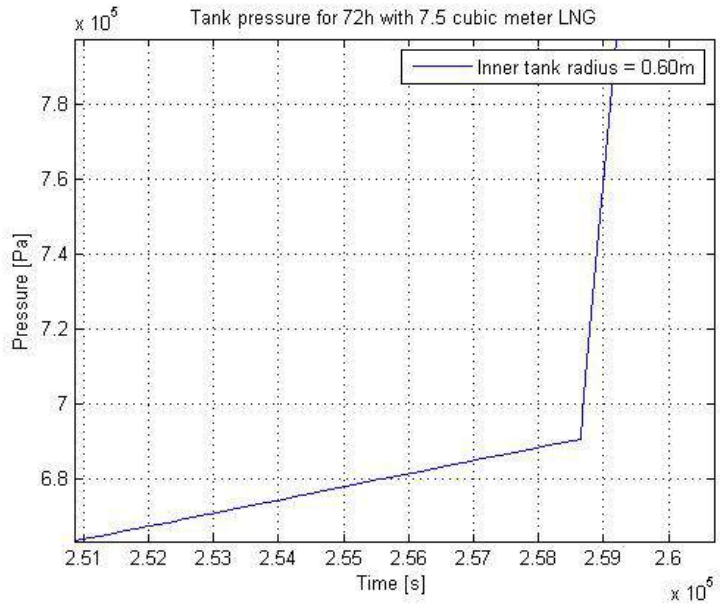

Figure 9-1: Rapid increase in pressure after all LNG reaches its liquid state

After this, different combination of radius and lengths were chosen and trade off was done as shown in the table 9-4. Weight and drag are given equal importance. Drag is based on the frontal area. The trade-off is based on the percentage change in drag and weight of a certain radius with respect to the previous radius. If the percentage of weight reduction is higher than the percentage increase in drag the design is considered preferable over another design.

Table 9-4: Fuel tank design trade-off

Radius	Weight	Frontal area	Weight change	Drag change	Total change
0.55 m	594.81	1.13	-	-	-
0.60 m	533.69	1.32	-10.28	7.65	-2.62
0.65 m	490.82	1.52	-8.03	7.42	-0.61
0.70 m	451.34	1.73	-8.04	6.76	-1.28
0.75 m	421.44	1.96	-6.62	6.47	-0.16
0.80 m	399.47	2.21	-5.21	6.20	0.99

The option chosen is the one with a radius of 0.75 m because this still has a higher relative weight reduction than the relative drag increase compared to a radius of 0.70 m. All values of the final design are given in table 9-5.

Table 9-5: Values of the final parameters which where changed for every iteration

Parameters	Value	Unit
Radius	0.75	m
Aluminium mass	303.93	kg
Insulation mass	147.13	kg
Insulation thickness	0.036	m
Total length of cylindrical part	3.81	m
Tank surface area	26.67	m^2
Insulation surface area	25.11	m^2
Inner tank surface area	25.02	m^2
Outer diameter	1.58	m
Outer length	5.39	m
Inner tank thickness	0.002	m
Insulation thickness	0.036	m
Outer tank thickness	0.002	m
Outer surface area	26.67	m^2
Total empty tank mass	421.44	kg
Frontal area	1.96	m^2
Max Pressure after 72h	6.9	bar

The pressure over time for the final design is given in figure 9-2. The boil off rate for the final design is given in figure 9-3, it can be seen in this figure that the mass of the vapour does not start at zero. This is because the volume of the tank ($8.5m^3$) is higher than the volume of the LNG ($7.5m^3$). At the end of 72h, the pressure is 6.9bar which is the maximum allowable pressure as stated before. But for a safety margin, the tanks is design to withstand 7.5bar. As shown in the figure 9-3, there is not vapour state as LNG leaves the saturation belt on liquid side of its T-s diagram also explained before.

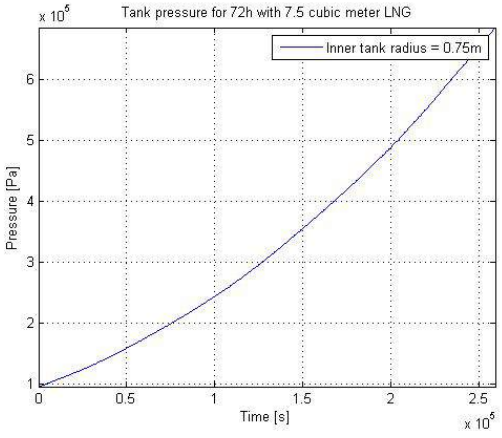

Figure 9-2: Tank pressure over time

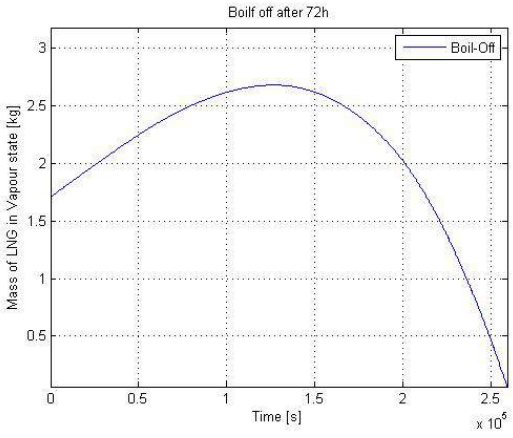

Figure 9-3: Mass of vapour over time

9-3-3 Fuel tank Analysis for flight conditions

Modelica is also used to build a flight model. This flight model simulates the physical conditions throughout a flight of 3.5 hours, taking into account the decrease in LNG mass due to the fuel consumption of the aircraft. The fuel consumption during take-off, climb, cruise, descent and landing are found using the software Piano. The simulation is made conservative by using maximum solar intensity values encountered during a day. During the simulation, there is venting of the boild off- os boil off stays in the tank. Figure 9-4 gives the pressure increase during the flight and figure 9-5 presents the mass of the vapour during the flight. It can be seen that more LNG evaporates during flight as compared to the 72 h simulation with no fuel flow. This can be expected since more space inside the tank is available for the vapour since the volume of the liquid LNG decreases over time. The pressure after 5 flight hours is less than the pressure after 72 hours on the ground. It can be concluded that the design is able to withstand the pressures encountered during flight. The boil-off rate during flight is approximately 6.9kg per hour. Hence, for a 3.5 hour flight the total boil off is 24kg, less than 1 percent of the total LNG used during flight. This is acceptable and the design can be considered successful.

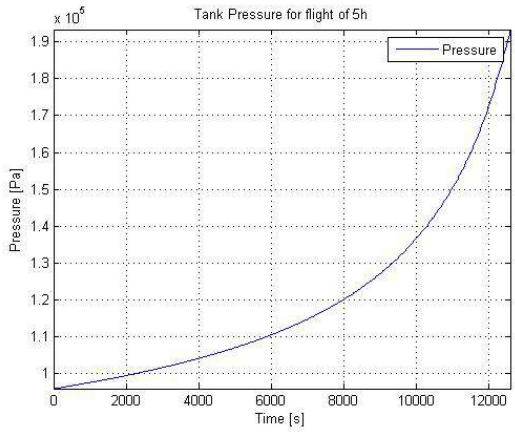

Figure 9-4: Tank pressure during flight

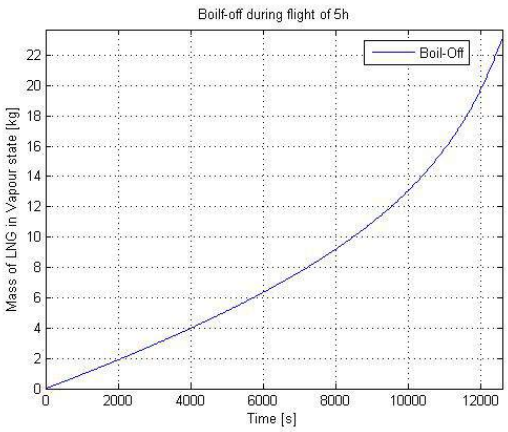

Figure 9-5: Mass of vapour during flight

9-4 Forces

In this section, forces acting on the fuel tank are analysed and an analysis for bending and buckling is done.

Drag force

To estimate the drag coefficient of the cylinder with spherical caps, [104] is used.
The slenderness ratio (l/d) of the design is 3.41 since the length is 5.39 meter and the diameter is 1.58 meter.
From [104], it is found that a cylinder with spherical caps with this slenderness ratio, has a drag coefficient of approximately 0.2.

The drag force is then be approximated by: $D = C_D \frac{1}{2} \rho V^2 S$
where S is the frontal area pointing into the flow. During cruise, at an altitude of 10,000 meter, the density is $0.414 kg/m^3$ [116] and assuming a cruise speed of 222 m/s this leads to a drag force of 4000N. The total drag of the aircraft is between 44 kN and 50 kN, see section 12-4. Hence, the pods account for approximately 16-18 percent of the total drag.

9-4-1 Bird strike

From [76] it is known that the impact force due to a bird strike is determined by: $F = \frac{2\Pi r^2 \rho V^2}{3}$
where r is the radius of the bird, V is the speed of the aircraft and ρ is the density of the bird. The assumptions used to arrive at this equations are:

- The bird has a spherical shape
- The impact angle is 90 degrees
- Bird is deformed by half its size on impact

The requirement CS 25.571 [46] is used which state that the airplane must be able to successfully complete a flight in case a bird of 1.8kg strikes. Since volume and radius are needed to determine the impact force they are estimated. The density is estimated to be $429 kg/m^3$. The radius is assumed to be 0.15m and the velocity of the aircraft is taking as maximum landing velocity of 78 m/s. This results in a force of 123 kN.

Compression analysis

First of all the local stress at the impact area due to a bird strike is calculated. Assuming a circular impact area with a radius of 0.1m this results in a stress of $\sigma = \frac{123000}{0.031} = 3.97 MPa$. It follows that the local tank structure at the place of impact is able to handle a bird strike since this is lower than the yield stress. In order to make sure the fuel tank does not fail under compression in case of a bird strike, the compression stress is calculated by $\sigma = \frac{F}{A} = \frac{123000}{0.019} = 6.53 MPa$ where F is the impact force due to the bird strike and A is the cross sectional area of the tank taking the loads somewhere along the cylindrical part of the tank. The resulting stress is much lower than the yield stress of the tank so the tank does not fail under compression [79]. This is not surprising since a high strength aluminium alloy is used for the tank design.

Buckling analysis

To make sure the fuel tank do not fail due to buckling under maximum compression forces, a buckling analysis is conducted. Since the fuel tank has a large radius and a thin wall (hence a large moment of inertia), it can be expected that the critical buckling load is high and is a less critical design condition when compared to failure under compression. This is found

to be the case since the critical buckling load is 373kN, much less than the force encountered due to a bird strike.

Bending analysis

Since the fuel tank is symmetrical, the bending stress equation $\sigma = \frac{My}{I}$ can be used [79]. The force is assumed to act at the tip of the fuel tank creating the largest moment, M, at the other end of the tank. y is the distance from the neutral axis which is equal to the radius of the fuel tank. I is the moment of inertia as determined in the previous section. To estimate the bending force a bird strike under an angle of 45 degrees from the horizontal is assumed. This gives a bending force of $F = cos(45) \cdot 123000 = 102.5kN$ This results in a moment of $M = F \cdot L = 102500 \cdot 5.39 = 552.6kN$. Hence, the bending stress is $\sigma = \frac{552600 \cdot 0.75}{1.534 \cdot 10^{-2}} = 27MPa$. Hence, the fuel tank does not fail under bending.

9-5 Fairing design

In order to make the fuel tank more aerodynamic and accommodate the venting system, a fairing is build around the nose of the fuel tank. From [125], it is known that a parabolic shape is a superior aerodynamic shape for a speed of around Mach 0.8. Therefore, the nose fairing is built with a parabolic shape. Besides the aerodynamic shape, the main design consideration comes from impact forces. Glare is chosen as the material to use for the parabolic fairing because it has good impact performance which can be attributed to its high failure strain.
However, it is not by definition better than aluminium since Glare is not optimised for impact resistance, it is optimised for fatigue [82].
It can be optimised for impact resistance as proposed by [82]. Further research for this is required.
At the back of the pylon a fairing can be built in order to reduce the pressure drag. Since this does not need to withstand impacts, a simple lightweight plastic fairing will be sufficient.

9-6 Pylon design

An important design issue to consider is the height of the pylon. The CFM56-3 series engine, which is used on the A320, has a diameter of 1.5 m [53]. The fuel tank has a diameter of 1.58 m. The aim is to keep the tank approximately as far above the ground as the current engine is above the ground. Since the diameter is almost the same, the pylon length is also taken the same. The current engine pylon can be taken as baseline design. Since the tank weight with maximum fuel is more than the engine weight, the pylon has to be reinforced to be able to carry the weight of the full tank. The main contribution to the force in vertical direction comes from the weight of the tank and fuel. Accounting for a maximum load factor of 2.5 this leads to a force of $F = m * g * n = 103kN$. The largest possible force in horizontal direction comes from the impact of a bird, the largest force in vertical direction comes from the tank

weight (incl. load factor). These are the design requirements for the support structure of the tank.

9-7 Venting system

The venting system consists of pressure gauges, pressure relief devices, valves, fuel volume indicator and a fill connector.

Pressure gauges

The pressure gauges used in LNG tanks shall be connected to a point above the maximum liquid level. They should be able to cope with the pressure and temperature conditions and have a minimum burst pressure safety factor of 4 [19].

Pressure relief device

A pressure relief device is needed in order to release LNG in case the pressure becomes too high inside the tank. Under normal operations this venting system will not be used. Only if the pressure becomes too high will the gas be vented. This can happen when insulation is decreased or if the fuel is left inside the tank for more than 72 hours. The fuel tank is designed to withstand a pressure of 7.5 bar. The valve will open once a pressure of 5 bar is reached such that the pressure remains within the allowable limits. The pressure relief device vents outside of the vehicle and communicate directly with the vapour space inside of the tank.
Loss of insulation is taken as worst case scenario to determine the required venting since this has a large effect on the boil-off rate. However, since complete loss of insulation is very unlikely, a 25 percent loss of insulation is taken in order to size the pressure discharge area. Assuming an outside temperature of -44 degrees Celsius this results in a boil-off rate of 0.06 kg/s. This maximum rate was found by comparing different boil-off values from simulations for different losses in insulation.
Pentair Pressure Relief Valve Engineering Handbook [14] is used to determine the size of the discharge area. Discharge area is defined as the measured minimum net area which determines the flow through the valve. The equations [14] used are valid for pressures above 1.03 bar.
The effective discharge area found is: $A = 253mm^2$. Assuming a circular discharge area this results in a circle with a diameter of 18mm. This area is used for the design of the LNG tank. It should be noted that this is only an initial estimation and the final discharge area depends on the actual pressure relief device used.

Refuelling System

Prior refuelling of the aircraft the fuel system must be bled with a non reacting gas such as helium or nitrogen to avoid any air entering the system, as it creates an explosive mixture with gaseous LNG. Due to difficult handling and storage requirements of helium, nitrogen bleeding is preferred. If the aircraft fuel system is drained, it is also advised to fill the tanks

and the fuel system with nitrogen to avoid presence of air. In order to fill LNG into the fuel tanks a fill connector and fuel volume indicator are required. The refuelling rate for LNG is 1.25 cubic meters per minute as determined in chapter 20. The main parts of the refuelling system are the fill connector, fuel volume indicator and fill check valve [58].

- **Fill Connector:** A connector needs to be used which is able to withstand the cryogenic temperatures of LNG. It is used to connect the refuelling station to the tank and create pressure a difference for the flow of LNG. The connector should have proper sealing to prevent any leakage during refuelling. The connection works with a spring system which shuts the connection when not in use. This also prevent leakage.
- **Fuel Volume indicator:** This is used to measure the volume of LNG in the tanks during refuelling.
- **Fill Check Valve:** This is needed to stop back flow of LNG in case of any accident.

9-8 Deicing and anti-icing procedure

Icing at the surface of the fuel tank might take place because the airplane is flying high altitude where the air is below freezing temperatures. This makes an ice mitigation system required. There are two types of ice mitigation systems that are considered: deicing and anti-icing systems. Anti-icing is usually done before take-off which prevents the build up of ice by coating the tanks with mixtures of water and glycol [34].
Several deicing procedures can be considered such as thermal melting, use of chemical compound, freezing point depressants,surface deformation and pneumatic boot systems etc. The area most prone to icing at the tank is the leading edge of the fairing in front of the tank. Thermal melting, use of chemical compound, freezing point depressants cannot be used as they add a weight penalty and surface deformation cannot be used as it can lead to fatigue of the tank. Therefore pneumatic boot systems shall be used which expand on the front of the fuel tank in order to remove ice [114].

9-9 Layout of the fuel tank

Figure 9-6 shows the layout of LNG fuel tank. It includes the actual tank with fairing, venting system, refueling system, pressure gages for measuring pressure and the fuel volume indicator.

9-10 Verification and Validation

The numerical model used for the calculation of the maximum pressure inside the fuel tank after 72 hours has to be verified and validated.
Verification is done while the numerical model is build. The solutions found by the numerical model are verified by analytical calculations in order to make sure the software performs the calculations correctly using the right equations. Furthermore, a more simplified model is used in order to verify the results of the model. This model is used to check whether the obtained results are similar to the results of the simplified model.

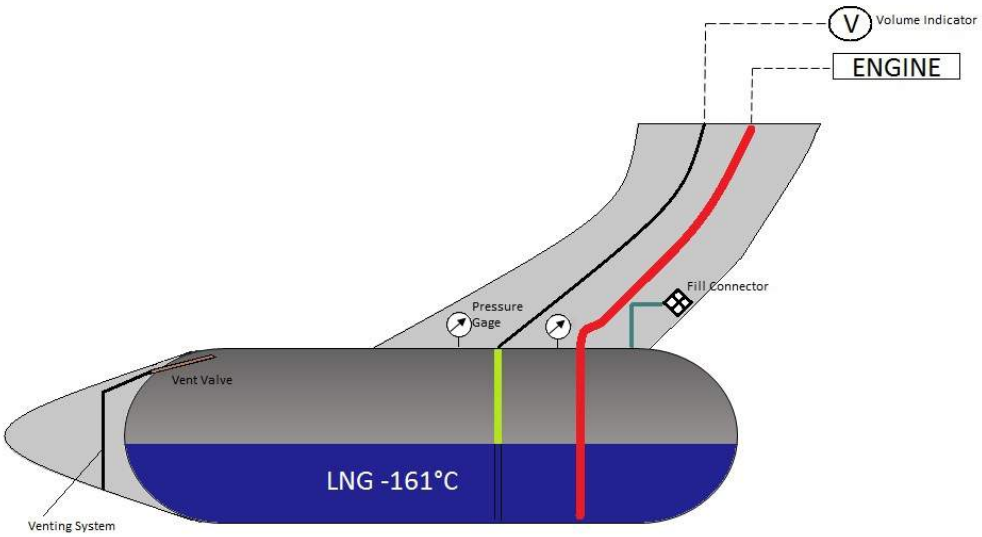

Figure 9-6: Layout of the fuel tank and subsystems

In order to validate the model the tank has to be built. A test can be performed by exposing the fuel tank to certain conditions, then comparing the results to the numerical model. The temperatures, pressure and total boil off from the experiment and numerical model are compared. The results should be within the allowable error limit of 5%. This limit is chosen because a small difference in results can be expected due to the assumptions made when setting up the numerical model. These assumptions can be found in section 9-3-2.

Chapter 10

ATA28/48 - Fuel System Design

After designing the fuel tank, a fuel distribution system is designed. Since the design under consideration is hybrid, LNG and kerosene fuel systems are presented individually.

10-1 Kerosene system

The kerosene system uses Jet A-1 fuel and comprises of multiple systems with different functionalities. The fuel lines and pumps are designed for the maximum fuel flow rate of 2600 kg/h (0.722 kg/s) [65] in an A320 aircraft. The overall system layout for kerosene is presented in figure 10-1. The different subsystems of the fuel system are described and explained.

Each wing is mounted with one electrical transfer valve to carry the fuel from outer tank to inner tank. Transfer valves connect the fuel tanks with the cross feed system and regulate fuel flow in both directions. The cross feed allows controlled distribution of fuel to the fuel tanks, ultimately allowing centre of gravity control. This process of balancing fuel between the wing tanks is automated.

A ball valve is placed before the APU pump because no flow control is necessary; the pump requires only a on/off feature which is used to provide the engines with the start up power. A cross feed valve is controlled by a two-way motor, which allows both engines to be fed from one wing or one engine to be fed from both wings[109]. A flow control valve is placed before each engine fuel pump, this valve controls the rate at which the fuel is fed into the engine. There are two flow control valves, one ball valve, seven transfer valves and one cross feed valve in this design. This selection and placement of valves are based on current kerosene fuel systems[109].

Fuel cleaning devices Two types of devices are used to clean the fuel: fuel strainer and fuel filter. Fuel strainers are made with rough wire mesh and are arranged to block large pieces of debris from entering the fuel system. Fuel filters are generally constructed with finer mesh. Strainers are placed at the outlet of the fuel tank and the inlet for the engine. Filters are placed somewhere between the outlet and engine driven fuel pump. Frequent inspection and cleaning of these fuel cleaning devices are necessary for operation. Two strainers and two filters are used in this design.

Auxiliary feed A fuel pump is connected to the auxiliary power unit (APU) to supply fuel for engine start-up. This fuel pump is used when fuel feed pressure is low and the engine driven pump is not yet capable for sufficient fuel delivery.

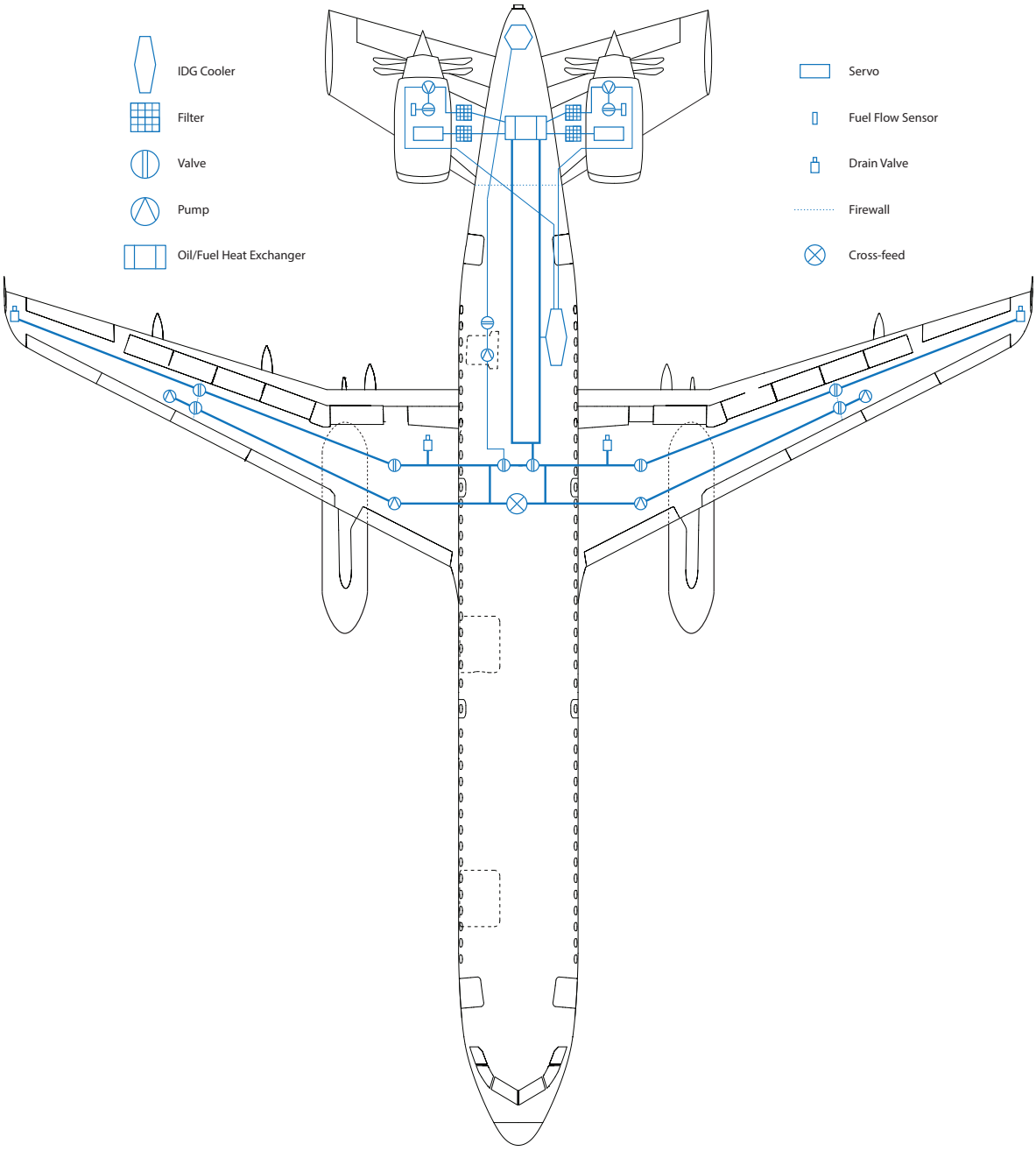

Figure 10-1: Fuel system schematic: Kerosene

Operational fuel system

For the operation of the aircraft, kerosene must be able to flow from the tanks to the engines. Fuel lines and relevant devices are to be designed to repeatedly perform this without failure.

Fuel pumps Four types of fuel pump are used in this design: boost pump, engine pump, APU pump and refuel pump. A boost pump is an electric motor driven centrifugal pump

mounted in the bottom of the fuel tank[59]. The boost pump is double ended, submerged in fuel and is able to deliver fuel both forward and backwards. The pump is also low pressure in order to supply fuel to the engine driven pump[5]. Boost pumps also maintain pressure in the fuel to prevent vapour lock in the fuel lines. A standby pump is also put into the fuel tank and operates only when the boost pump is defective or set to off. A high pressured engine driven pump is located inside each engine for fuel injection.

An APU pump is used to supply power to start the main engines when the aircraft is on ground. Engine-driven generators are used to power the pumps when the aircraft is in flight. Refuelling pumps are used to transfer fuel from tankers in order to fill up empty wing tanks. Four boost pumps, four standby pumps, two engine pumps and one APU pump are used in this design. According to Eaton corporation, a main pump supplier for Airbus, the average weight of a fuel pump is approximately 20 kg[39]. With nine pumps, a total of 180 kg is accounted for fuel pumps.

Fuel system lines and fittings Rigid lines are made of aluminium alloy. These are connected with Army/Navy or military standard fittings. In this design, stainless steel reinforced hose assemblies are used at locations in which abrasion, frequent vibrations and heat exchange occur. The fuel lines also have to be supported to withstand aircraft vibrations, loads due to fuel flow pressure and accelerated flight conditions[5]. Another design consideration is that the fuel lines have to be able to supply twice the maximum fuel flow rate in the case that one wing has to supply fuel for both engines. Taking this into account, the thickness of the fuel lines of both aluminium and stainless steel can be determined. A factor of 1.5 is used for safety design purposes.

The fuel lines are cylindrical for optimal pressure distribution. Common aircraft hose dash sizes are used as reference for determining diameter of the fuel delivery lines[111], as listed below.

- Fuel delivery and oil cooler lines, 12.7 mm
- Large aircraft, oil and fuel, 15.875 mm
- Large aircraft, oil and fuel, 19.05 mm
- Large aircraft, oil and fuel, 25.4 mm

To determine the thicknesses, the flow velocity is first determined using:

$$v = \frac{Q}{A} \tag{10-1}$$

A is the area of the pressure vessel and is calculated using πR^2. Q is the volume flow rate, this is deduced from the maximum mass flow rate given that the density of jet fuel is 0.81 kg/m^3. With the flow velocity, the pressure in the vessel can be calculated using Bernoulli's equation:

$$q = \frac{1}{2}\rho v^2 \tag{10-2}$$

The pressure allows us to determine the thicknesses of the pipe using the hoop stress formula[47]:

$$\sigma = SF \cdot \frac{Pd^2}{(d+2t)^2 - d^2} \tag{10-3}$$

σ is the ultimate yield stress of the material, SF is the safety factor and d is the design diameter mentioned above. Corrosion allowance has to be taken into account. According to World Corrosion Organisation, aluminium is assigned a corrosion allowance of 0.5 mm and stainless steel 1.0 mm. However, the aluminium fuel lines inside the wing tanks are exposed to fuel both internally and externally, a total allowance is 1.0 mm is necessary for safety[89]. The thicknesses are then rounded up to the nearest 0.5 for ease of production[36]. The table below shows the thicknesses and kg/m of aluminium, aluminium inside fuel tank and stainless steel:

Table 10-1: Thickness and kg/m of aluminium, aluminium inside fuel tank and stainless steel fuel lines

	Thickness inc. corrosion allowance [mm]			**kg/m**		
Diameter [mm]	Al	Al (tank)	Steel	Al	Al (tank)	Steel
12.700	2.0	2.5	2.0	0.465	0.592	1.014
15.875	1.5	2.0	1.5	0.423	0.573	1.253
19.050	1.0	1.5	1.5	0.332	0.504	1.493
25.400	1.0	1.5	1.5	0.439	0.665	1.972

For oil delivery and cooling purposes, the 12.7 mm aluminium configuration has the lowest weight and is used for engine oil line. For stainless steel assembly hoses, the 15.875 mm configuration is used. As for fuel lines inside the wing tank, the 19.05 mm aluminium (inside tank) configuration is used. The 19.05 mm aluminium configuration is also used for fuel lines inside the fuselage.

Then, the total weight for each configuration is calculated. Given the kg/m, the total length of each configuration is measured using a schematic of the current A320. The individual weight of each configuration and total weight of fuel lines are presented in the table below.

Table 10-2: Individual length, weight of different fuel line configurations and total weight

Diameter [mm]	Configuration	kg/m	Length [m]	Weight [kg]
12.700	Aluminium	0.465	36.5	17.0
15.875	Stainless Steel	1.253	10.1	12.7
19.050	Aluminium (inside tank)	0.504	75.5	38.1
			Total	67.7

The total weight contributed by kerosene fuel lines is 67.7 kg. Fittings are necessary to connect the fuel lines and at the same time allow structural flexibility[6]. One fitting is required at each fuel line intersection. A fitting weighs approximately 0.05 kg[20]. According to schematic, 60 fittings are used to connect the fuel system, this adds up to 3 kg.

Fuel recirculation system In order to cool the engine when engine oil temperature is high or aircraft is operating at low engine power settings, an IDG (integrated drive generator)[50] heat exchanger is required [50]. The fuel recirculation system is also necessary for heating the fuel and engine oil at cold temperatures to prevent frost formation.

Heating and ice prevention devices Temperature is significantly lower at operational altitudes. There is the risk of ice formation from water in the fuel, ice blocks the flow of fuel through the filter. In this design, the APU can be used as a fuel heater and the heated fuel is circulated around the system for defrost purposes.

Refuelling system

To keep the turnaround times low, multiple fuel connections are needed. Also, multiple refuelling locations are selected to make sure that all the fuel in the wing tanks is accessible. An automatic shut off system is used to prevent overfilling of the fuel tank.

Drains An easy to open and close drain valve is required for defuelling purposes. This is necessary to remove the fuel so that the fuel pump can be detached from the tanks for cleaning and maintenance. This is also to remove any water which may have accumulated in the fuel lines. For efficient and effective drainage, two drainage valves are implemented into each wing. Take note that fuel dump systems are not installed as this contradicts Airbus fuel handling policy.

Indicators

Two types of indicators are used to provide real time information on the amount of fuel remaining in the tank and engine feed rate.

Fuel quantity indicator Electric fuel quantity indicators are used in this design. Servo heaters for each engine are separately connected to the heat exchanger to monitor the fuel feed temperature and pressure[107].

Fuel level sensing control unit Also known as a fuel flow meter, this device displays the engine's use of fuel in real time. An electric fuel management gauge is used for this design. Both indicators are managed by the electronic centralised aircraft monitor[12]. The central processing unit of this monitor is placed at the cockpit. This information is used to manage refuelling, inter-tank fuel transfers, and overfill.

Safety system

Fire walls are necessary to maximise protection of passengers and crew in the occurrence of a fire. The main fuselage is sealed from the engine compartments and auxiliary power unit. Fireproof and corrosion proof material is used to seal the fire wall. Shrouds are also necessary

to cover the fuel lines to prevent any passage of hazardous air, fluids or flame[4]. According to FAA, the stainless steel hoses do not need fireproof shrouds because it is thicker than 0.015 inches[64]. According to the schematic, 60 m of the fuel lines require heat shrouding because they are made of aluminium and/or are not inside the fuel tank. Using [127] shroud sleeve numbers (FAA approved heat shroud) , the shroud weighs 0.116 kg/m. The entire heat shroud weighs 7 kg.

For safety purposes, all fuel pump and valve electrical wiring are routed outside of the fuel tanks to eliminate the potential of ignition into the fuel tanks[43]. Summing up the weight components of the fuel system, the kerosene system weighs a total of 257.7 kg.

10-2 LNG system

Use of liquified natural gas as an aircraft fuel poses multiple technological difficulties for the design of the fuel system, in particular from combination of the conventional kerosene fuel system and cryogenic fuel system in the proposed hybrid A320LNG design. This leads to increased complexity and places a cap on cooling potential of the cryogenic fuel because each of the fuel will only be used for the respective part of the mission and the aircraft must be able to safely operate on jet fuel alone. The layout of the LNG fuel system is illustrated in the figure 10-2.

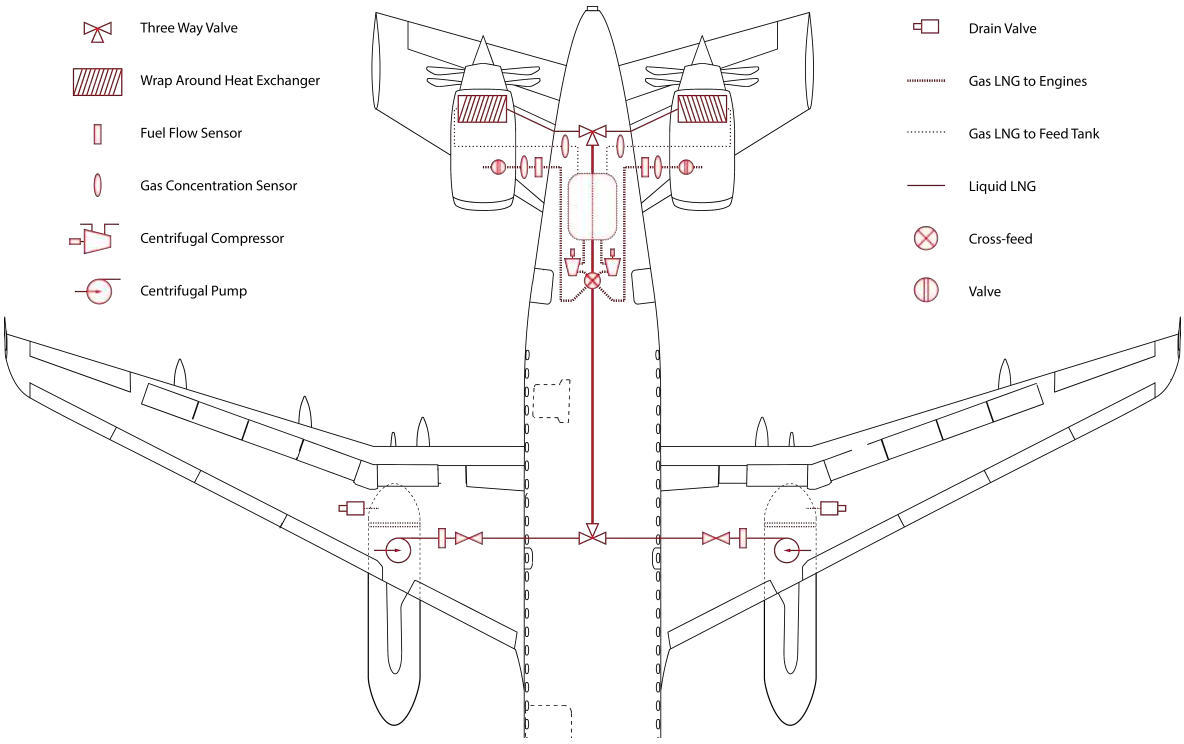

Figure 10-2: A320 LNG Fuel System

The fuel is extracted from the wing podded tanks through the boost pumps, tank shut-off valves and fuel supply lines to the engine. From there it passes though the exhaust gas-to-LNG

heat exchanger and is returned to the engine feed tank. The gaseous LNG is then directed to the engine through centrifugal compressors, cross-feed valve and flow control valves. The thrust output of the engine is controlled by the adjustments of the valve settings as well as the compressor output.

Fuel pump

The first part of the fuel systems ensures delivery of LNG from the wing podded tanks to the heat exchanger for vaporisation. This is done through booster pumps operating at a wide range of flow rates to ensure continuous fuel supply. The aircraft shall have two booster tanks per compartment, such that the failure of a single pump will not compromise aircraft safety. The booster pumps are followed by shutoff valves that are activated in case of tank failure.

As the pump operates at low inlet pressure and LNG is stored near its boiling point, cavitation is a very prominent issue, causing such problems as decrease in efficiency, hindering continuous fuel supply, excessive vibration and reduced pump life due to cavitation erosion. Use of an impeller inducer is chosen as the most adequate way to manage the cavitation problem by reducing required net positive suction head (NPSH). This effectively minimises the pressure drop across the pump to avoid boiling.

Four fuel pump types for aircraft applications can be differentiated. Among these are vane and piston positive displacement pumps and centrifugal and inducer dynamic pumps. The displacement pumps are too heavy and require lubrication on large surface area, which compromises maintainability and is impractical at cryogenic temperatures. Centrifugal pump in combination with an impeller inducer is chosen for its wide operating range, moderate mechanical friction, low wear on impellers, and thus manageable lubrication requirements.

The pump can be powered hydraulically, electrically or by engine bleed air. Since the engines are located far from the fuel tanks, use of turbine or compressor bleed air is not technologically beneficial. On-board hydraulic system has large weight and complexity drawbacks, therefore electrical pump operation is favoured. It involves using an alternator to convert some of the engine's mechanical work into electricity, which is then directed to a generator that operates the pump.

Heat exchanger

Heat exchanger (HE) is required to vaporise and sufficiently heat the fuel prior feeding it to the combustion chamber. This can be achieved by using the excess heat from the engine, while also exploiting enormous cooling potential of LNG to boost the engine efficiency. However, location of the heat exchanger poses a large problem. There are three general possible positions for the heat exchanger placement. These include placing the HE at the compressor for either pre-cooling or inter-cooling of compressor air, at the high pressure turbine, or at the exhaust for regenerative fuel heating or hydrogen expander cycle. Pre-cooling is the simplest method, which requires least engine modifications, but provides a very limited temperature difference across the HE and causes icing problems at the engine inlet, which poses a risk of foreign object damage. As well as with compressor pre-cooling, the pressure drop on the air side of the heat exchanger is the offsetting disadvantage of the inter-cooling HE. Placing the HE at the

high pressure turbine itself offers the great efficiency benefits, yet is the most complex solution and produces an adverse temperature gradient in turbine blades, making them prone to low cycle fatigue failure. The first three options for heat exchanger placement are illustrated in the figures 10-3 - 10-5.

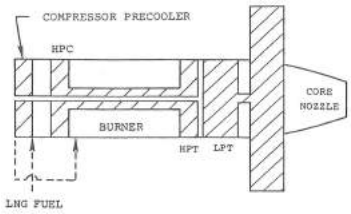

Figure 10-3: Compressor pre-cooling HE

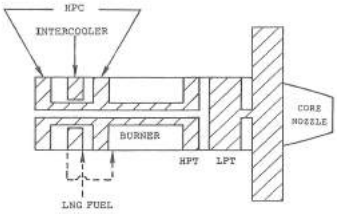

Figure 10-4: Compressor inter-cooling HE

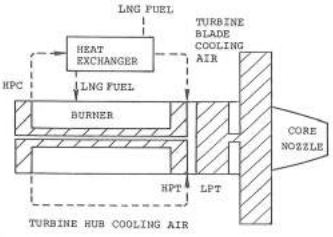

Figure 10-5: Turbine cooling HE

Before exploring the last option for HE placement, it has to be noted that in the chosen hybrid configuration it is not possible to solely rely on the LNG cryogenic capacity for engine cooling. This is because only a part of the mission is performed on LNG, while during the rest of the flight the cryogenic fuel must be kept in the tank in it's liquid form. This means that efficiency benefits of the cryogenic fuel cooling are very limited. The main purpose of the heat exchanger is therefore evaporation and heating of the fuel before it enters the combustion chamber, while cooling can only provide minor extra efficiency benefits during LNG operation.

With this in mind an exhaust gas heat exchanger can be considered as the most favourable arrangement. Such placement provides the largest temperature difference across the HE for the fastest evaporation, avoids such issues as foreign object damage due to icing and does not pose large technological drawbacks in terms of weight and complexity. The regenerative fuel heating at the exhaust gas is a simple solution that allows efficient heating of the cryogenic fuel as illustrated in figure 10-6. Hydrogen expander cycle on the other hand provides aircraft accessory power by using a hydrogen expansion turbine rather than extracting it from a gear box shown in figure 10-7. This method has similar efficiency impacts and weight penalties to the regenerative fuel heating, yet it is more technologically complex. With that in mind exhaust gas regenerative fuel heating is selected as a heat exchanger option.

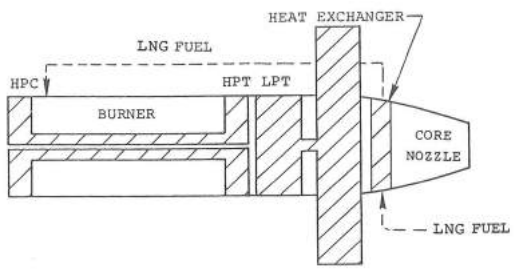

Figure 10-6: Exhaust gas HE

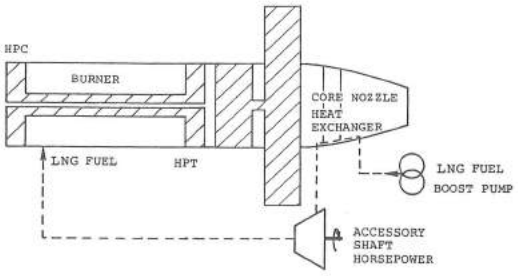

Figure 10-7: LNG expander cycle HE

Regarding the type of the heat exchanger, several options exist, such as tubular, plate or ribbed HE. Multi-tube ring heat exchanger shown in the figure 10-8 is the most lightweight

of them all and is chosen for its simplicity and least number of modifications to the engine layout.

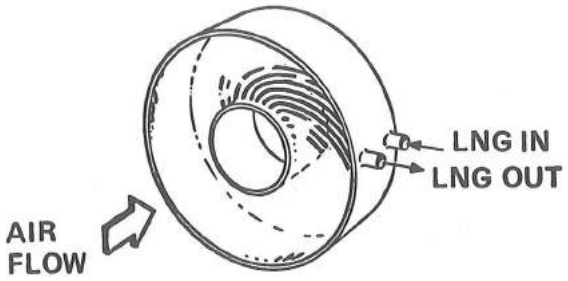

Figure 10-8: Multi-tube ring heat exchanger [26]

Engine feed tank

Vaporisation of a fluid is never an even process, therefore evaporated LNG cannot be fed to the engines directly from the heat exchanger as it is impossible to sustain continuous fuel flow. As a means to resolve that issue an engine feed tank is introduced to store vaporised LNG prior directing it to the engines. Initially it was proposed to also route the boil-off from the main LNG tanks to the engine feed tank via compressors, however the amount of LNG evaporated throughout the flight was not found to be significant to justify implementation of such system. Even though an additional tank adds extra weight to the system, it does not store cryogenic fuel and therefore does not need to be thermally insulated, only pressurised.

Two suitable arrangements exist for the engine feed tank positioning. Placing the tank inside of the wing box is beneficial for stability of the aircraft, as it moves the center of gravity forward, however such placement requires longer piping, increasing the weight of the fuel system. Aft location of the engine feed tank as shown in figure 10-2 is preferred as it decreases the complexity of the system, overall length of the fuel lines and therefore it's weight. This allows for the compressors to be placed directly before the engines. According to regulations each engine has to be supplied from a separate tank during fuel intensive parts of the flight, therefore the engine feed tank is separated in two equal compartments. Due to hybrid operation the feed tank only stores 2 m^3 of evaporated LNG at 10 bars, before the compressors feed it to the engine at 17 bars, slightly above the maximum pressure of the combustion chamber during cruise. The tank is able to store 13.4 kg of evaporated LNG. The maximum fuel consumption is 0.6 kg/s per engine, which means that there is a buffer time of 11.16 seconds between the vaporised LNG entering from the heat exchanger and being fed to the engines.

Engine feed system

A conventional turbine engine utilises multi-point fuel injection through a large number of nozzles to ensure a homogeneous mixture in the combustion chamber. As the requirements for the injection nozzles vary between the kerosene and natural gas, they cannot be used interchangeably. Based on SFC values 45% of fuel injectors operate on LNG while the rest of

them are reserved exclusively for kerosene. This way a smooth transition can be achieved when switching between the two fuels mid flight. A shut off valve is chosen as a means of stopping the kerosene supply to the engine and turning off the kerosene feed pumps. Meanwhile the LNG pumps and compressors are activated and the throttle lever is rewired to control the LNG supply. The difficulty in this method is matching the LNG flow to the kerosene flow in terms of the thrust levels it produces, so the pilot get the same thrust response in a certain lever position.

Gas LNG Compressor

The LNG in its gas form is directed to the engine from the feed tank through a compressor. Since it is desired that the fuel enter the combustion chamber at elevated temperature, the compressor no longer has to be working in a cryogenic environment, which relieves multiple limitations. For the compressor operation an electric motor operation is chosen as it offers the greatest flow control flexibility. Shaft power from the running main engine is directed into an alternator that generates the electricity required to drive the compressor, as illustrated in the figure 10-9. The rest of the options were neglected due to their weight, complexity, or operational inflexibility.

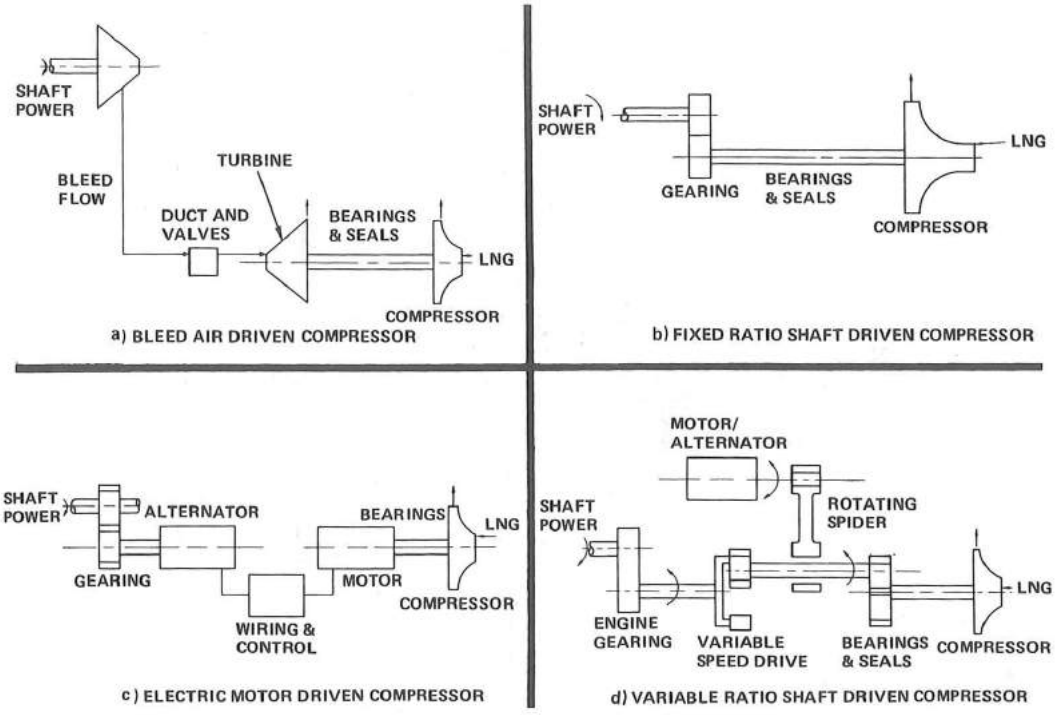

Figure 10-9: High pressure compressor drive options [26]

Fuel transfer system

Transferring a cryogenic fuel such as LNG poses several difficulties. All the piping has to be thermally insulated to minimise the heat losses, yet even with the most sophisticated

insulation it is impossible to ensure homogeneous flow of cryogenic fuel. Thermal losses, bends, friction against the pipe walls, valves, sensors, pumps and compressors cause pressure drops in the fuel lines that lead to boiling of cryogenic liquid. Therefore typical cryogenic flow consists of constantly interchanging proportions of liquid and vapour. Such two phase flow is illustrated in the figure 10-10.

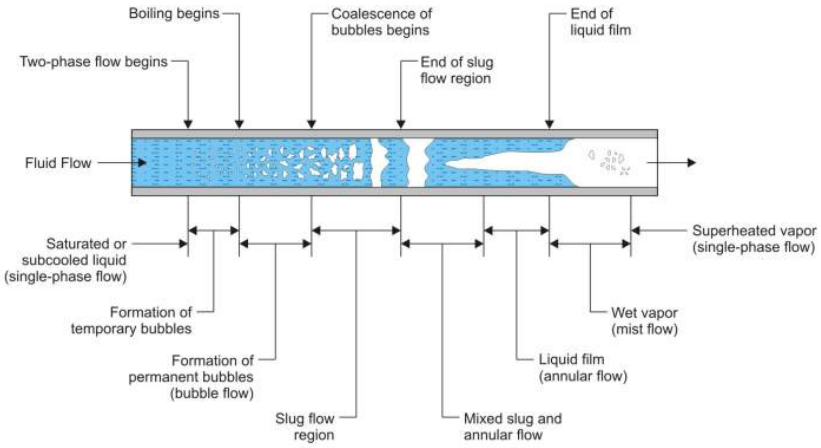

Figure 10-10: Two Phase Cryogenic Fluid Flow Through Pipe [94]

This is one of the main designing constraints when dealing with cryogenic fuel system, particularly it illustrates the necessity of the heat exchanger for continuous fuel supply. It also complicates the pipe sizing process as the the three typical types of two-phase flow are observed, each with its own flow rate. Single phase flow is preferable for its homogeneity but cannot always be achieved due to pressure variations in certain parts of the pipe. Bubble flow is preferable when a single phase flow cannot be achieved, as it does not result in a dramatic mass flow reduction, but can, however cause unwanted destabilising vibrations of the fuel system. Slug flow consists of alternating areas of liquid and vapour that introduce dynamic loading and intense vibrations as well as a drastic drop in the mass flow. Annular flow consist of a thin film of cryogenic fuel alongside the walls of the piping with vapour in the center. This virtually renders the piping system ineffective.

To minimise the two phase flow and heat losses, the fuel lines need to be thermally insulated. Two basic types of cryogenic piping insulation are in use, vacuum-jacketed (VJ) and rigid, closed-cell foam. VJ insulation has unparalleled performance in terms of heat loss per unit diameter, set back by costly manufacture, poor reliability and difficult installation and maintenance. A single leak in a VJ piping would compromise the entire fuel line and render it unusable. Foam insulation on the other hand is much more reliable and easy in service, but suffers from added weight. A commercially available insulation material is a polyisocyanurate bun stock ISO-C1, which is highly moisture resistant, strong, durable, and lightweight. The foam can be infused with such low conducting gases as nitrogen to avoid condensation. Low friability and ease of installation and handling make it appealing for LNG insulation in the fuel lines of the aircraft.

The thickness of the insulating foam was determined by comparison to the vacuum jacket insulation, which is taken as a golden standard. It can be seen that while foam insulation is quite inferior to vacuum jacket, there is an initial drop in the heat input after which the

rate of the heat leak decrease is much smaller than the increase in insulation thickness. It has been decided that the input of 25 W/m is an acceptable penalty at ground conditions as halving it would require increasing the insulation thickness by a factor of 5. Resulting insulation thickness is therefore 3 cm.

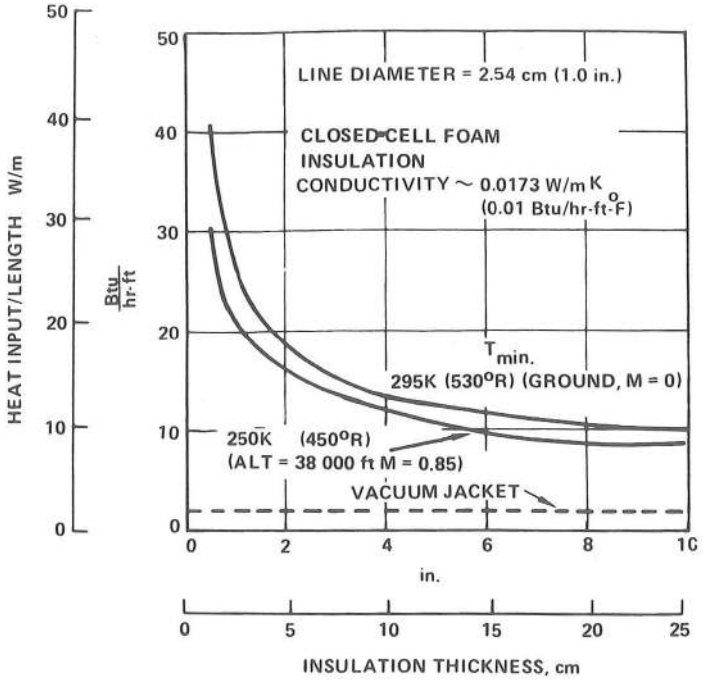

Figure 10-11: ISO-C1 Fuel line heat leak for foam and vacuum insulation [26]

Materials used in the construction of fuel feed system must be resistant to LNG embrittlement, capable off retaining sufficient structural properties at cryogenic temperatures. The isolating foam is placed around the inner stainless steel tubing containing LNG. Outer aluminium tubing around the foam serves as means of mechanical protection and vapour barrier. It is estimated that the upper bound of the engine fuel flow is 0.8 kg/s while the density of LNG is 410 kg/m^3. An booster pump is able to provide a velocity increment of 2.5 m/s to LNG in cryogenic form, therefore the optimal pipe thickness is found to be 35.25 mm. The thickness of the inner piping is dictated by manufacturing restrictions rather than structural strength requirements. The minimum thickness for austenitic stainless steel pipes with external diameter between 21.3 and 48.3 mm is 1.6 mm, which is chosen for the cryogenic fuel lines to minimise weight. The outer aluminium tubing needs to be as light as possible, as it does not bear any significant mechanical loads, so the minimum available thickness of 0.41 mm is selected. Cross section of selected fuel line is depicted in the figure 10-12.

After the LNG has been vaporised in the heat exchanger, the requirements to the piping are much less stringent, as they no longer need to be thermally insulated. Therefore the same design is utilised as for the cryogenic LNG but without the outer aluminium jacket and foam insulation. Despite the density drop after vaporisation, the compressor is able to ensure sufficient flow rate, so the diameter and thickness of the tubing remain the same. All the evaporated fuel is directed to a feed tank, from where it is directed to the engines using a set

of compressors.

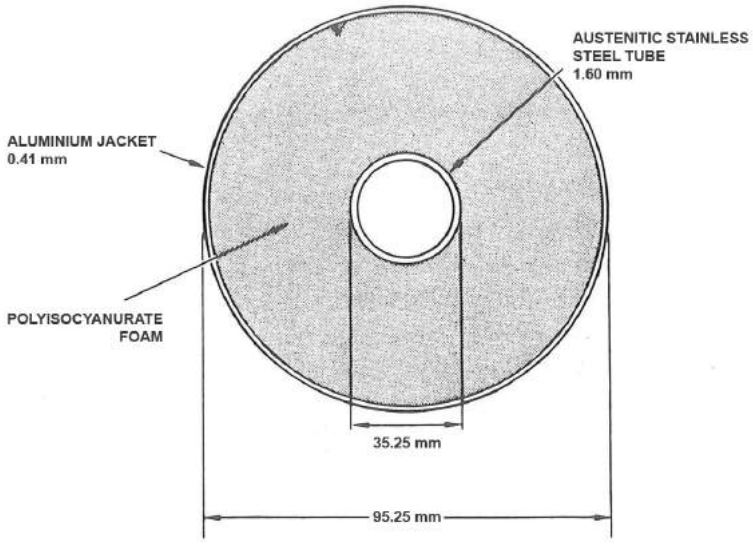

Figure 10-12: Cross section of cryogenic LNG fuel line [26]

Safety system

Even though LNG is a highly volatile substance, it only poses explosive danger in the gas form. This means that a variety of gas sensors can be used to analyse the LNG vapour concentrations in the crucial linkage and feed points. The combination of sensors acts as a fire prevention system to ensure the safety of the aircraft. In case of the fuel system malfunction that poses a threat the purging valves can be used to dump cryogenic fuel.

System Weight and CG

The surface area of the walls of austenitic stainless steel fuel lines is 196.12 mm^2 and the total length of the piping is 58.66 m, which results in 0.00992 m^3 of material used for inner tubing, contributing 78.97 kg to the fuel system weight. The density of polyisocyanurate foam is only 33 kg/m^3, adding 5.85 kg of weight. Aluminium jacket around cryogenic pipes contributes further 27.10 kg to the weight of the system. No reference heat exchangers exist in production yet, so estimating the weight of their casing, tubing and mounting, they are found to weigh 98 kg each. The engine feed tank, four booster pumps, two high pressure compressors and cross feed system along with the valves and pressure sensors contribute another 200 kg to the system. Total weight of the LNG fuel system is 508.3 kg, making it 70% heavier than the kerosene system. As can be seen from the diagram 10-13 the center of gravity of the fuel system is located quite aft and its estimated position is 29.5 m from the nose.

10-3 Combined kerosene/LNG fuel system

The entire fuel system of the A320LNG is illustrated in the figure 10-13. This system is a hybrid using both LNG and Jet-A fuel for operation of the aircraft, where each of the engines is capable of operating on both fuels and seamlessly transition from one another mid flight.

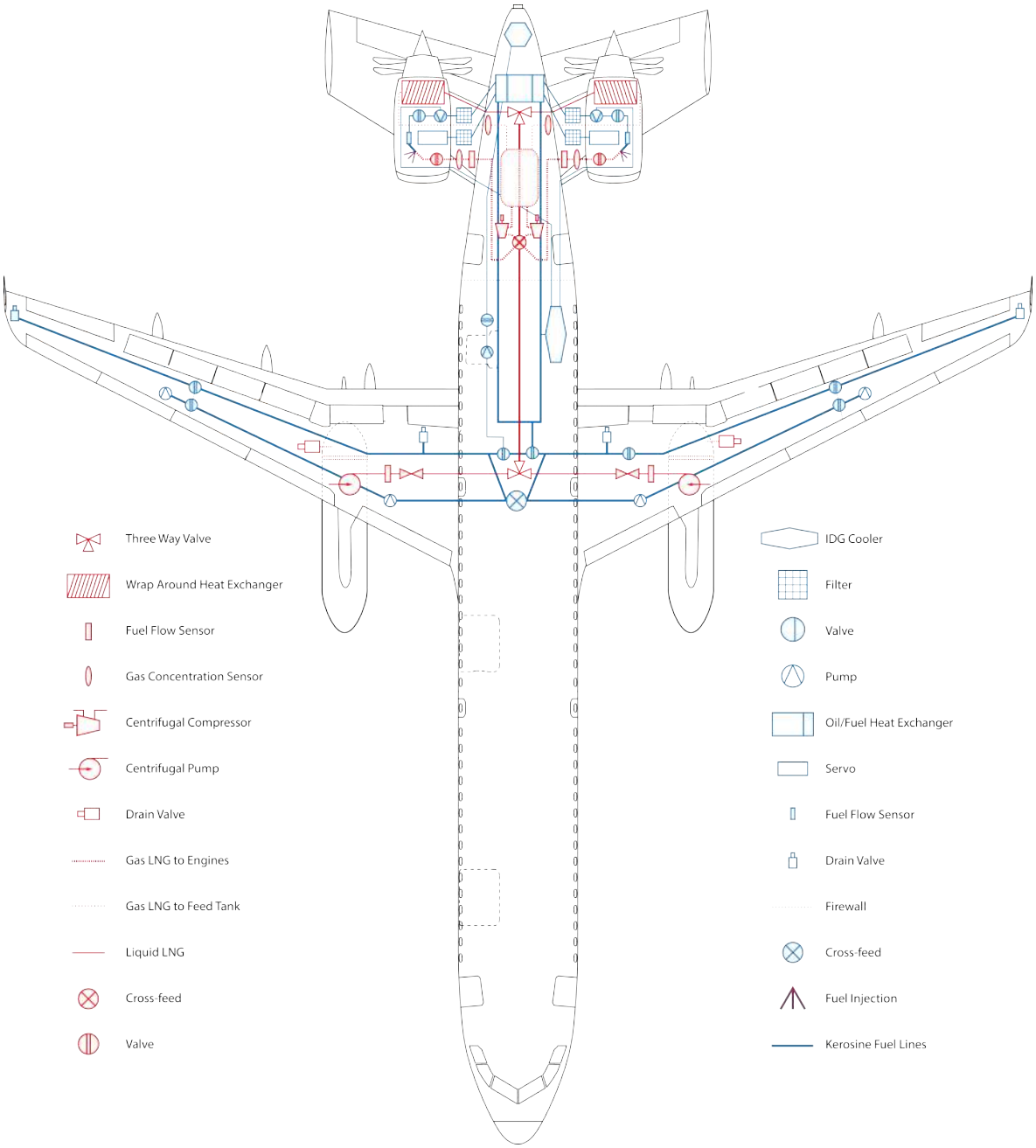

Figure 10-13: A320LNG Hybrid Fuel System

Chapter 11

ATA25/53 - Fuselage Design

This chapter will describe the preliminary design of the fuselage. The design options considered in the different subsections are the overall sizing, the passenger cabin, the cargo compartment, the integration of fuel lines, the structural design of the fuselage and reinforcements of the aft fuselage to account for the possible impact of an open rotor blade.

11-1 Preliminary design

The fuselage mainly has to withstand the pressure differences and the forces induced by weight, wings, landing gear and control surfaces. At the current fuselage diameter, the A320 can use LD3 containers and experience exists in manufacturing this fuselage size, therefore it was decided to keep the outer dimensions the same. However it was decided to build the fuselage from carbon fibre reinforced polymers to benefit from the weight savings, which were found to possibly decrease the structural fuselage weight by 24.6 % [75].

From literature [75] it was found that the structural weight of the current A320 is 4547kg. This structural weight was found to possibly decrease by 24.6 % with the use of CFRP. The use of composite materials and by flying at lower altitudes during the average mission, an increase in the fatigue life of the fuselage is possible.

The possibility of increasing the cabin width by reducing the thickness of the hull structure was investigated. It was found that the thickness of the hull is restricted by the height of the stringers. Therefore it was decided that the increased weight by reducing the height of the stringers is not worth the increase in passenger comfort as the A320 already has a superior cabin width compared to its direct competitors.

11-2 Passenger cabin

Based on the current floor plan of the A320, an optimised configuration was investigated. It was found that by resizing the aft galley and changing the position of the rear galley and the two rear toilets, additional space could be created. This space can be used to fit 3 additional seats into the cabin or increase the pitch of the seats thereby increasing the comfort of the passengers. In figure 11-1 the current layout and the modified layout are shown for a high density single class and a typical two class configuration.

Evacuation plan

The increased amount of passengers requires an adapted safety concept. As the current A320 is certified for 180 passengers only, the amount of emergency exits has to be increased as it

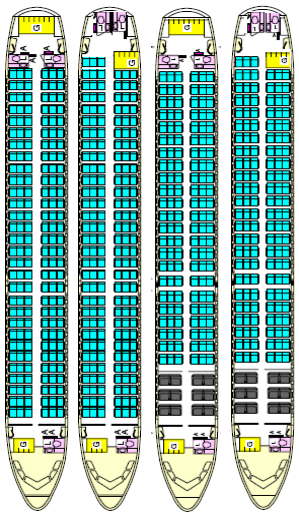

Figure 11-1: Comparison of current and suggested cabin layout. Current layout high density left, modified layout high density second from left, current layout typical configuration third from left, modified layout typical configuration right

should now be certified for a capacity of 183 passengers. However the current A320 is equipped with one pair of special Type I and two type III emergency exits on each side[45]. According to CS-25 regulations §25.807 this amount is sufficient for 2*55 + 2*35 = 180 passengers. Therefore the amount of emergency exits is not sufficient for 183 passengers and changes to the emergency exit layout have to be made. An option to increase the maximum occupancy of the aircraft is to increase the height of the over wing exits by 2 inches, from 40 to 42 inches thus making them type II exits. The new configuration would be suitable for 2*55 +2*40 = 190 passengers and thus sufficient for the new amount of 183 passengers. The advantage of this solution is that the modifications required in the fuselage are minimal and the space requirement is the same. The room gained by the rearrangements is not sacrificed for the new emergency exits. As the wing will move backwards with respect to the fuselage, the over wing emergency exits will have to move back as well. The exits have to move by the equivalent of 11 windows.

11-3 Cargo compartment

As for the passenger cabin, it is aimed to optimize the cargo bay. Again the considerations are based on the current A320 design. Through the movement of the wing towards the aft, the distribution of the big cargo compartments will shift. This will result in a configuration of one bigger cargo compartment in front of the wing that can take 7 LD 3 containers and an bulk cargo compartment in the rear for the aircraft. The fact that the fuel tanks are removed from the center wing box, gives room for storage space. However the centre wing box is not accessible therefore the feasibility of using this space for cargo storage is not given. However the integration of the lower mounted horizontal stabilizer might require a longer cylindrical form of the fuselage and less of a cone form. This might give the chance to increase the size of the aft bulk cargo compartment. However as more volume in the cone is required to

house the fuel system components, it was decided to not increase the size of the bulk cargo compartment. Figure 11-2 shows the distribution of the cargo compartments.

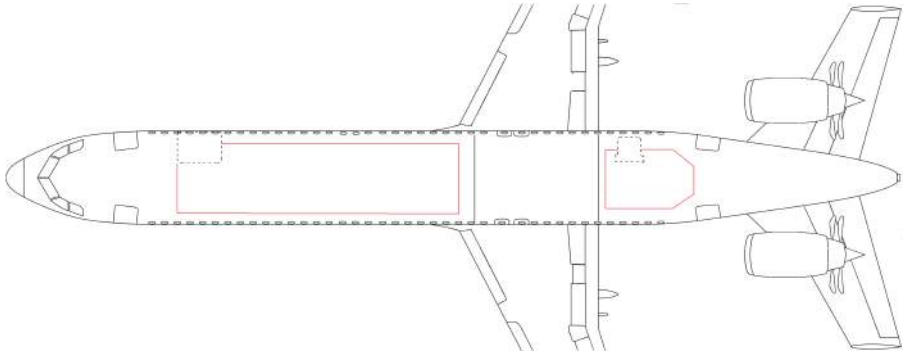

Figure 11-2: Location and sizing of the cargo bays

11-4 Fuel line integration

As the fuel lines are running through the fuselage, the risks of a gas leakage into the fuselage has to be eliminated. Therefore it was decided to let the fuel lines run in an extra, gas tight compartment along the fuselage hull. Inside this compartment there will be gas detectors to detect leakage and the hull will be protected by an additional layer of insulating material to avoid thermal stresses in case of fuel leakage.

11-5 Structural design

To withstand the loads applied to it, the fuselage has to be designed sufficiently strong. This section describes the design of the fuselage and the loads it has to withstand. As load case the cruise condition was used. To account for dynamic loading, a load factor of 3 was used. Due to time reasons, the taxiing/touch down condition was not investigated. The different loads applied to the fuselage are:

- Internal pressure load
- Bending moments
- Shear forces
- Compressive forces due to the thrust

The shear forces are induced by weight and lift forces. The bending moments are derived from this shear force distribution. The internal pressure is constant over the fuselage and depends on the outside pressure at the service ceiling and the pressure inside the fuselage. The compressive force due to drag and thrust start with a high value due to the form drag of the aircraft front. After this it increases linearly because of the skin drag and makes a jump at the location of the wings. At the engine location, the force decreases to zero. As material, quasi isotropic carbon fibre reinforced polymers with a maximum tensile stress of 375 MPa, a Poison ratio of 0.39 and an E-modulus of 55 GPa were used.

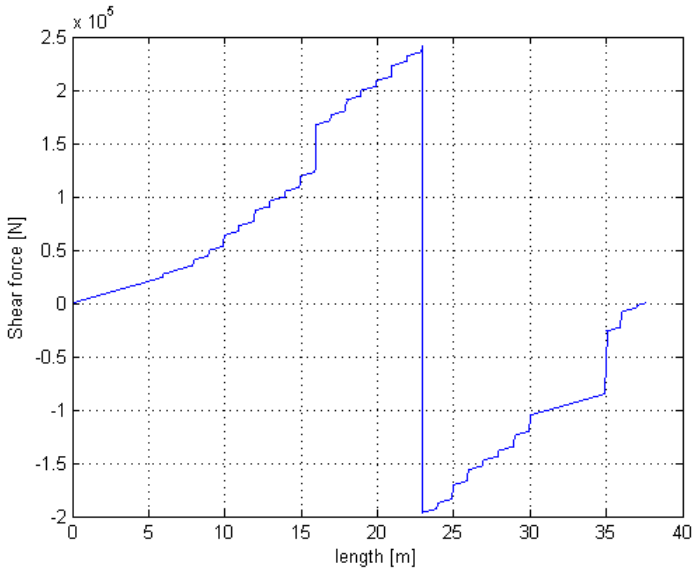

Figure 11-3: Shear force diagram for the fuselage during cruise flight

The internal pressure causes stresses in the skin in longitudinal and the circumferential direction.

$$\sigma_{hoop} = \frac{pr}{t} \tag{11-1}$$

$$\sigma_{long} = \frac{pr}{2t} \tag{11-2}$$

The bending moment causes normal stresses in the skin and in the stringers in longitudinal direction according to the flexure formula. It is assumed, that the neutral line of the fuselage is in the middle of the fuselage cross section.

$$\sigma = \frac{My}{I} \tag{11-3}$$

Next to this, the panels have to be sized to withstand plate buckling and the skin has to be able to handle the shear stresses caused by the shear forces. The critical force for plate buckling is given by

$$\sigma_{cr} = \frac{\pi^2 k_c E}{12(1-v^2)}(\frac{t}{b})^2 \tag{11-4}$$

as the k_c value depends on the ratio of stringer spacing to frame spacing and increases rapidly for values smaller than 2, the minimum stringer spacing to frame spacing value was set to 2. This results in a k_c value of 7.9. The cargo and passenger floors are assumed to act as stringers in that they clamp the skin panels.

Fuselage design

Based on the loads, a detailed design of the fuselage was created. The skin thickness of the fuselage is 5.4mm. This design has a frame spacing of 2m, a maximum stringer spacing of 1m. An isotropic view of the fuselage is given in figure 11-4.

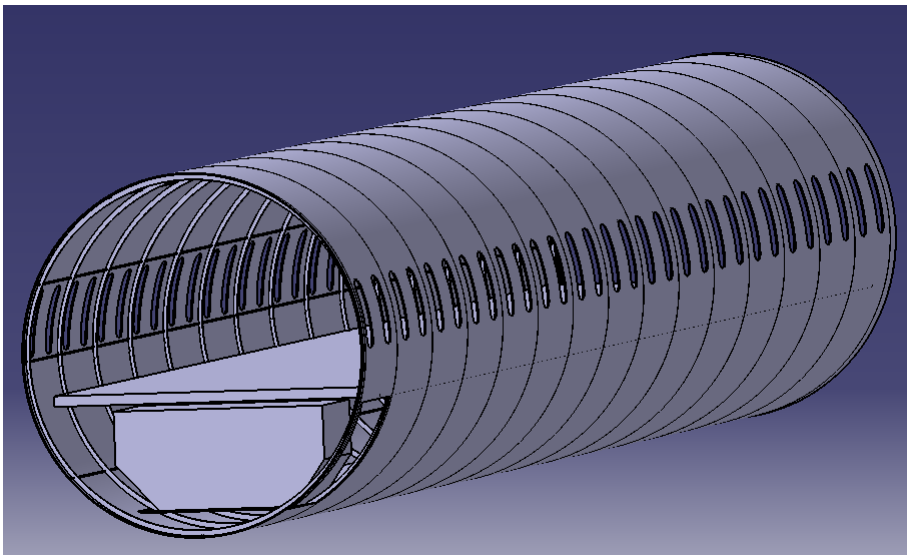

Figure 11-4: CAD model of the fuselage section

11-6 Empennage integration

Behind the cylindrical passenger cabin, the empennage cone begins. This part requires the highest changes compared to the current A320 as a different tail configuration is used and the engines are now mounted onto the back. Therefore the form of the empennage has to change and it has to be reinforced to be able to survive the possible impact of a propeller blade.

Layout change

The overall shape of the empennage changes as now a H-tail is used and the open rotor engines are placed in the back. Therefore the empennage has to house not just the control lines and the APU but also many parts of the fuel system. Also as the two engines have to be separated to eliminate the risk of a catastrophic failure, the horizontal tail should be placed as low as possible. This requires a lower empennage. As the landing gear is placed further to the back, thus decreasing the overhang of the tail, the tail can be formed less conical without an increase of the tail strike risk compared to the current A320. At the same time, the available volume inside the tail cone is increased. A comparison of the current and the proposed empennage side view is shown in figure 22-5.

11-7 Impact resistance

The open rotor engines bear the risk of a blade failure. In the case of a fan blade failing, the blade could impact the fuselage. To protect the second engine and the Apu, the fuselage skin in the aft section has to be able to withstand this impact and stop the blade. As high speed impact modelling is a very complex field, the finite element modelling tool ANSYS 14.5 was used to obtain reliable results. Two different models were created to predict the impact of a blade on the structure. The different models and the design that was obtained using them is described in this section.

Static impact model

For this simplified model, the average force of a propeller blade onto a rigid fuselage panel is calculated. Based on this force, the stresses in the panel are calculated. As a failure criterion, the Tsai-Wu failure criterion is used. This failure criterion determines if a composite material fails, whether it is due to fibre failure or matrix failure. However the criterion can not identify the failure mode. The Tsai-Wu failure criterion is given as [86]:

$$F_1\sigma_1 + F_2(\sigma_2+\sigma_3) + F_{11}\sigma_1^2 + F_{22}(\sigma_2^2+\sigma_3^2) + 2F_{12}\sigma_1(\sigma_2+\sigma_3) + 2F_{23}\sigma_2\sigma_3 + 2F_{44}\sigma_4^2 + F_{66}(\sigma_5^2+\sigma_6^2) >= 1 \quad (11\text{-}5)$$

Furthermore $X1T$ and $X2T$ give the maximum material strength in tension in the corresponding dimension while $X1C$ and $X2C$ represent the maximum compressive stress in this direction.

The kinetic energy of the blade is known as its velocity and mass are known. For more details see chapter 12. It is assumed that the fuselage does not deform and that the blade decelerates with a constant deceleration over its length.

$$s = \frac{1}{2}a * t^2 \quad (11\text{-}6)$$

$$t = \frac{v}{a} \quad (11\text{-}7)$$

Based on this the deceleration is calculated. Using the Newtonian relation, the average force is calculated.

$$F = m * a \quad (11\text{-}8)$$

This average force was used to calculate the stresses inside the plate for the case of a static force. The plate is modelled as being rigidly clamped at all its edges and no forces act except for the impact force. In this way the outer dimensions determine the stringer spacing or the frame spacing respectively. However the model gives poor results as it does not model the force peaks at the beginning of the impact and the energy dissipation due to the material deformation. The stress distribution of the plate is shown in figure 11-5.

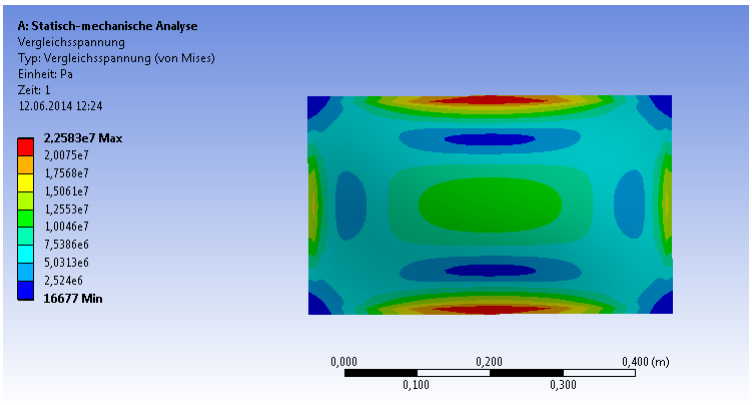

Figure 11-5: Stress distribution inside the panel due to impact force

Verification of the static model

To verify the model of the plate bending due to a point force, a second model was created. This model was based on Matlab and uses classic beam bending theory. Therefore 2 beams that are clamped on both ends and loaded by a point load in the middle are super positioned. The boundary condition is that both beams have to have the same displacement in the middle and the deflection angle in the middle has to be zero. The size of the beams is determined so that the thickness and the ratio of width over length is the same as for the plate. Also the volume has to stay the same. This results in beams half the width of their corresponding plate side.

With the condition that the displacement of both beams in the middle is equal, the force carried by each beam can be calculated. With the force known, the maximum moment can be calculated and using the flexure formula, the maximum stress is calculated. This value is compared to the results of the ANSYS simulation.

As the results differed significantly, it was decided to adjust the ANSYS model and bring it closer to the model calculated in the matlab code. Therefore the model was changed to a cross with the same dimensions as in the matlab code. The results of this second simulation are shown in figure 11-6. The stress values differed by maximal 16.5% and the general pattern met the expectation. The difference in stresses can be explained by the different theories that are used in the calculations and the overlap of material in the matlab code. Therefore the ANSYS model with force and boundary condition definition is considered to be verified.

Validation of the static model

Next to the Verification, the model also has to be validated to ensure correct results. This paragraph describes how the model could be validated. For validation a plate with identical dimension and the same material properties as in the model is clamped on all edges and a small projectile is shot onto the plate. The mass and velocity is chosen in a way that the resulting average force is equivalent to the one in the model. The deformations of the plate can be measured using strain gauges. These measured values can be compared to the simulated ones. It is expected that the values will be much smaller than the simulated ones as no static

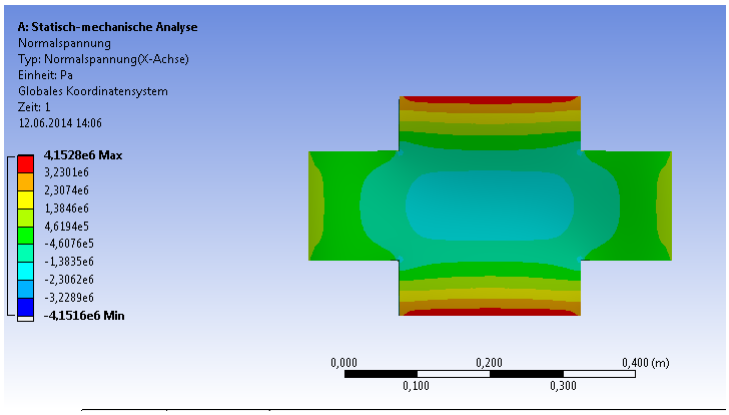

Figure 11-6: Normal stress of the verification model

equilibrium is reached. Furthermore a lot of damage at the impact point is expected due to the high velocity and force peaks.

Dynamic impact model

As the assumption of a constant deceleration of the blade induces big errors, a dynamic model was generated as well. This model was created using the explicit dynamics workbench of ANSYS. The simulation modelled the impact of a blade with an initial velocity onto a plate clamped rigidly on all edges. The results of the simulation are shown in figure 11-7.

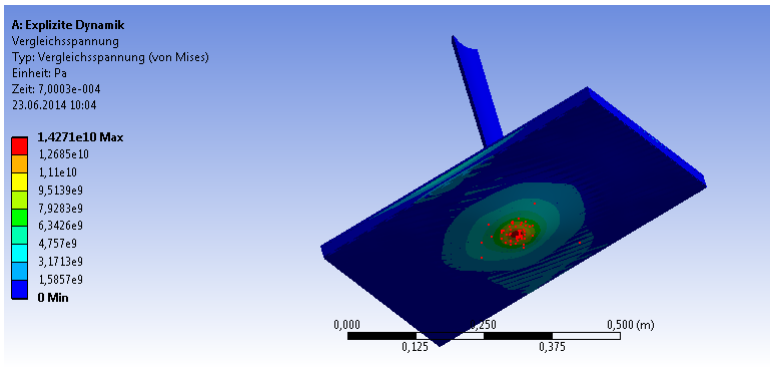

Figure 11-7: Results of the dynamic model

This model showed a combination of high modulus Carbon fibre composites in ±90deg on the outside and inside and Kevlar fibre composites in ±45deg in the middle as most suitable material combination. This design comes with a weight increase of 149kg as compared to the not reinforced design.

Verification of the dynamic model

To verify the finite element model a grid refinement study was conducted to show that the solution is independent of the chosen grid size. This was done by running three simulations

that only differed in the chosen grid size. Further verification is very difficult as analytical solutions for intermediate impact speeds with high impact energies do not exist. Furthermore there are only very few solutions available that cover the entire failure range of composites. Therefore a complete verification is not possible. However an option using the analytical code of the phd candidate in computational mechanics at TU Delft Fardin Esrail was identified. This code is not able to determine penetration and is intended for low impact velocities and energies only. By checking for a complete fibre failure in the analytical solution, penetration can be predicted. In any case a validation is required to validate the numerical model and the comparability of analytical and numerical solution.

Validation of the dynamic model

To validate the dynamic model, an experiment is required. In this experiment a panel with the same dimensions and same material as in the model is rigidly clamped on all edges. A similar open rotor blade is than shot onto the panel with a speed of 100m/s. The deformation over time can be watched by high speed cameras and the damage after the test can be assessed. The results are compared to the results of the numerical simulation.

Reinforcement layout

The empennage reinforcements were designed using the dynamic model. As material, Kevlar composites, Dyneema composites and Glare were investigated. Kevlar composites were chosen as empennage material, as the Dyneema was not suitable under the given temperature conditions. Furthermore the empennage section is not load critical. Following from this the higher load bearing capabilities of Glare were not required and thus a Glare solution would result in a heavier construction. Different combinations of thickness, frame spacing and stringer spacing and their impact to the stress distribution in the static model were investigated. This lead to the optimal panel size. The stringer spacing is 400mm. the frame spacing is 600mm. The panels are made from two layers of 5mm thick carbon fibre on the inside and outside and a 20 mm thick Kevlar core in $\pm$ 45° direction in the middle. This design results in an additional weight of 149 kg.

11-8 Conclusion

In this chapter the design of the fuselage is described. Through the use of composite materials a weight reduction of 24% can be achieved. The passenger capacity was increased by 3 through layout rearrangements and the safety measures were adjusted accordingly. Through the back shift of the wing, the cargo distribution changed, however the total available volume stayed constant. Also a safe method for integrating the LNG fuel lines into the fuselage has been identified. Furthermore the empennage section was adjusted to house the open rotor engine and the H-tail. This required a new aft fuselage layout as fuel system components have to be stored in the aft fuselage. Furthermore the aft fuselage was reinforced by Kevlar and an additional layer of carbon fibre composites to be able to protect the enclosed systems from a possible blade impact.

Chapter 12

ATA26/49/70 - Powerplant System

The propulsion subsystem of an aircraft plays a major role in the amount of emissions produced. In order to reduce the emissions of the aircraft, engine manufacturers continuously come up with innovative solutions and new designs on reducing the specific fuel consumption ($SFC = \frac{\dot{m}_{fuel}}{F_T}$ (F_T =Thrust)). Currently, High-bypass Turbofan (HBT) firmly holds its place in modern engine technology, but this will likely change in the near future as open rotor engines are predicted to become the new propulsion technology.

The outline of this chapter is as follows:

1. Study of A320-200 engines
2. Study of (counter rotating) open rotors
3. Analysis of turboprop engine
4. Development of counter rotating open rotor
5. Estimation of mass of counter rotating open rotor
6. Evaluation of performance of counter rotating open rotor
7. Design verification

12-1 High-bypass Turbofan

The two engine options, both HBT, of the A320 are studied in order to obtain a clear picture of their design and performance characteristics. The benefit of HBT comes from the bypassing airstream providing improvements in efficiency as it increases thrust and decreases the noise level. A schematic of a HBT can be seen in figure 12-1. The amount of bypassed air is represented by the bypass ratio (BPR).

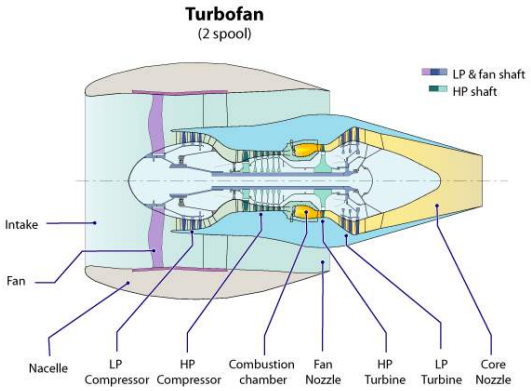

Figure 12-1: Schematic of a Turbofan [124]

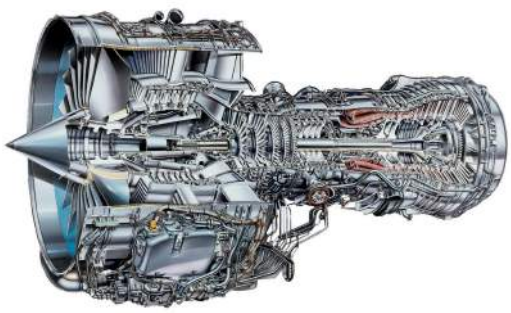

Figure 12-2: V2500 Engine cutaway [93]

Currently, the A320 is available in two engine options, the HBT V2500-A5 by international aero engines (a cutaway is displayed in figure 12-2) or the HBT CFM56-5B by CFM international.

In table 12-1 the parameters for the engine options of the A320 are listed.

Table 12-1: Engine parameters of HBT of the current A320 and the A320neo

	V2500 [93]	CFM56-5B [32]
Diameter fan tip [m]	1.6	1.73
Length [m]	3.2	2.6
Dry mass [kg]	[-]	2381
Takeoff thrust [kN]	111	120
Cruise thrust [kN]	[-]	22
Bypass ratio	5.4	5.7
Overall pressure ratio	29.8	32.6
Thrust range [kN]	98-146	98-146

12-2 Open Rotor Engine Characteristics

Open rotors (as depicted in figure 12-3) are engines that are not enclosed by a nacelle around the rotors (only around the engine core), hence the engine will have a decreased drag penalty compared to turbofan engines. The engine fan blades are also not limited by the nacelle and can be made much larger, increasing the bypass ratio drastically. This allows open rotor engines the capability to deliver significant amounts of environmental improvement for single aisle aircraft.

There are two types of configurations for open rotors, namely puller and pusher. The two configurations can either have a single propeller or a pair of contra-rotating propellers. The advantage of using contra-rotating open rotors (CROR) is an increase in effective engine thrust, since the swirl of air origin from the first set of blades is corrected by the second set. As a result, the diameter of the propellers can be reduced, thus the tip speed compared to a single propeller and hence the noise generated by the engine. However, there is still noise generated due to the interaction of the blade rows. Another drawback of using a pair of blades is the added complexity to the design and weight.

The propellers can be driven directly or by a reduction gearbox. But a geared engine will be more complex and heavier, hence its maintenance requirements will be higher compared to a direct driven engine. However, a direct driven engine will pose a performance penalty.

Decision for CROR

In this subsection, the reasoning for using a geared CROR is presented. Advantages and disadvantages are listed in table 12-2.

The consequences of the disadvantages has to be analysed. The limitation on speed has been evaluated in chapter 8. Next, certification should be feasible by 2025. Currently, propeller

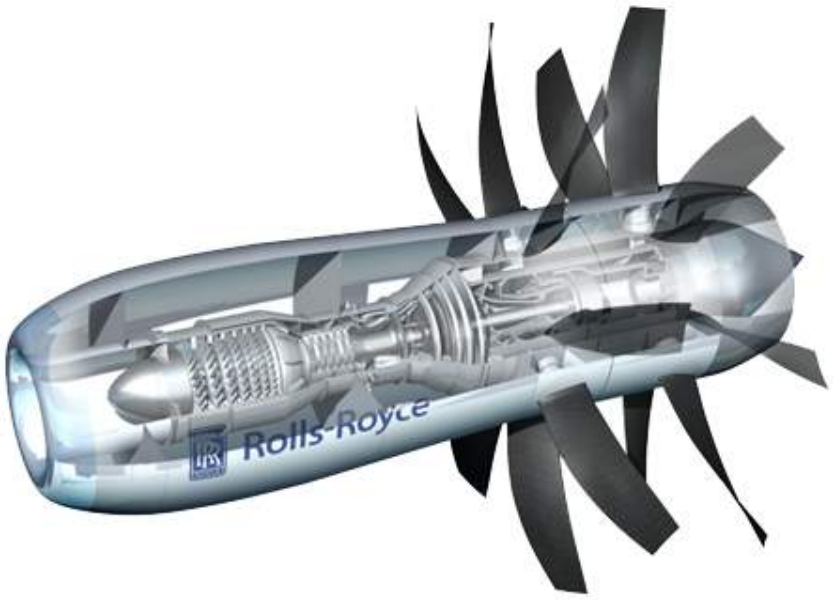

Figure 12-3: Open rotor jet engine design by Rolls Royce

Table 12-2: Advantages and disadvantages of an CROR

Advantages	Disadvantages
- 25-30 % predicted reduction in fuel consumption relative to existing single aisle aircraft [112] - Decrease in drag induced by the nacelle - Possible higher overall efficiency compared to turbofans and propeller engines - Reduction in NOx emissions	- The optimum Mach number is limited to 0.73, hence the open rotor will not be suitable for long haul flights - Meeting noise compliance poses a challenge - Certification is an issue due to blade containment complications

aircraft are operating successfully, dealing with the same issues of engine blade release and noise, and hence a solution should be feasible. In order to reduce the noise, the engine is surrounded by the upper part of the H-tail and placed at the rear fuselage, reducing passenger and ground noise levels. Therefore, the use of a geared CROR for the new aircraft is concluded to be the best option that helps achieve the emission goals.

Current Manufacturers

At present, open rotor engines are being developed by a few leading engine manufactures such as Rolls Royce, General Electric (GE) and Snecma [121]. Therefore, in 2025 airlines will most likely at minimum be able to choose between these three manufactures. The open rotor being developed by Rolls Royce, as seen in figure 12-3, was initiated by the 'clean sky' program. Rolls Royce claims that its open rotor will be an ideal replacement engine for single aisle aircraft and it is likely to be in service in 2025 (A320LNG-REQ-ATA26-01). Furthermore, GE and Snecma are working towards delivering an open rotor to the market in 2030 [121].

Rationale: Pusher Configuration Use

Since the centre of gravity of the aircraft is in front of the engines, a pusher configuration is chosen as it improves both longitudinal and directional stability [100], while the puller produces a destabilising effect. Furthermore, having propellers at the rear of the open rotor engine will reduce the noise transmitted to the cabin compared to a puller configuration.

Benefit of Contra-Rotating Open Rotors

A study conducted by DLR [103] states that CROR are better than single rotating blades in terms of both propulsive efficiency and fuel consumption. Due to the swirl free exit of the flow, the overall propulsive efficiency increases by 5 percent compared to single rotating blades [103] at its optimum Mach number of 0.73 for fuel efficiency [103].

The overall propulsive efficiency, η_{net}, is the product of the thermodynamic efficiency η_{th} and the propulsive efficiency η_{prop}. Due to the increase in exit velocity, the η_{prop} decreases and hence for a single blade set the decrease is more due to the influence of the swirl angle, γ. Therefore, according to [103] an optimum η_{net} can be achieved by having a zero γ, which can be obtained by introducing contra-rotating blades.

12-3 Development of CROR

In this section the CROR development procedure is explained.

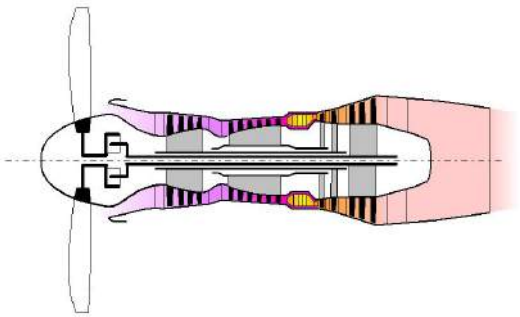

Figure 12-4: Geared Three Spool Turboprop by GasTurb

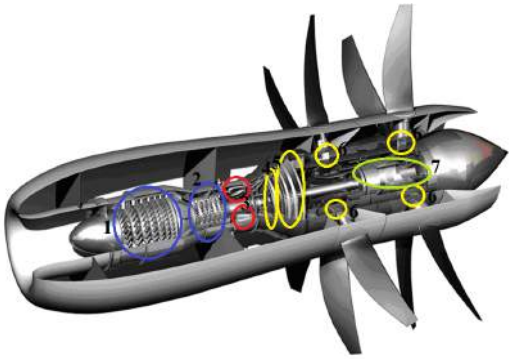

Figure 12-5: CROR structure [112]

The design of the CROR is based on the TP400, currently used on the A400M, a military cargo aircraft [11] and on the technical paper from *Chalmers University of Technology* [74]. The internal structure is copied from the TP400 and performance values for a geared three spool turboprop using TP400 structure and some dimensions of the new CROR are determined by using GastTurb [1]. A schematic of a geared three spool turboprop, such as the TP400, is

[1] GasTurb is a gas turbine simulation software tool which determine the performance of different engines

depicted in figure 12-4. Moreover, input values inserted only into Gasturb are listed in table 12-3.

After the performance was estimated with GasTurb, a Matlab [2] script was written. Some results obtained with GasTurb are inputs for the script (they are marked with * in table 12-5). The script finally outputs the specific fuel consumption (SFC) and thrust of the CROR. Inputs to GasTurb and Matlab are listed in table 12-4. Inputs for Matlab only are listed in table 12-5. The data for the efficiency estimation was obtained in an interview with Dr. Arvind G. Rao [3] hence it is considered reliable.

Table 12-3: Inputs to GasTurb only

Engine characteristics	
Propeller diameter [21]	$4.2m$
Turbine stages (HPT/IPT/LPT)	1/1/3
Pressure ratio (IPC/HPC)	3.6/7
Propeller efficiency	0.55
Cruise speed (Mach)	0.73

Table 12-4: Inputs to GasTurb and Matlab

Engine characteristics	
Intake isentropic efficiency	0.92
Compressor pressure ratio CPR	25
Isentropic efficiency	0.91
Mechanical efficiency	0.99
Main combustor efficiency	0.98
Combustion chamber pressure ratio CCPR	0.96
Turbine isentropic efficiency	0.92
Nozzle efficiency	0.98
Exit pressure ratio at cruise	1.1
Temperature at sea level	$288K$
Pressure at sea level	$101325Pa$
LHV kerosene	$43MJ/kg$

Apart from the values listed, it has to be mentioned, that the length of the engine is $3.5m$.

12-4 Comparison to A320-200 Engines

In this section, the performance of the A320-200 HBT is compared to the CROR. In order to determine realistic values for the A320-200 a software called PIANOx[4] was used.

The comparison between the HBT of the A320-200 and the CROR of the A320LNG is executed in table 12-6.

[2]Matlab is a software where different scripts can be programmed and executed

[3]Dr. Rao is an assistant professor at the department of Flight Performance & Propulsion at TU Delft and is also the principle tutor for this thesis project

[4]PIANO-X is a professional tool used for the analysis of commercial aircraft performance studies

Table 12-5: Inputs to Matlab only

Engine characteristics	
Rotor efficiency	0.8
LHV LNG	$48.632 MJ/kg$
Diameter of engine inlet*	$0.445m$
Engine inlet area*	$0.16m^2$
Engine nozzle area*	$0.59646m^2$
BPR*	89
Fuel flow of LNG and kerosene [kg/s]	0.14 : 0.01 : 0.8
Freestream Mach number	0.5 : 0.01 : 0.8

Table 12-6: Use of kerosene during cruise (Mach 0.73)

Software	**PIANOx**		**Matlab**	
Aircraft + Engine	A320-200 HBT		A320LNG CROR	
Altitude [km]	10.973	8.992	11	9
Thrust [kN]	38.4	39.7	43.6	49.20
Fuel Flow [kg/s]	0.65	0.7	0.56	0.64
SFC [g/(kN*s)]	16.9	17.6	12.6	13
SFC improve in % of A320-200	0	0	25.4	26.1

Summarizing, an improvement in SFC of about 25 % was achieved. This was judged as a realistic value hence, emission calculations can be based on the SFC reduction further on.

Performance Range of CROR

The performance variance depends on the airspeed and the fuel flow. For different fuel flows the engine thrust is plotted (see figure 12-6 and 12-7). Moreover, the aircraft drag at 9 and 11 km cruise altitude depending on airspeed is determined. The corresponding drag curve is plotted in figures 12-8 and 12-9. Additionally, these figures contain the thrust delivered by the two CROR for a certain fuel flow, which equals the drag at Mach 0.73.

12-5 CROR Engine Mass

In this section, the mass breakdown is determined, i.e. the weight and the centre of gravity position of the engine. The mass breakdown is listed in table 12-7. Verified by [74], the total mass is determined to be 2980 kg.

Result

In conclusion, engine characteristics of the A320-200 are compared to the newly designed A320LNG. The most impacting changes comparing the two are:

- 25% increase in engine weight compared to CFM56-5B

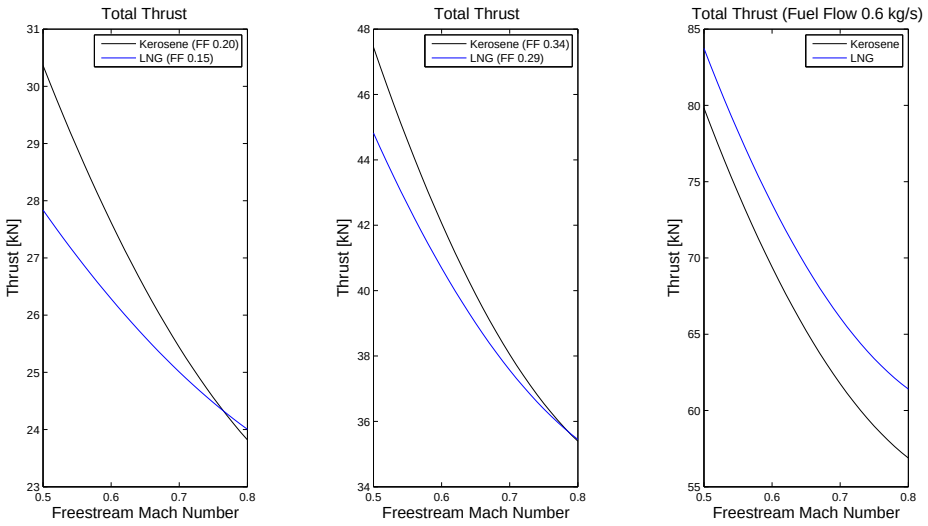

Figure 12-6: Total Thrust of one engine operating on either LNG or Kerosene for different fuel flows at 9 km

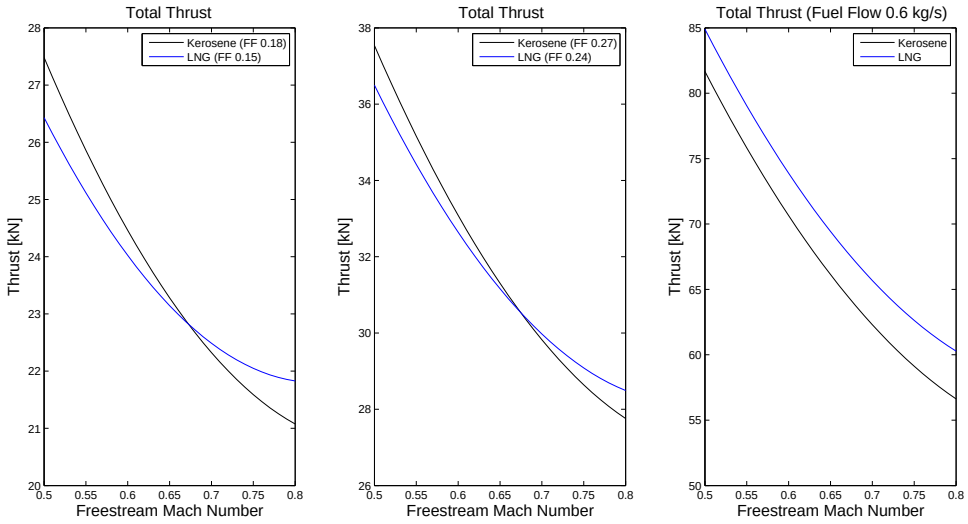

Figure 12-7: Total Thrust of one engine operating on either LNG or Kerosene for different fuel flows at 11 km

- C_{D_0} of 0.02341 instead of 0.01921 (LNG tanks)
  Drag increase by 15-25%
  L/D decrease from 17.26 to 15.35 (12%)
- Specific fuel consumption reduced by approximately 25%

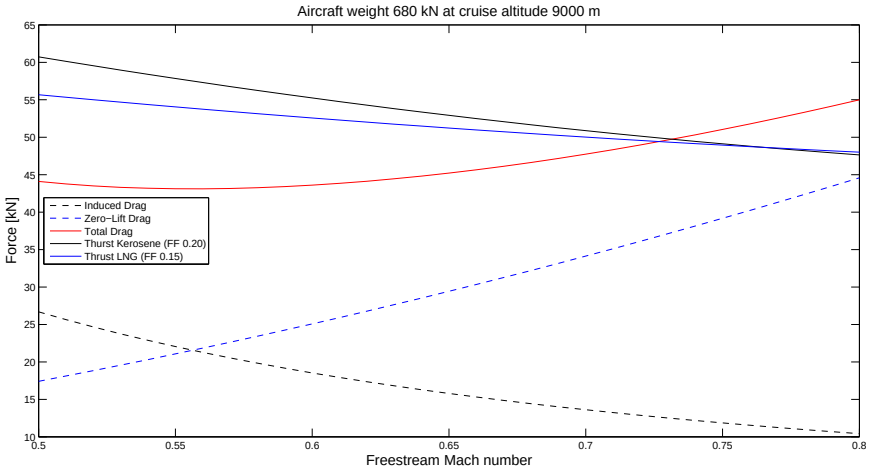

Figure 12-8: Drag and Thrust of the A320LNG (Mass approx. 69 tonnes) at cruise (9 km)

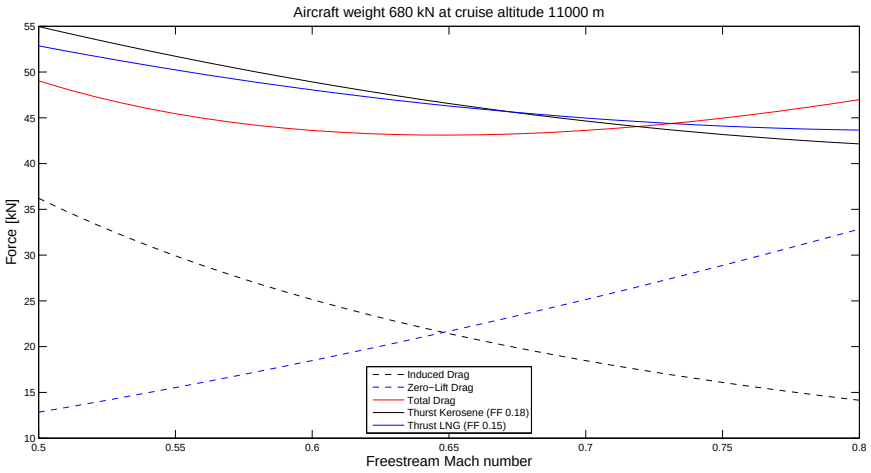

Figure 12-9: Drag and Thrust of the A320LNG (Mass approx. 69 tonnes) at cruise (11 km)

Table 12-7: Weight breakdown of new Open rotor

Components	Mass [kg]	CG from front [m]	CG as fraction
Engine inlet and LPC + HPC	280	0.875	0.25
Combustion chamber and HPT	150	1.7	0.49
LPT, nozzle, exhaust cone	500	3.2	0.91
Gearbox and shafts	450	1.8	0.51
Propeller and nacelle	1500	2.3	0.66
Accessories, bearings	100	1.75	0.5
Total	2980	2.193	0.63

12-6 Performance Risk and Certification Requirements

This section outlines the risk of operation and presents key certification requirements.

CROR Noise

This section outlines the aeroacoustic noise generated by CROR engines and discusses about the certification of aeroengines in general.

Tonal vs broadband noise

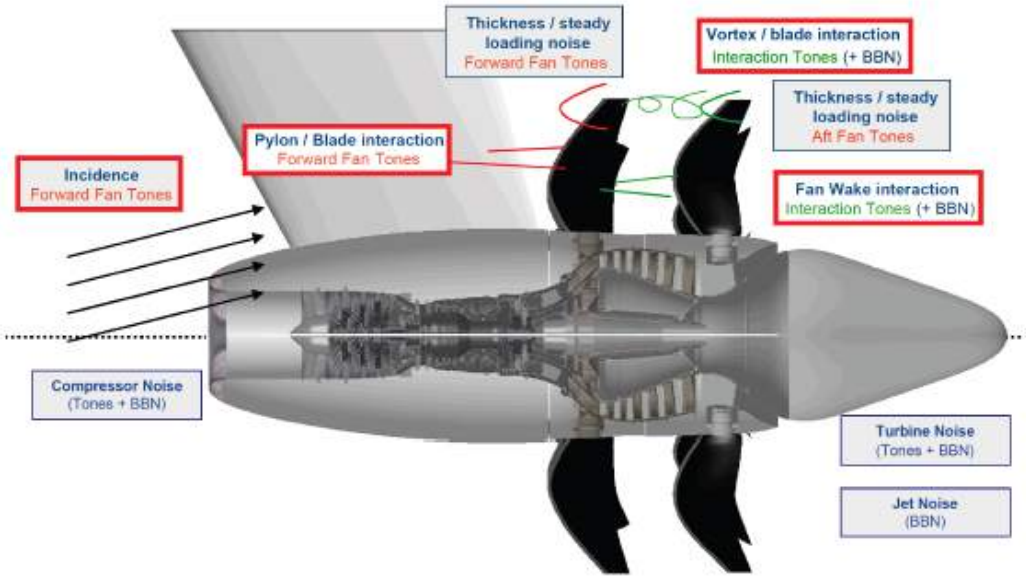

Figure 12-10: Overview of CROR noise sources reproduced from [25]

CROR engines are rather complex aeroacoustic systems which emit a variety of tonal and broadband noise sources [25]. From figure 12-10 it can be seen that open rotor noise can be divided into rotor noise and other noise sources. CROR engines generate much higher noise than a single rotating open rotor and with increase in rotor spacing, this is due to the interaction of viscous wakes and tip-vortex shed (figure 12-11) from the front and rear rotors [25]. Therefore, research is currently under way to investigate the aeroacoustic of CROR engines as it is still not completely understood. The tonal noise is caused by the two sets of rotors, aeroacoustic and aerodynamic interaction between the rotors and the interaction between the rotors and the pylon, horizontal tail and fuselage [15], [80]. This same interaction produces broadband noise when flow turbulence is involved in the interaction [15], [71].

Open Rotor Noise Certification

When open rotor engines were first developed 25 years ago, noise was the main concern that halted the program. But now with technological advancements, both Airbus and Snecma believe that by 2030 open rotor engines will be able to meet the International Civil Aviation Organisation (ICAO) requirements [121]. Snecma is currently working on the optimization of blade performance to decrease noise [121]. Furthermore, using a pusher configuration, the

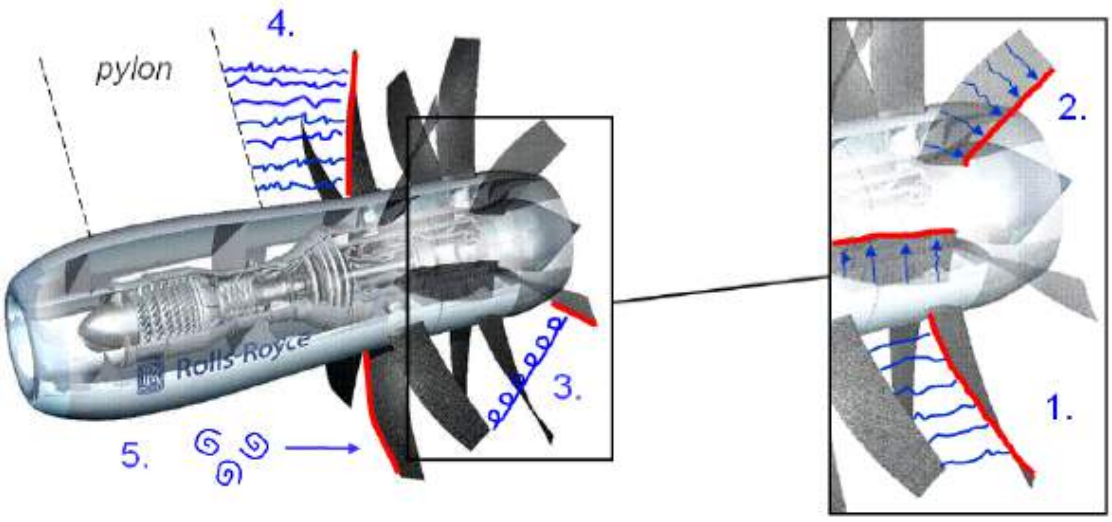

Figure 12-11: Sources of broadband noise in an installed CROR [25]

cabin noise transmission is reduced compared to a puller configuration. In addition, by opting for a H-tail arrangement noise propagation to the ground will be blocked.

Aircraft acoustic certification involves the measurements of noise levels at three reference points in terms of Effective Perceived Noise Level (EPNL) in dB, according to the ICAO chapter 14 [42]. Furthermore, General Electrics (GE) states that CROR engines will be able to meet the noise goal of 15-17 EPNdB cumulative noise margin set by the Federal Aviation Administration [48] which adheres to ICAO chapter 14. The sum of the noise at each point dictates the cumulative noise levels. The three reference points are given below and depicted in figure 12-12:

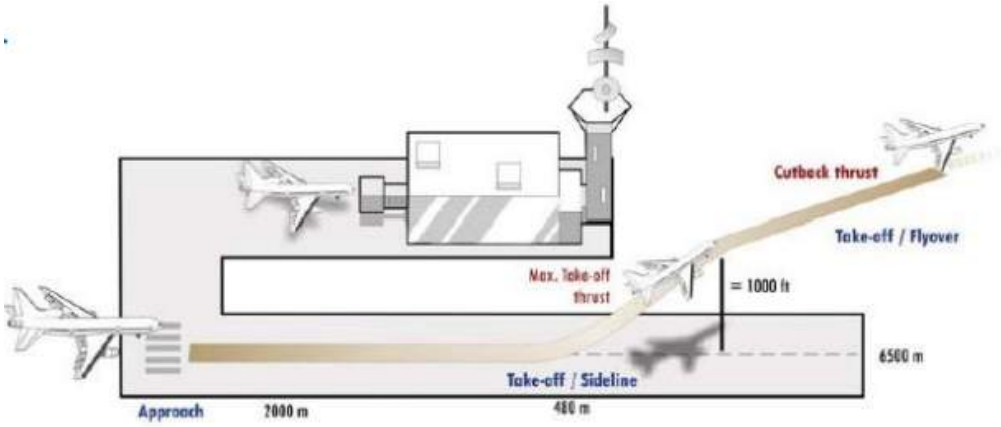

Figure 12-12: Illustration of noise reference points [42]

1. **Fly over:** From the moment the brakes are released until a distance of $6500m$ on the take-off flight path
2. **Takeoff:** the highest noise measurement is recorded at any point after $450m$ on the

runway
3. **Approach:** $2000m$ above the runway threshold during approach

Blade Containment Certification Requirements

Blade containment is a major certification requirement concerning the safety of the aircraft. The same philosophy can be employed by propeller engines i.e. by demonstrating the probability of a blade being released is one failure per 100 million flying hours. Therefore, the open-rotor will be designed such that it meets this safety requirement. Also, if a blade release occurs, the fuselage area close to the engine must be sufficiently reinforced in order to prevent hydraulic and electrical lines being demolished by blade release. This issue can also be tackled by re-positioning the aircraft systems.

Combustion chamber, heat exchanger, switch mechanism, position, weight prediction, engine control, (gear design), APU, Engine type, Engine start up.

12-7 Engine Performance Risk Map

The risk map seen in figure 12-13 provides an overall risk assessment for the engine performance and aids in identifying suitable risk mitigation methods further on in the design process. The risk elements are;

1. Bird strike
2. Blade release
3. Water ingestion
4. Engine rip out at take-off
5. Blade failure
6. Debris ingestion
7. Flame out in combustion chamber
8. High engine oil temperature
9. Abnormal engine vibration

The first three elements have been treated previously. Engine rip out during take-off (4) may occur due to excessive torque, blade failure (5) due to blade material yielding. It might be a result of blade vibrations. Furthermore, failure of the blade may occur due to initiation of cracks caused by high temperatures or stress concentration. Foreign object ingestion (6) is possible if the runway contains debris which may be sucked into the engine during take-off or landing. Flame extinction in combustion chamber (7) may be caused if the CROR experiences a fuel or oxygen starvation [77]. High engine oil temperature (8) is a consequence if the engine is not cooled properly. High engine oil temperature will deposit in the engine which may degrade the performance of the engine. Finally, abnormal engine vibration (9) may occur if fan blades contain manufacturing flaws.

12-8 Auxiliary Power Unit (APU)

As the name already states, the APU is an alternative power system, that supplies the required power to the engine for start up. In addition, the APU delivers pneumatic and electrical

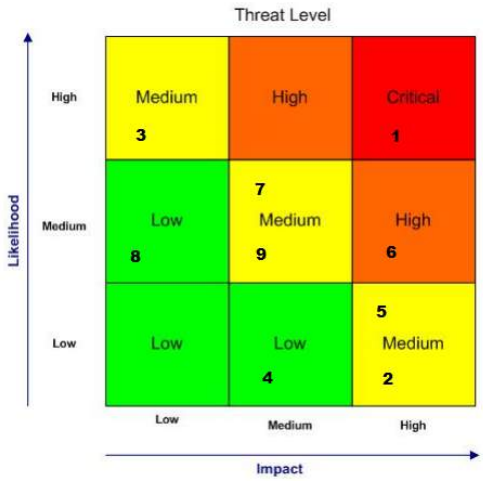

Figure 12-13: Engine performance risk map (Risk = impact × likelihood)

power. Current APUs stem from gas turbines and operate at a 15 percent load cycle while also contributing to nearly 20 percent of ground based emissions [70]. Furthermore, the study conducted by DLR [70] states that APUs cause 50 percent of the maintenance delays which accounts to 12 % of the maintenance, thereby subsequently increasing DOC. Therefore, replacing the current APUs with improved and more efficient APUs is crucial for achieving the emission targets. The current APU for the A320 is a twin-axial turbine APU that provides a maximum shaft output of $126.7kW$ and has a dry mass of $140kg$ [67].

It can be assumed, that by 2030 the technology of APU will improve and thus will the efficiency. Hence, more environmental friendly APUs will exist compared to today's technology. Moreover, it is likely, that the mass will decrease by implementation of lightweight materials.

12-9 CROR Blade Release Impact on Fuselage Structure

In order to assess the impact of a blade release an analysis on the blade dynamics is done and a trajectory is obtained at its cruise speed. The blades tip is 2.1 m apart from the engine centre line, and the blades are rotating at a maximum speed of 500 rpm. The released blade will have a tangential trajectory which is determined by its initial conditions. However, since the clearance distance of the blades to the fuselage will be in the order of 0.25 m the trajectory will be assumed to be straight. At the moment of release, the blade will have a tip speed of 110 m/s (point A in figure 12-14) and a rotational speed of 52.36 rad/s. Considering the distance between the fuselage and the blade, the velocity will be constant. After a discussion with Dr. Derek Gransden [5] the worst possible scenario of impact of the blade will be if the blade pierces through the structure with point A. The piercing of the blade will cause the most amount of plastic deformation to the structure hence being the worst case scenario. Furthermore, the blade was modelled as a rigid rectangular homogeneous beam while assuming a blade mass

[5]Dr. Derek Gransden is a post-doctorate researcher at TU Delft. Currently he is working on aircraft crash simulations and previously worked on helicopter rotor dynamics.

of 5 kg. This results in kinetic energy of 40.32 kJ at impact. Knowing the impact energy, the material of the structure will be chosen. In addition, in the event of a blade out, there will a large imbalance in mass which alters the moment of inertia of the rotor causing an asymmetric rotation of the remaining blades. However, this will only have a large effect if there are multiple blade outs since each disk contains a minimum of 10 blades.

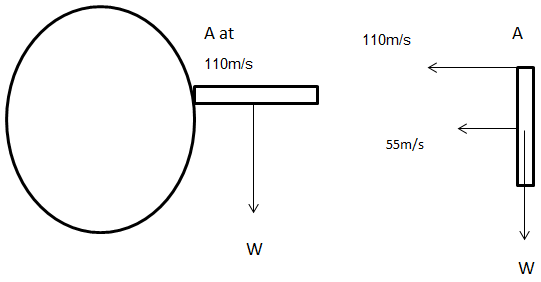

Figure 12-14: Exaggerated diagram of a blade impacting the fuselage

12-10 Low-velocity Impact on CROR Engine

Low-velocity impact from foreign object such as bird strikes on the engine can lead to severe damage, however finite element methods have enabled bird-proof designs. According to [96] 92 % of the bird strikes occur at landing and take-off phases. Certification regulations such as CS 25.571, 33.76 require demonstration of the structural integrity and continued thrust level of 75 percent power for birds impacts of 1.8 kg mass [96]. Assuming the velocity of impact to be the average velocity of the aircraft (78 m/s) at take off and landing. This results in 5.5 kJ of average kinetic energy in which the blades will have to resist the impact. According to Rolls-Royce [99], blades are capable of withstanding impact from foreign objects. This is achieved by using titanium alloys together with advanced processing techniques. Furthermore, certification requirements also stipulate the engine inlet to withstand a 1.8 kg bird impact without damage to critical engine components [96].

12-11 Engine Start-up Procedure

The functional flow chart shown in figure 12-15 describes the nominal procedure that needs to be taken when starting up the engines.

12-12 Engine Operations

This section elaborates on the engine operations also taking into account its dangers.

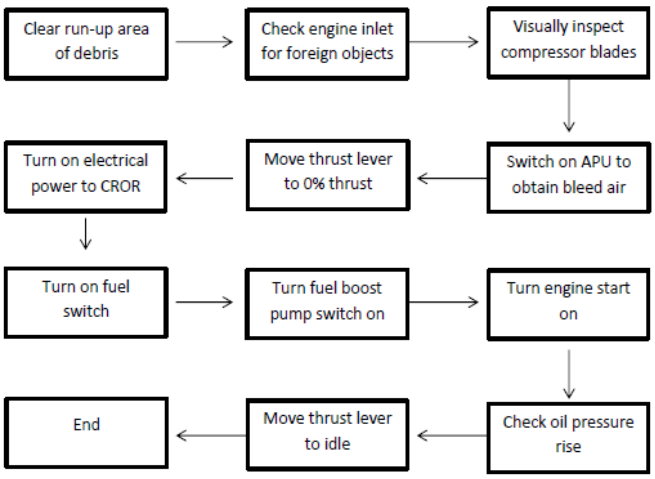

Figure 12-15: Functional flow diagram for the engine start up procedure

Fuel Transition Control

As previously stated in section 10-2 the use of LNG or kerosene in the combustion chamber will be controlled by a primary fuel switch which is connected to a fuel selector valve. This primary fuel switch will control the transition of LNG to kerosene and vice versa depending on the type of mission and altitude. Similar to a conventional aero engine, each CROR engine will have its individual thrust lever which will control the fuel flow-rate and consequently the rotor speed.

Engine Fire Protection

The CROR engine fire protection system consist of detection and extinguishing systems similar to a conventional jet engine. The detection is achieved by fire loops which are placed at potential heat sources that triggers a warning alarm if there is an abnormal temperature rise [64]. An electrically operated extinguisher will be installed at the nose cowl which will extinguish a fire. Furthermore, if a fire starts in the engine core it can be put off by shutting the engine down.

Engine Flame-out

Under adverse climatic conditions there is a risk of excessive water or ice ingestion into the gas turbine which could cause flame-out. Therefore, the open rotor ingestion system shall be capable of continuous operability. In the event of a flame-out, the engines will not generate any thrust and hence, the gas turbine shall enable flame relight.

12-13 Verification & Validation

Verification is an important process of result determination. Most mistakes can be avoided by verifying the model continuously. In this section the verification of various models is treated.

At first the Matlab model for the engine thrust, SFC and the aircraft drag is analyzed, followed by the blade model. The Validation of the model was never executed, since experiments are a common method to do so. Nevertheless, methods of possible validation in future are presented.

Engine

The final fuel flow of a given thrust output is compared to the results of GasTurb. However, a tree spool turboprop is used, whereas in Matlab a three spool CROR is simulated. Verification is done during the whole process of writing the scripts. Values are checked with literature during the process and the improved fuel consumption should be about 25 %, based on literature.

To validate the model, data of an existing open rotor has to be used, to compare the input, with the output values. Companies keep most of it a secret, and thus, a validation is hard to execute.

CROR Blade Release Model

Verification for the CROR blade release analytic model was carried out by consulting Dr. Derek Gransden. Note this model is a rather simplified model due to the used assumptions.

In order validate this model, a test can be carried out by performing a blade release test of an actual open rotor engine. Furthermore, the results from the test are likely to be within the 10 percent error limit which would have mainly been constituted by the used assumptions.

12-14 Conclusion

To briefly summarize the main concluding points from carrying out a preliminary design on the propulsion subsystem is as follows; the CROR engines provide a 25 percent increase in efficiency compared to turbofan engines thereby improving the fuel efficiency. After expert consultation with Dr. Arvind Rao, it was decided to derive design characteristics for the open rotor from the TP400 turboprop engine. Furthermore, specialized software tools such as Gasturb and Piano-X were used to aid in the design process. In addition to the design, certification with respect to noise and blade release were researched.

It was concluded that the open rotor will be able to reach its noise target limit of 15-17 EPNdB by the year 2030. Moreover, the blades were modelled using a CAD software and its dynamics were carefully analysed. From this it was concluded that in the event of a blade failure, the aft fuselage will pose as a potentially target for the impact hence, the aft fuselage was designed to withstand such blade impact. On the same token, low velocity blade impact was also analysed concluding that the engine core will be able to withstand a 1.8 kg object ingestion and also the blades will be able to withstand low-velocity impact without undergoing severe damage. Finally, operational aspects of the open rotor engine were also looked while deriving the operationally aspects from conventional turboprop engines.

Chapter 13

Preliminary Weight Estimation

The weight both affects and responds to changes in subsystem design. Given the preliminary designed subsystems, namely the fuel system, fuselage, tanks and engine, a new weight of the A320 aircraft can be estimated. This knowledge is required for wing and empennage sizing, and consequently stability analysis. The process is thus iterative, as this sizing will affect the aircraft operational empty weight (OEW), and hence an optimisation process begins.

The preliminary weight estimation is determined by taking the weights from the redesigned subsystems. For the other aircraft weights, the Torenbeek class II method [118] and statistical data of the current A320 is applied. The aircraft components are split up into the following categories:

Empty Weight Components

- Wing
- Pylons
- Empennage
- Fuselage
- Landing gear
- Powerplant
- Pods
- Fixed equipment

Operating Weight Components

- Operating items (includes flight crew)

Fuel and Payload Weight Components

- Kerosene
- LNG
- Payload (Passengers + Cargo)

By splitting up the components, each preliminary weight change can be evaluated. Table 13-1 indicates the changes in each category and gives the reasoning for these preliminary values. From this, waterfall chart 13-1 shows the individual component percentage changes to arrive from the original A320 MTOW to the new A320LNG MTOW.

Figures 13-2 and 13-3 show the weight distribution of the A320-200 and A320LNG respectively for the major weight components. The same is shown in figures 13-4 and 13-5, however here the detailed subsystem weights are given. The A320LNG component weights are also shown in table 13-2.

Table 13-1: Components and their preliminary weight change estimations

Components	**Percent Change [%]**	**Reasoning**
Wing	-4.17	Sweep angle reduced to 20 degrees. Lighter materials used.
Pylons	0	Engines exchanged with pods, roughly equivalent average weight
Empennage	+55.6	Rotor blade containment, redundancy design and larger tail
Fuselage	-10	Composite fuselage
Landing Gear	0	MTOW remains similar (same worst case scenario landing)
Powerplant	+0.58	Fuel systems & engine heavier, nacelle lighter
Pods	+100	Usage of pods
Fixed Equipment	-5.48	Largest factors: increase in pneumatic system, flight controls; decrease in hydraulics and handling equipment
Operating Items	-20.0	Improved materials and better usage
Fuel	-32.3	50/50 LNG hybrid configuration
OEW **MTOW**	-2.07 -5.16	

Table 13-2: Preliminary weights of A320LNG - Maximum Payload

Components	**Weight [kg]**
Wing	8434
Pylons	907
Empennage	1693.6
Fuselage	8044.2
Landing Gear	2275
Powerplant	7239.8
Pods	842.9
Fixed Equipment	7184.5
Empty Weight	**36621**
Operating Items	2572.0
Operating Empty Weight	**39193**
Kerosene	3984.0
LNG	3207.3
Passengers	13500
Cargo	9822.1
Maximum Takeoff Weight	**69706**

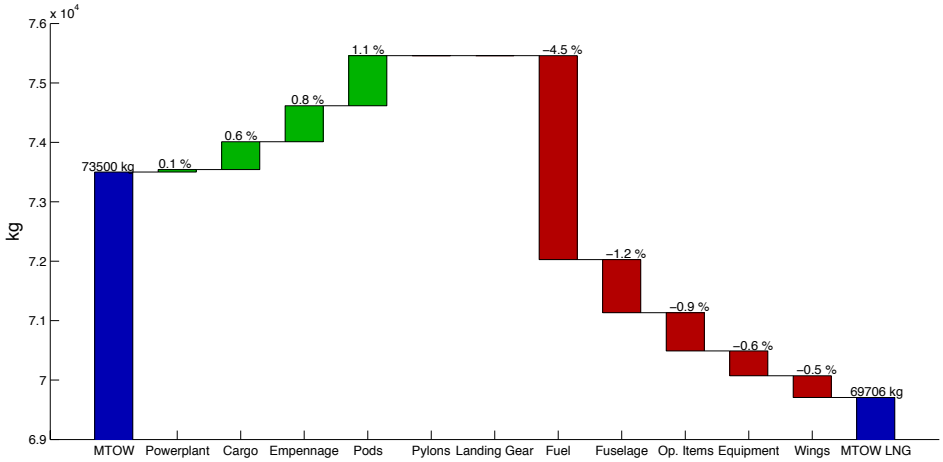

Figure 13-1: Weight changes MTOW breakdown

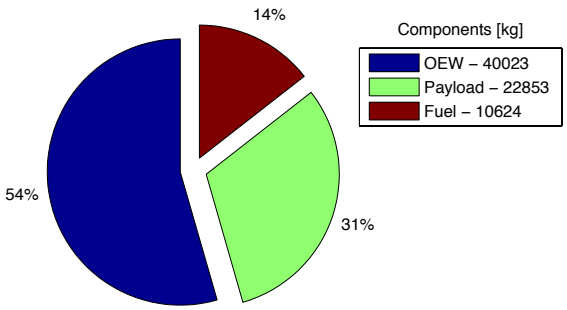

Figure 13-2: A320 major weights

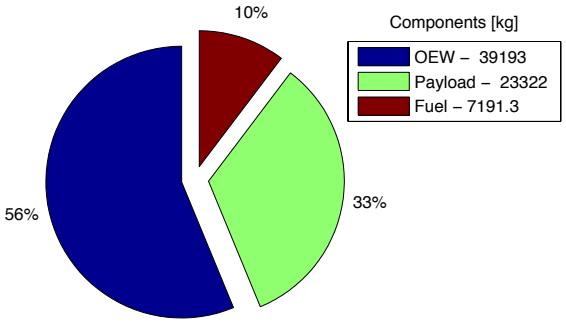

Figure 13-3: A320LNG major weights

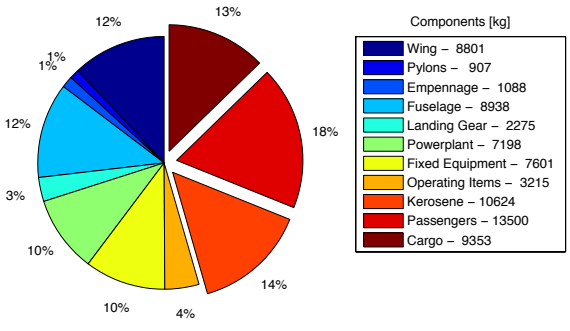

Figure 13-4: A320 weight components

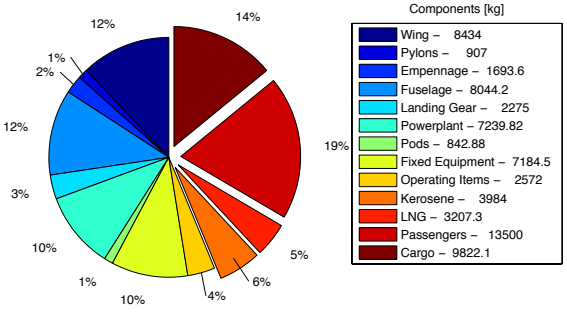

Figure 13-5: A320LNG weight components

Chapter 14

ATA57 - Wing

The design of the wing has the following sequence in this chapter; determining the wing loading and the wing area, selecting the high lift devices, choosing wing airfoils and finally designing wing geometry to satisfy flight conditions.

14-1 Wing Loading

For all aircraft a certain W/S and T/W is required to be able to preform takeoff and climb within the set requirements and for landing the required stall speed drives a certain required wing loading as well. These requirements are analysed and plotted in the same graph (see figure 14-1). The design point is shown in yellow, next to the current A320-200 W/S and T/W in green. Due to similar requirements the design point is found to coincide. From the preliminary weight analysis presented in chapter 13 the MTOW was found to be nearly the same and hence with the same W/S and T/W the required wing area will stay the same as for the current A320-200.

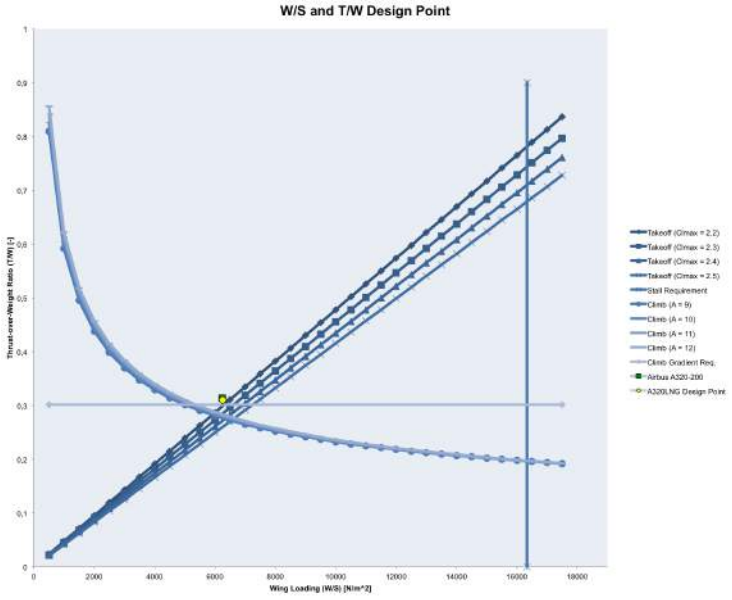

Figure 14-1: Wing loading design point

14-2 High Lift Devices (HLD)

High lift devices are used to increase the maximum lift coefficient of the wing. The design process involves the following four steps:

1. HLD location along wing span
2. Type of HLD
3. HLD chord (c_f)
4. HLD span (b_f)

Points 1 and 2 are determined by analysis of reference aircraft, whereas 3 and 4 are first estimated and then adjusted to allow for take-off (and landing). The HLD location along the wing span is taken from the current A320 wing, and hence for the trailing edge high lift device begins at the visible portion of the wing span (i.e. not within fuselage). The leading edge runs along the full wing.

For the trailing edge, Fowler flaps (see figure 14-2) are taken as they offer a significant C_l increase, by increasing not only chamber but also wing area. The industry additionally has had a tendency of moving towards simpler devices [117]. , as they offer savings in aircraft weight, maintenance costs and also reductions in noise and drag penalties. Hence, no double or triple slots are chosen. Powered leading edge slats are the choice of HLD for the leading edge of the wing. There is ongoing research into making both efficient and silent leading edge slats, called VLCS (Very Long Chord Slat) [61], which would be highly suitable for the A320LNG.

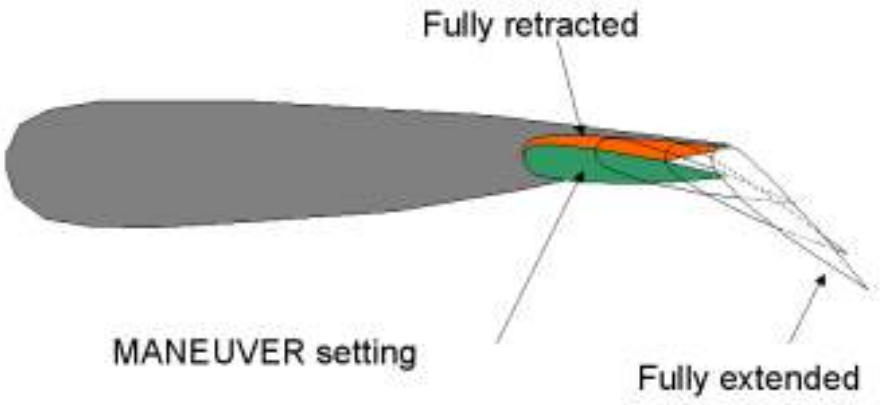

Figure 14-2: Fowler flap [38]

The chord (c_f/c) and span (b_f/b) require an initial value for further calculations in this part. Therefore looking at reference data [102] and schematics of the current A320, c_f/c is chosen to be 0.35 and b_f/b 0.6. It is decided that of the 0.35 chord ratio, 0.25 makes up the flaps and 0.1 the slats. Thereby, the Fowler flaps run 60 % of the visible wing span and have a chord ratio of 0.25. The leading edge slats run along the full visible wing span, and have a chord ratio of 0.1.

14-3 Airfoil Design

From 14-1, the surface area is found to be 122.8 m^2. Thereby the design requirements for the new wing are:

$$S = 122.8\ m^2,\ m = 69706\ kg,\ V_c = 218.2\ m/s,\ V_s = 61.43\ m/s$$

Two assumptions are made, first that if the wing is shown to be able to perform take-off, then landing is also guaranteed, and secondly the high lift devices by 2030 will generate slightly more lift than presently. Furthermore, the chord root and tip root have a first estimation based on current A320 (see appendix D).

Airfoil Design Points

The complete design of a new airfoil for the A320LNG is beyond the scope of this project. Therefore, the airfoil is selected from the NACA database and is chosen based on the below calculations. First the airfoil ideal lift coefficient has to be found.

$$\underline{\text{Aircraft Ideal Cruise Lift Coefficient}} : C_{Lc} = \frac{2 * W_{avg}}{rho * V^2 * S} = 0.4751 \quad (14\text{-}1)$$

$$\underline{\text{Wing Cruise Lift Coefficient}} : C_{Lcw} = \frac{C_{Lc}}{0.95} = 0.5001 \quad (14\text{-}2)$$

$$\underline{\text{Wing Airfoil Ideal Lift Coefficient}} : C_{li} = C_{Lcw}/0.9 = 0.5557 \quad (14\text{-}3)$$

Second, the airfoil maximum lift coefficient has to be determined.

$$\underline{\text{Aircraft Maximum Lift Coefficient}} : C_{Lmax} = 2 * W_{TO}/(rho_0 * V_s^2 * S) = 2.8 \quad (14\text{-}4)$$

$$\underline{\text{Wing Maximum Lift Coefficient}} : C_{Lmax_w} = C_{Lmax}/0.95 = 2.9474 \quad (14\text{-}5)$$

$$\underline{\text{Wing Airfoil Gross Maximum Lift Coefficient}} : C_{lmax_{gross}} = C_{Lmax_w}/0.9 = 3.2749 \quad (14\text{-}6)$$

The maximum lift coefficient of the airfoil however is largely increased by the high lift devices on the wing. Given the choice of powered slats and fowler flaps as stated in section 14-2, it was estimated that the change in C_l (dCL) is 1.3 [102]. Therefore the clean airfoil maximum lift coefficient is:

$$\underline{\text{Wing Airfoil Net Maximum Lift Coefficient}} : C_{lmax} = C_{lmax_{gross}} - dCl = 1.5049 \quad (14\text{-}7)$$

Consequently, the two design points to look for in this airfoil are:

1. Ideal lift coefficient **0.56**
2. Airfoil net lift coefficient **1.51**

Airfoil Selection

The choice of airfoil is made by looking at figure 14-3. As can be seen, the design point lies between 4 airfoils. However, given that the NACA four digit series (namely the 4418) are simpler airfoils, where the aerodynamics was modelled without taking into account phenomena such as flow separation . the decision is made to not select this one. Hence, the 63_3-618, 64_3-618 or 65_3-618 airfoil could be a possible selection. From their naming, it can already be seen that they all have a design lift coefficient of 0.6 and a maximum thickness-to-chord ratio of 18%. Their differences lie in their chord-wise position of minimum pressure.

The following criteria are considered for the airfoil selection:

- Lowest C_{m_0} for controllability

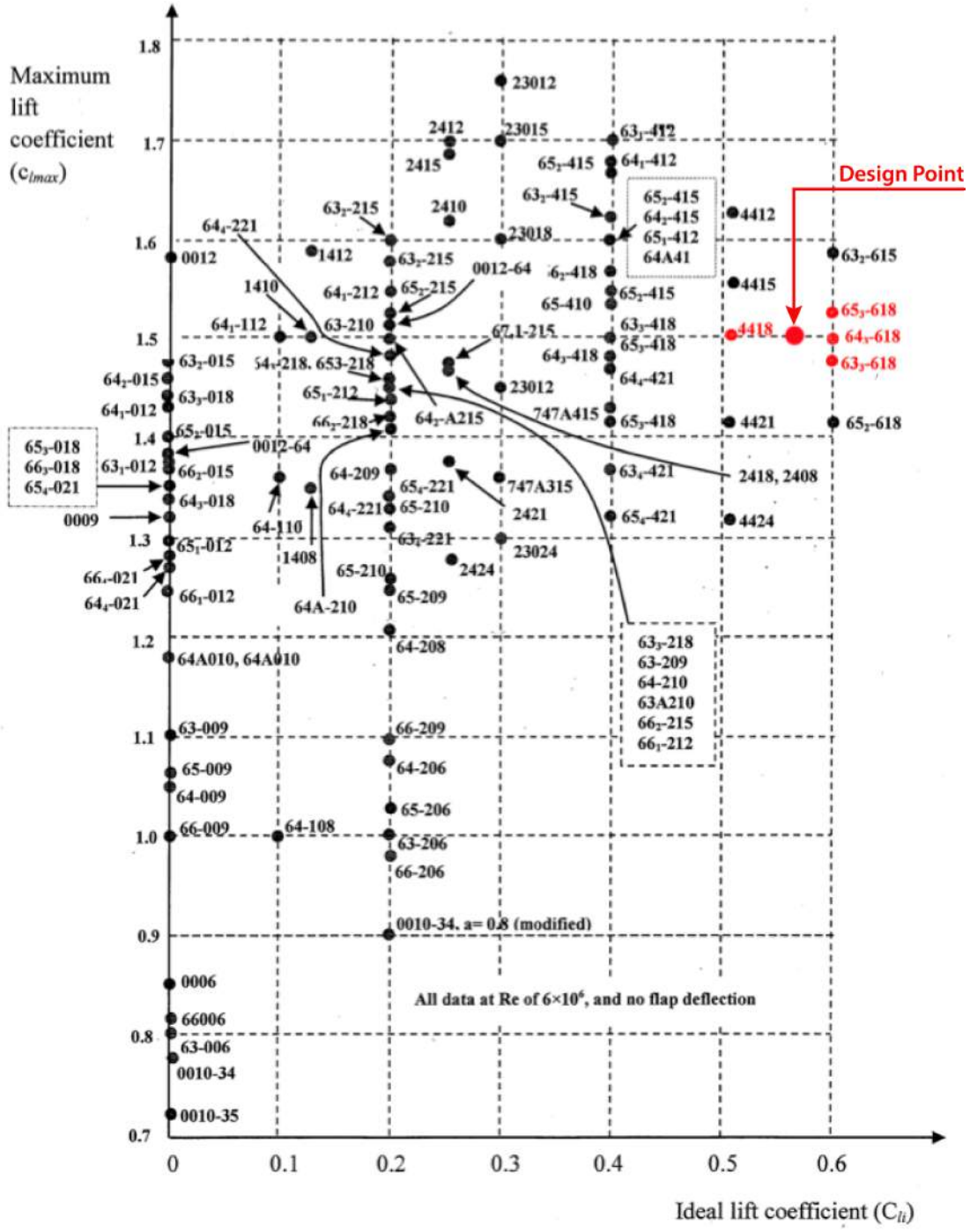

Figure 14-3: NACA airfoils - $C_{l_{max}}$ vs C_{l_i}

- Lowest $C_{d_{min}}$ for drag and maximum flight speed
- Highest a_s for minimum flight speed
- Highest C_l/C_d for aircraft endurance
- Highest M_{cr} for wing sweep

Given this criteria, numerous NACA airfoils were considered including the three listed above.

Table 14-1: NACA airfoil selections

NACA	$\mathbf{C}_{m_0}$	$\mathbf{C}_{d_{min}}$	$\boldsymbol{\alpha_s}$	$(\mathbf{C}_l/\mathbf{C}_d)_{max}$	$\mathbf{M}_{cr}$
63_2-615	-0.121	0.00646	12	171	0.697
63_3-618	-0.120	0.00709	14	169	0.671
63_4-421	-0.080	0.00727	16	157	0.672
64_3-418	-0.081	0.00676	15	180	0.696
65_3-618	-0.125	0.00685	13	200	0.677

The five best airfoil found are shown in table 14-1 and as can be seen are extremely similar in their properties. *JavaFoil* and statistical data were used to determine these values.

NACA 63_2-615 is chosen as the root airfoil, as it has the lowest $C_{d_{min}}$ and a good M_{cr}. NACA 64_3-418 is then chosen as the tip airfoil, given the same M_{cr} and low $C_{d_{min}}$, and additionally the higher stall angle. This ensures the root stalls before the tip, hence ailerons can be used for recovery procedures. Figures 14-4 and 14-5 show the airfoil geometry.

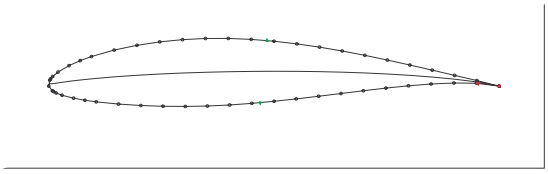

Figure 14-4: 63_2-615 airfoil geometry

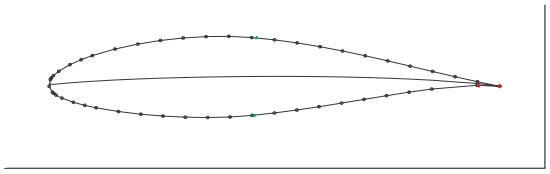

Figure 14-5: 64_3-418 airfoil geometry

14-4 Wing Design

The geometry of the wing has to be sized for the chosen airfoils and mission requirements. To do this, the wing has to satisfy both cruise and take-off requirements (base assumption that take-off ensures landing capabilities). This will ensure both efficiency and capability of the aircraft. Additionally, the wing sweep has to be determined such that Mach critical (M_{cr}) is larger than the cruise Mach, to minimise drag.

Wing sweep

The chosen cruise Mach to minimise DOC is 0.73 (see section 8). Mach critical for both the root and tip airfoil are approximately 0.696 (see table 14-1). The required sweep angle can then be calculated from equation 14-8:

$$cos(\Lambda) = \frac{0.696}{0.73} \tag{14-8}$$

From this it is found that sweep required is 17.55 degrees. To allow for minor tolerances in flight cruise speed without having sonic flow over the wing, the sweep angle is chosen to be 20 degrees.

Cruise Wing Parameters

Figures 14-6 and 14-7 indicate a preliminary incidence angle for the wing (i_w). This is displayed in the ideal lift coefficient versus section angle of attack. Hence, a first guess for i_w of the root and tip airfoils are respectively 1 and 2 degrees, or averaging it out for the whole wing, 1.5 degrees. Aspect ratio (AR) is 8.87, taper ratio (λ) is 0.277 (see appendix D) and as an initial guess the twist angle (α_t) is chosen to be -1 degree. Using this information, the wing lift distribution and wing lift coefficient (C_L) can be calculated with a Matlab program based on the lifting line theory, verified with known airfoils and aircraft [102], [68].

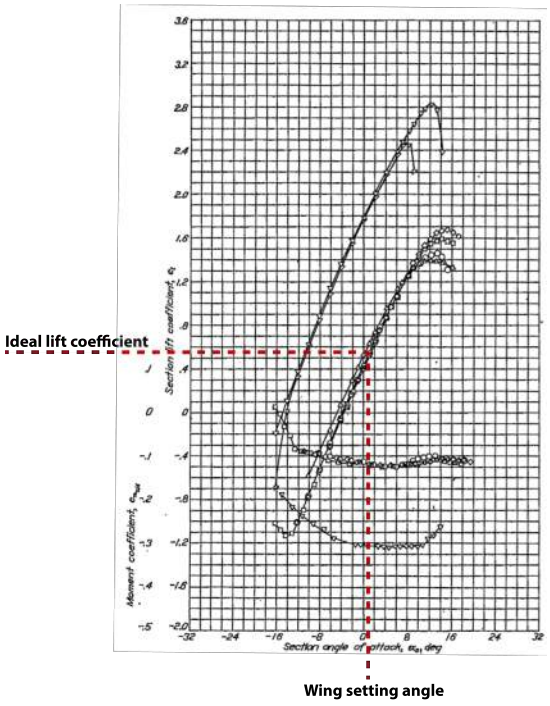

Figure 14-6: Root airfoil wing setting for C_{l_i}

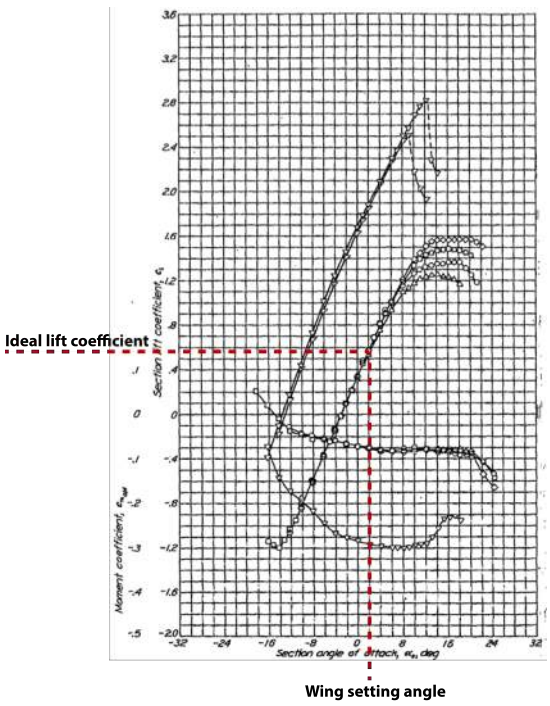

Figure 14-7: Tip airfoil wing setting for C_{l_i}

C_L is found to be 0.554 for the above set parameters. However, the required lift coefficient ($C_{L_{req}}$) is found to be 0.504. Additionally, the lift distribution loads the tips too much as shown in figure 14-8 (i.e. the distribution should be more elliptical). By adjusting the values, the following values were found to satisfy cruise requirements as well as making the lift distribution more elliptical (see figure 14-9).

$$\text{AR} = 8.87,\ \lambda = 0.277,\ \alpha_t = \text{-}4,\ i_w = 2.02$$

C_L is calculated to be 0.5045 which is equal to $C_{L_{req}}$ and therefore the wing cruise requirements have been met.

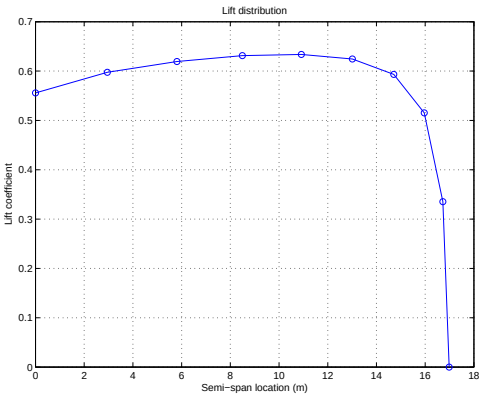

Figure 14-8: Wing cruise lift distribution - initial parameters

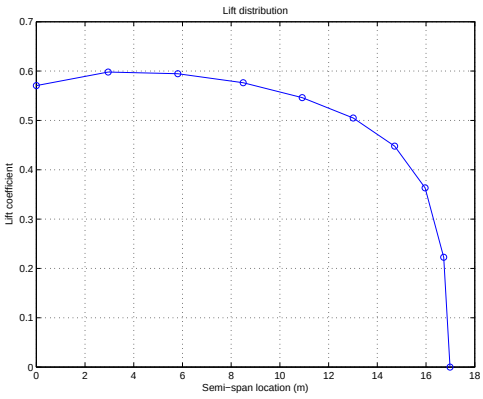

Figure 14-9: Wing cruise lift distribution - modified parameters

Take-off Wing Parameters

Take-off velocity (V_{TO}) can be approximated to be 1.2 times stall velocity (V_s). Stall velocity is calculated in equation 14-9 and thereby lift coefficient required at take-off ($C_{L_{TO,req}}$) is determined in equation 14-10.

$$V_s = \sqrt{\frac{2 * W_{TO} * 9.81}{\rho_0 * S * C_{L_{max}}}} = 56.87 m/s \tag{14-9}$$

$$C_{L_{TO,req}} = \frac{2 * W_{TO}}{\rho_0 * {V_{TO}}^2 * S} = 1.837 \tag{14-10}$$

From section 14-2, b_f/b and c_c/c are respectively 0.6 and 0.35. From table 14-1, α_s of the root airfoil is 12 degrees. Therefore, take-off angle of attack of the wing (α_{TO}) is initially assumed to be 10 degrees. Take-off lift coefficient ($C_{L_{TO}}$) is now determined with the Matlab program to be 1.9715.

Consequently, $C_{L_{TO}}$ is larger than $C_{L_{TO,req}}$. By adjusting α_{TO} and c_c/c, $C_{L_{TO}}$ becomes 1.84 which fulfils take-off lift requirements. The wing parameters are then:

$$b_f/b = 0.6,\ C_f/C = 0.3,\ \alpha_{TO} = 9°,\ i_w = 2.02°,\ \alpha_{TO,fus} = 6.98°$$

Final Wing Design

Figure 14-10 shows the designed wing geometry and important parameters. Figure 14-11 shows a rendering of the final wing. The changing airfoil from root to tip, as well as twist angle can be seen on this figure. Additional important parameters for the wing are:

$$AR = 8.87,\ \lambda = 0.277,\ S = 122.8\ m^2,\ i_w = 2.02°,\ \alpha_t = -4°$$

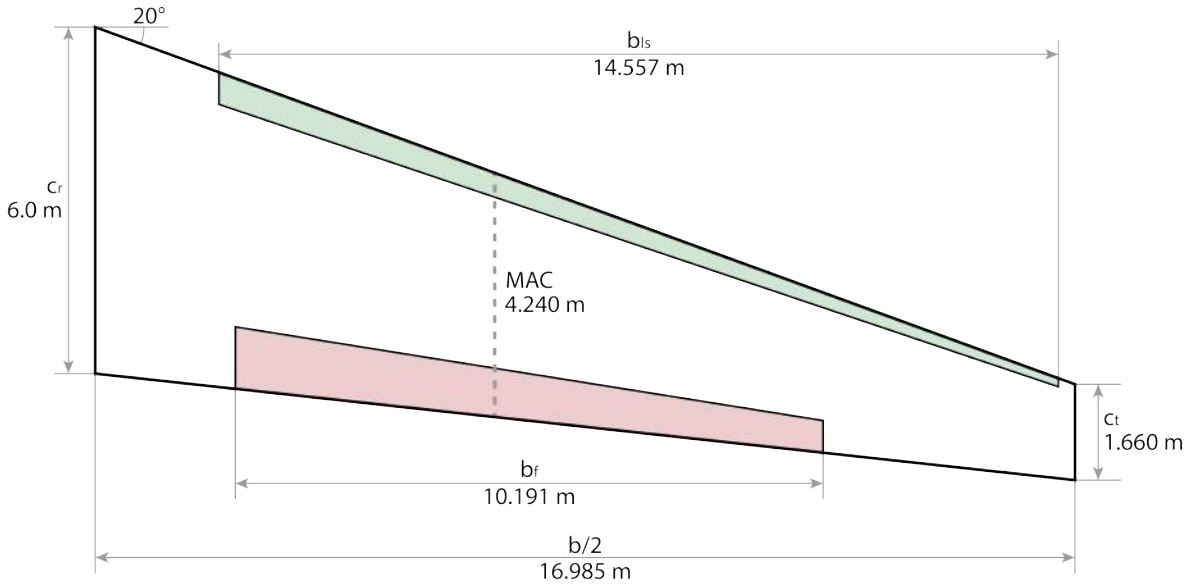

Figure 14-10: A320LNG Wing Geometry

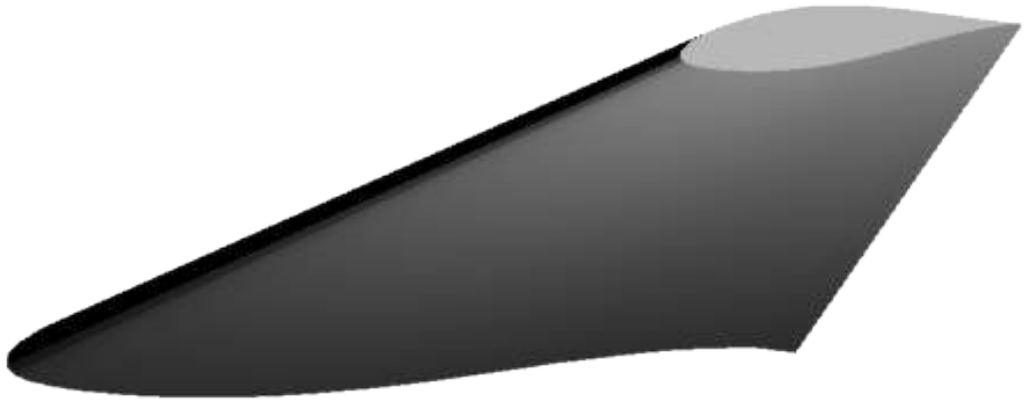

Figure 14-11: A320 wing redering

14-5 Wing Stress Distribution

It is important to simulate the stress distribution in the wing box to be able to understand where the highest stresses take place, as these areas should be able to take the internal forces. Figures 14-12 and 14-13 show the stress distribution. As can be seen, the wing box root and the pod location, have the largest stresses. The front plate and top plate stresses versus wing span are shown in figures 14-14 and 14-15. Figure 14-16 shows the wing box inside the wing.

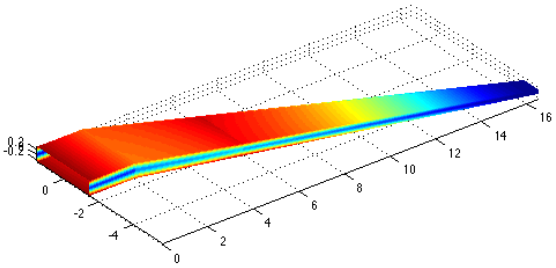

Figure 14-12: A320LNG wing stress distribution

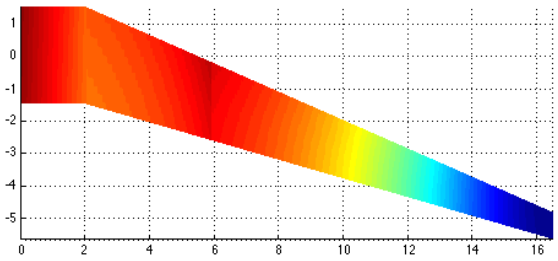

Figure 14-13: A320LNG wing stress distribution - top view

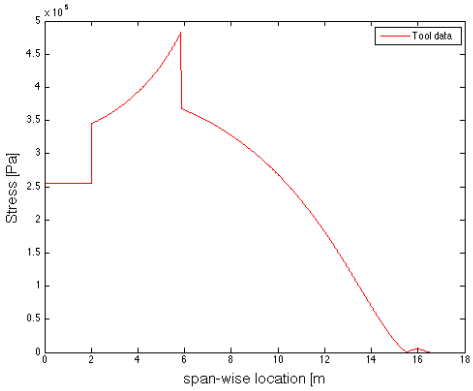

Figure 14-14: A320LNG front plate stress

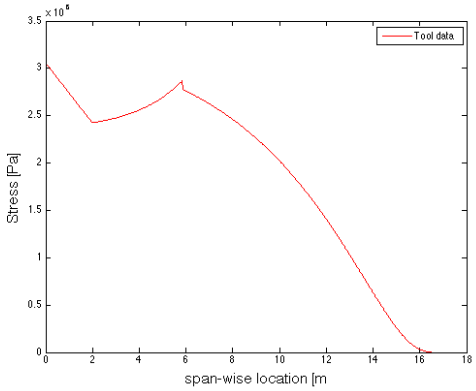

Figure 14-15: A320LNG top plate stress

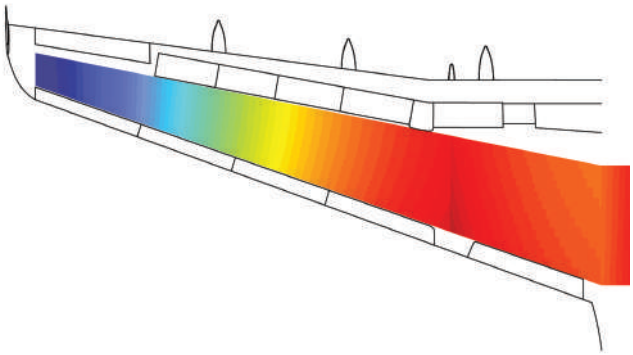

Figure 14-16: A320LNG wing box within wing

Material Choice

The choice of material for the wing box that will be able to take these stresses, whilst being light weight is carbon fibre reinforced plastic (CFRP). This material is already being used in the industry, and is what the Boeing 787 wing box is made out of [81] as well as the Airbus A350 [51].

Chapter 15

ATA55 - Stability and Control

Once the preliminary design of the fuselage, wing, fuel system and LNG tanks are computed, a stability and control analysis can be made. The aim will be to size the horizontal and vertical tail as well as finding the optimal position for the landing gears. In order to do so the weights of the components found in chapter 13 will be used to generate a load diagram followed by a centre of gravity range plot which will be used to determine the horizontal tail's surface and the wing's position to have a stable and controllable aircraft. In addition the vertical tail will be sized for the new configuration and finally the landing gear will be placed and designed.

15-1 Loading Diagrams

Due to the repositioning of the engines at the back of the aircraft in comparison to the current A320, the centre of gravity (cg) of the aircraft was shifted backwards. This changes its stability when on the ground and therefore a loading analysis has to be made to ensure its stability.

The OEW used for this analysis was taken from chapter 13. In addition it was decided to make the analysis for maximum payload which corresponds to a cargo capacity of 9353 kg that was divided as follows; a compartment of 7860.5 kg in front of the aircraft at a distance of 13.25 m from the nose and the remaining 1492.5 kg were placed in an aft compartment, at 23 m of the nose. Furthermore the fuel weight was divided in 3984 kg for kerosene and 3207 kg for LNG. Finally it was assumed that each passenger weighs 75 kg and the layout is, as mentioned in chapter 11, 3 seats on each side of the aisle.

With the above information a fore and aft shift analysis of the limits for the cg due to different loading condition was computed for the original wing position of the A320. This analysis is illustrated in figure 15-1, where the OEW, cargo, the passengers placement and the fuel weight are indicated with the cg shift caused by their loading. The different weights in kg were plotted against their cg position with respect to the leading edge of the mean aerodynamic chord, x_{LEMAC} divided by the mean aerodynamic chord, MAC.

Thereafter the wing location was shifted back in steps of 5% until 30% of its original x_{LEMAC} position. The minimal and maximal cg location for each different wing position in terms of x_{LEMAC}/l_{fus} were estimated and increased by 2%; this margin is used to allow variations in weights and to take into account movements of passengers and staff in the cabin. This cg range was plotted against the location of LEMAC and can be found in figure 15-2.

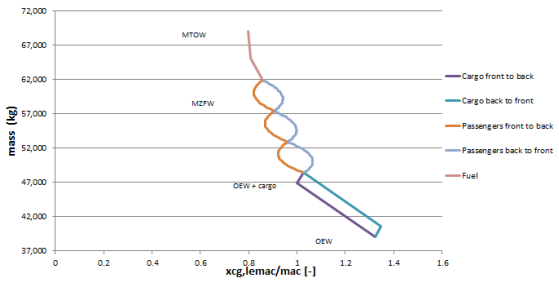

Figure 15-1: Loading diagram for original wing position

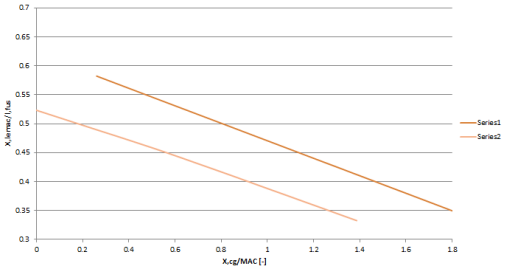

Figure 15-2: x_{LEMAC}/l_{fus} vs x_{LEMAC} over MAC

While changing the wing position, the location of the main landing gears with respect to the centre of gravity of the entire aircraft was examined, in order to make sure that it was positioned after the aircraft's cg with respect to the nose. This is crucial to maintain the aircraft in equilibrium when on the ground. It was found that when the wing is positioned 20% backwards of its original location that this requirement will be met. The landing gear's requirements for stability will be treated in more detail in the next section 15-3

15-2 Tail Design and Sizing

In this section the sizing and the dimensions of the tail will be dealt with.

Horizontal Tail

The horizontal tail will be sized taking into account the stability and controllability of the aircraft, followed by the tail's geometry.

The Sizing of the Tail

The stability and control curves will be generated and plotted along with the cg ranges to see if the aircraft satisfies the longitudinal stability and control requirements. If this is not the case the wing position and the tail size can be adjusted through an iterative process. To compute the two curves the following assumptions have been made.

- The maximum lift coefficient during landing is 2.8
- The cruise lift coefficient is 0.5
- The lift coefficient at zero angle of attack is 0.6
- Use a fuselage mounted stabilizer, hence Vh/V=0.85
- The tail is adjustable hence C_{L_h}=-0.8
- The airfoil used is a NACA63$_2$-615 which as a Cm_{ac_0}=-0.121

In addition equation 15-1 is used to generate the stability curve, it is used to calculate the centre of gravity with respect to the mean aerodynamic chord.

$$\bar{x_{cg}} = \bar{x_{ac}} + \frac{C_{L_{\alpha_h}}}{C_{L_\alpha}} \left(1 - \frac{d\eta}{d\alpha}\right) \frac{S_h l_h}{S\bar{c}} \left(\frac{V_h}{V}\right)^2 - S.M. \tag{15-1}$$

In equation 15-1 C_{L_α} represents the changing lift with varying angle of attack of the aircraft, $\frac{d\eta}{d\alpha}$ represents the down-wash. In addition the aerodynamic centre, $\bar{x_{ac}}$ is composed by the aerodynamic centre of the wing and fuselage, the jet-strums and the nacelles. Nevertheless the nacelles have only a very small contribution with the new configuration due to the use of open rotors as mentioned in chapter 12. Furthermore with equation 15-2 the controllability curve of the aircraft was generated, it similarly to the previous one calculates the cg with respect to the mean aerodynamic chord.

$$\bar{x_{cg}} = \bar{x_{ac}} - \frac{C_{m_{ac}}}{C_{L_{\alpha-h}}} + \left(\frac{C_{L_h}}{C_{L_{A-h}}}\right) \frac{S_h l_h}{S\bar{c}} \left(\frac{V_h}{V}\right)^2 \tag{15-2}$$

In equation 15-2, $C_{m_{ac}}$ is the pitching moment coefficient around the aerodynamic centre which was found to be approximately 1, C_{L_h} was assumed to be -0.8 as mentioned above. With the above equations the stability and control curves in figure 15-3 were plotted.

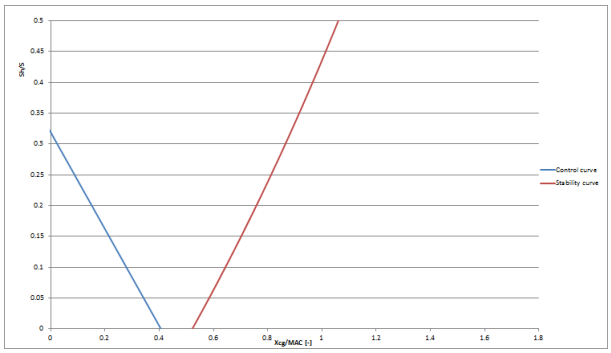

Figure 15-3: Scissor plot, the tail surface over the wing surface against the cg

As can been seen in the figure the curves do not meet which is due to the fact that the Cm_{ac} is positive. This is caused by the location of the aerodynamic centre as percentage of the chord which is very large compared to the conventional design of the A320 with a value of 53.63%. This high percentage can be explained by the relocation of the engines which results in a large positive contribution of thrust on the aerodynamic centre. When matching the scissor plot in figure 15-3 with the cg range plot in figure 15-2 it is possible to read off the tail surface and the wing position and to use the values as input to plot these graphs again. This was done numerous times and the last plot result can be found in figure 15-4.

From figure 15-4 it can be concluded that the ratio between tail and wing area is 0.285 which results in a horizontal tail of 35.5 m^2. The leading edge of the mean aerodynamic chord of the wing should be located at around 52% of the fuselage length, thereby repositioning the wing 25.5% backwards. The final position of the wing along with the centre of gravities of the entire aircraft and the main landing gear can be found in figure 15-5.

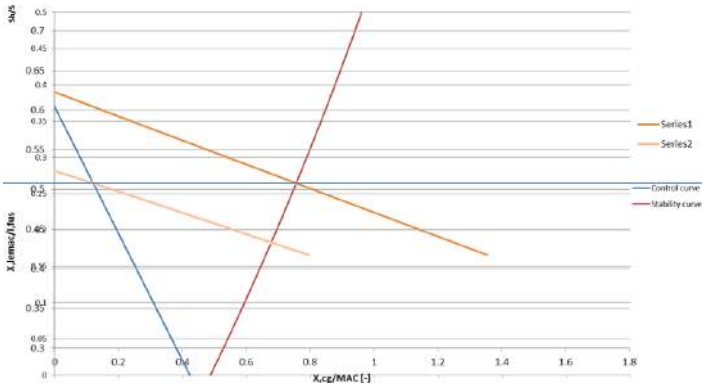

Figure 15-4: cg Range vs Wing Longitudinal Position

Geometry of the Tail

Next to its stabilizing effect the horizontal tail also serves as a shield for the open rotors to reduce the noise. Therefore the length and chord root of the tail have to be large enough to cover the engine. The engine is 3.5 m long and has a diameter of 4.2 m. It requires a sweep of 27 degrees, which is 7 degrees higher than the wing's sweep. With these constraints in mind and using an area of 19 m^2 for half of the tail, a design was chosen which can be found along with the dimensions in figure 15-7.

Vertical Tail

The vertical tail will follow the same sizing procedure as the horizontal tail.

Sizing of the Tail

Similarly to the longitudinal stability, the aircraft's lateral stability must be investigated. As the engines are mounted on the fuselage, crosswind during landing will determine the critical lateral stability instead of engine failure, which is decisive for the wing mounted engine configuration. During landing a maximum crosswind capability is imposed by certification, the aircraft must be able to land safely with a crosswind up to 20 knots.

Therefore the vertical tail must be sized as such that it can sustain this side wind velocity by determining the weathercock stability C_{n_β} contribution of the wing and the fuselage. The wing contribution was selected to be $C_{n_{\beta_i}} = 0.024$ because of the use of a low wing configuration. Furthermore, the fuselage's contribution was determined with equation 15-3 and was found to be -0.155.

$$C_{n_{\beta_f}} = -k_\beta \frac{S_{fs} l_f}{Sb} \left(\frac{h_{f_1}}{h_{f_2}}\right)^{\frac{1}{2}} \left(\frac{b_{f_2}}{b_{f_1}}\right)^{\frac{1}{3}} \tag{15-3}$$

Adding the two coefficients up and using the graph shown in figure 15-6 a $\frac{S_v l_v}{Sc}$ of 0.97 was found. Using the aircraft's dimensions it was found that the vertical tail surface had to be 29.8 m^2 which results in 14.9 m^2 per tail.

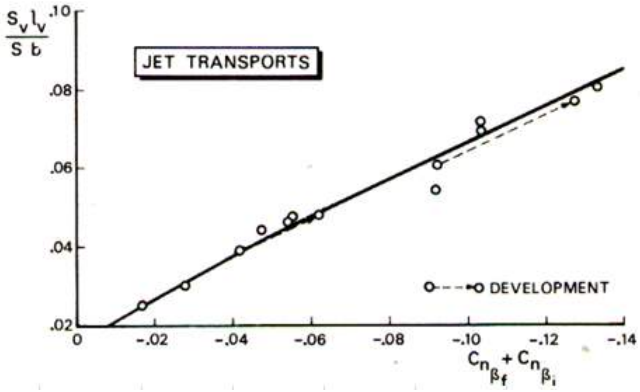

Figure 15-6: Vertical Tail Sizing using C_{n_β}

Geometry of the Tail

The vertical tail also serves as a shield for the open rotors to reduce noise during take-off, landing and climb procedures. As the rotors are 4.2 m high the tail will have to have approximately the same height, furthermore as it was chosen to use a h-tail design, 1/5 of the total height will be placed under the horizontal tail. This means the tail will have a total height of 5.5 m. The completed design of the tail along with the important dimensions can be found in the schematic in figure 15-8.

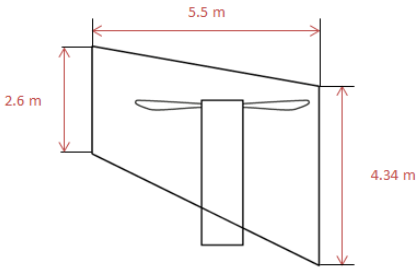

Figure 15-7: The Tail's Geometry

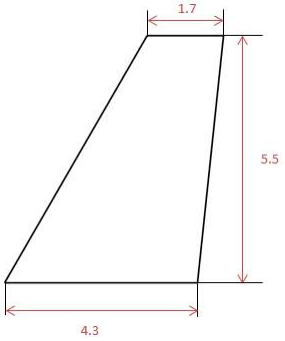

Figure 15-8: The Vertical Tail's Geometry

15-3 Landing Gear Sizing

In this section the landing gear will be designed, this will include the type, the height and track of the main gear, the location of the gears and the resulting stability of the aircraft on the ground. The design choices will be based on the following requirements; the ground clearance, tip-back and clearance angle at take-off angles and the aircraft ground stability and controllability.

The Configuration

For the A320LNG outlined it was decided to keep the same landing gear design base; a tricycle configuration with one wheel at the nose and two main wheels under the wing. This was mainly chosen for the comfort of passenger's and the ease of boarding, as the aircraft is straight with this design. In addition the MTOW is not extremely high which eliminates the configuration with more wheels. The main gears are located aft of the main cg of the aircraft and are closest to it, which means they carry most of the weight. The nose gear carries therefore only a small load which should be between 5 to 20% of the complete weight. The gears are retractable, which means that after take-off there are fully retracted inside the aircraft. This is essential as it will decrease the drag during flight and therefore lower the fuel consumption. The main gears will be stored inside the wing and the nose wheel in the fuselage.

The Height

The height is a very important factor as it allows ground clearance. It must prevent tip-back and ensure fuselage clearance during take-off. The ground clearance is calculated by measuring the lowest point of the aircraft to the ground, which in the case of the A320LNG are the LNG tanks podded under the wing. As the tanks contain fuel it was chosen to take a clearance of 0.6 m which is larger than the certification clearance mentioned in section 17. This results in a height from the lower part of the fuselage to the ground, H_f of 1.39 m . The overall dimensions can be found in figure 15-9.

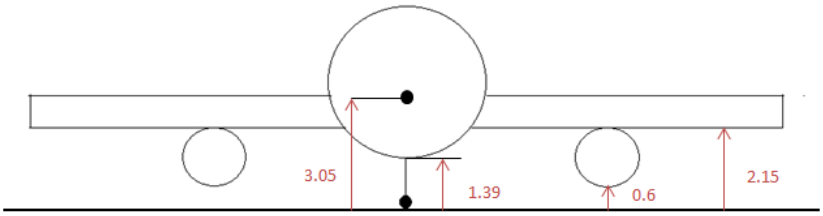

Figure 15-9: Ground clearance dimensions

The main gear is attached to the wing, hence its total height H_{LG} is the distance from the lower part of the wing to the ground, which was found to be 2.15 m.

Location

The location of the main and nose wheels will be decided taking into account the stability and ground clearance of the aircraft.

The Main Gear

To determine if the location of the main gear ensures stability and fuselage clearance during take-off the tip-back angle and take-off rotation clearance angle have to be calculated. Concerning the tip-back angle, α_{tb}, which is the maximum aircraft nose-up altitude with the tail touching the ground as illustrated in figure 15-11, it must always be 5 degrees larger than the take-off angle of attack, $\alpha_{TO,fus}$ [102]. This angle was found to be 7 degrees in chapter 14, hence the tip-back angle has to be larger than 12 degrees. To calculate the tip-back angle the distance between the main gear and the cg of the aircraft, x_{mg} is needed which was determined to be 0.81 m in section 15-2. In addition the main gear was positioned at 80% of MAC in order to be located behind the aircraft cg during the tail sizing. These positions correspond to a tip-back angle of 12.2 degrees which is large enough to meet the requirement hence the actual main gear position will be kept at 21.8 m from the nose.

In addition the take-off rotation clearance angle, α_c must be checked to make sure the fuselage nor tail will touch the ground during take-off. This angle must be larger than $\alpha_{TO,fus}$ which is 7 degrees [102]. In figure 15-11 the angle is depicted and is the angle between the ground and the line passing from the main gear to the beginning of the up-sweep of the fuselage. Using the height of the fuselage, H_f and the distance from the gear to the start of the up-sweep it was found that the angle is 11.8 degrees which is larger than the take-off angle. This means the ground take-off requirement is met. This angle allows for a clearance height during take-off, H_c of 0.8 m.

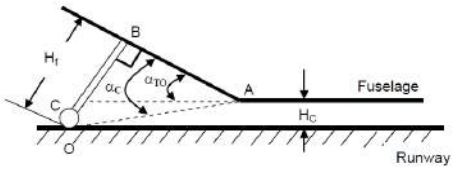

Figure 15-10: Clearance height during take-off

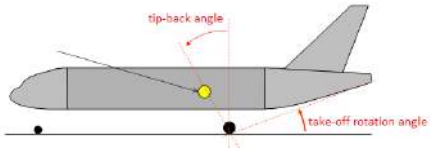

Figure 15-11: The tip-back and rotation angle

The Nose Gear

To guarantee ground controllability the nose gear must carry between 5 and 20% of the total load of the aircraft. Due to design constraints, which shifted the cg of the aircraft backwards, it was decided that the nose wheel would carry the lower limit of 5%, as it is situated further away from the cg than for a conventional A320. The nose wheel location for this percentage was found to be 6.5 m from the nose, which is a distance of 16.25 m from the main gears.

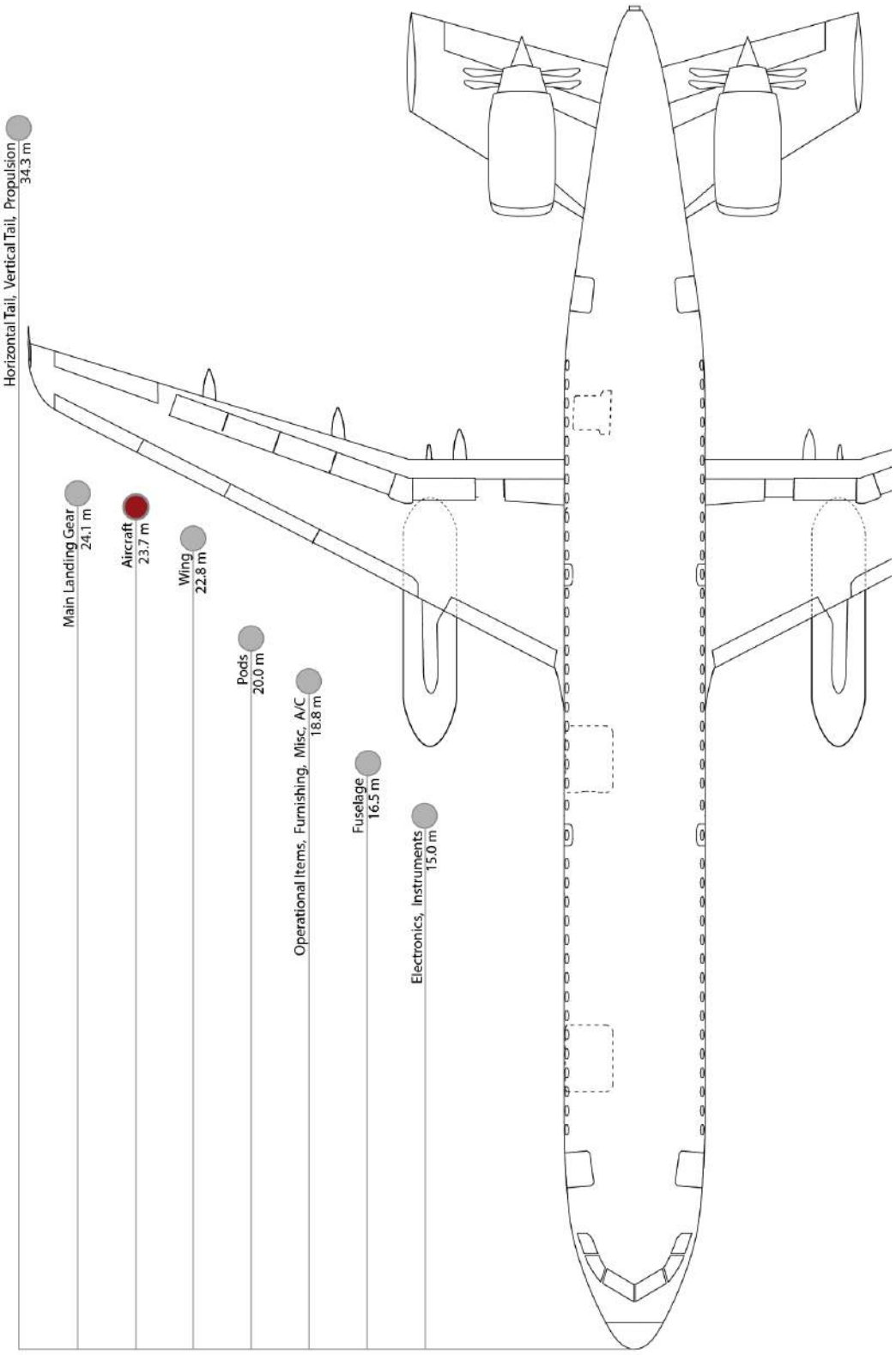

Figure 15-5: The different cg components of the aircraft after repositioning of the wing

Chapter 16

Preliminary Flight Dynamics Analysis

Aircraft with similar mission and geometric characteristics are used as benchmark for the stability derivatives. Then, symmetric and asymmetric aircraft motions are evaluated to provide a initial validation of aircraft stability.

16-1 Stability derivatives

The stability derivatives of various aircraft are investigated and compared[60][113]. Two aircraft control databases are used: Aircraft Stability and Control Data by Gary L. Teper and Aircraft Handling Qualities Data by Robert K. Heffley. Both are contractor reports for NASA. The benchmark derivatives are used as starting point for determining the stability derivatives of A320LNG. The flight condition and aircraft aerodynamic properties used for calculating the derivatives is:

- Altitude: 10000 m
- Velocity: 248.41 m/s
- α_0: 0.5°
- Initial mass: 72955 kg
- Oswald factor: 0.7945
- C_{L_α}: 6.875
- C_{D_0}: 0.0188

The stability derivatives are plotted for different eigenmotions and modified accordingly to satisfy stability requirements. This is an iterative process and the resulting stability derivatives can only be used as an initial control model. The stability derivatives used in this preliminary analysis are presented in table 16-1.

To provide a basic assessment on the static stability of the aircraft, several main stability derivatives from table 16-1 are discussed in further detail below:

- C_{m_α} is negative, the aircraft is statically stable because when the aircraft encounters a gust which pitches the aircraft nose up, the aircraft returns to equilibrium position by pitching nose down
- C_{n_r} and C_{l_r} are negative, the aircraft is statically stable because when the aircraft experiences a clockwise yaw contribution, the aircraft is able to return to equilibrium position
- C_{n_β} is positive and C_{l_β} is negative, the aircraft achieves spiral stability and has a convergent Dutch roll

Table 16-1: A320LNG aircraft stability derivatives

C_{X_0}	0	C_{m_u}	0.0699	C_{l_β}	-0.1326
C_{X_u}	-0.0279	C_{m_α}	-0.5626	C_{l_p}	-0.4809
C_{X_α}	-0.4797	$C_{m_{\dot{\alpha}}}$	0.178	C_{l_r}	0.176
$C_{X_{\dot{\alpha}}}$	0.0833	C_{m_q}	-8.7942	$C_{l_{\delta_a}}$	-0.0309
C_{X_q}	-0.2817	$C_{m_{\delta_e}}$	-1.1642	$C_{l_{\delta_r}}$	0.014
$C_{X_{\delta_e}}$	-0.0373	$C_{m_{\delta_t}}$	0	C_{n_β}	0.1448
$C_{X_{\delta_t}}$	0	C_{Y_β}	-0.75	$C_{n_{\dot{\beta}}}$	0
C_{Z_0}	-0.4573	$C_{Y_{\dot{\beta}}}$	0	C_{n_p}	-0.0602
C_{Z_u}	-0.3762	C_{Y_p}	-0.0304	C_{n_r}	-0.1961
C_{Z_α}	-5.7434	C_{Y_r}	0.8495	$C_{n_{\delta_a}}$	-0.01
$C_{Z_{\dot{\alpha}}}$	-0.0035	$C_{Y_{\delta_a}}$	-0.04	$C_{n_{\delta_r}}$	-0.0694
C_{Z_q}	-5.6629	$C_{Y_{\delta_r}}$	0.23		
$C_{Z_{\delta_e}}$	-0.6961	$C_{Z_{\delta_t}}$	0		

16-2 Modeling

A MATLAB model is produced to simulate each eigenmotion. Although the eigenmotions are fundamentally different, eigenmotion simulations follow a similar coding procedure, as illustrated in figure 16-1. The first part of the script initializes the system by reading/calculating the aircraft parameters. The second part of the script reads the stability derivatives and loads them into the state-space system. The script then calculates the eigenvalues and plots the respective aircraft eigenmotions.

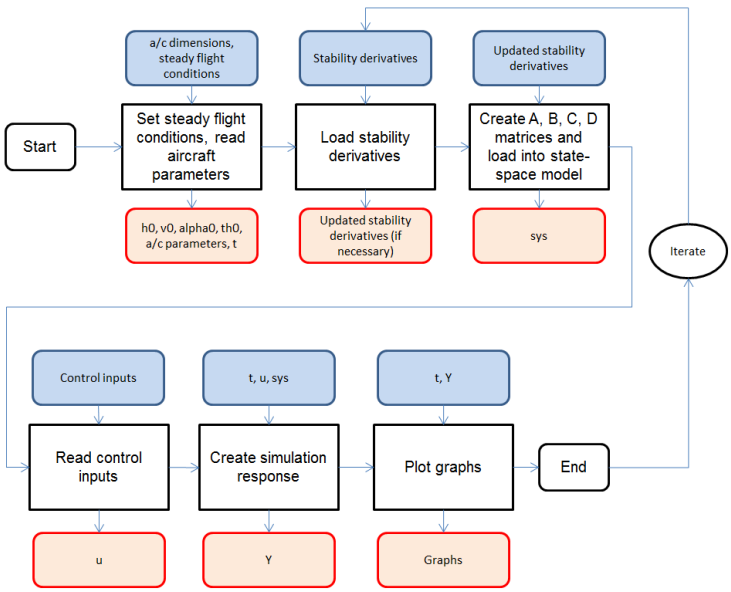

Figure 16-1: Stability model flow chart

16-3 Symmetric motion

Short period Short period oscillation is performed by initiating a step input to the elevator deflection. In this simulation, the elevator deflects upward slightly. This results in a decrease in lift generated at the tail, inducing an increase in pitch rate and ultimately an increase in angle of attack. This is shown in figure 16-2.

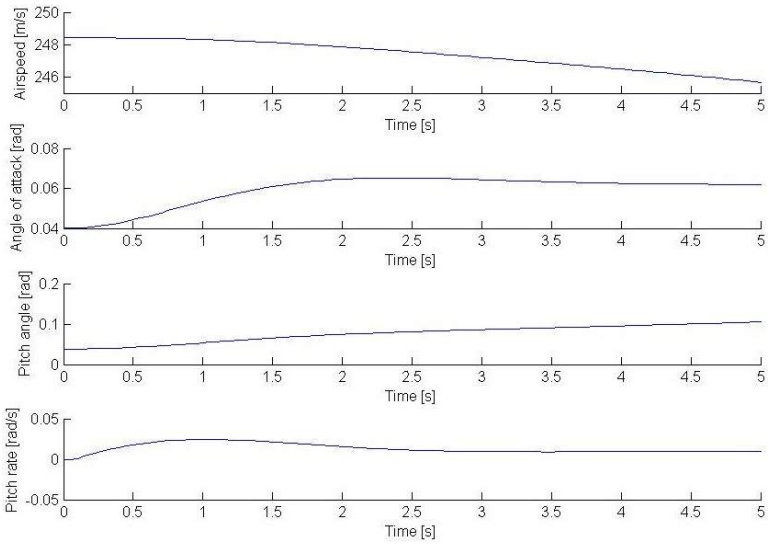

Figure 16-2: Simulated short period motion

The short period motion occurs within a small time frame with a negligible change in aircraft velocity. The eigenvalues are evaluated in table 16-2. All the real values are negative. From this, it can be concluded that the short period motion is stable.

Table 16-2: Eigenvalues of short period motion

-0.0165	± 0.0213 i
-0.0001	± 0.0008 i

Phugoid In this motion, an impulse deflection is initiated instead of a step input.

As expected, there is a large fluctuation of airspeed and pitch angle, but negligible variation in angle of attack. The eigenvalues are evaluated in table 16-3. The real values are negative, thus the Phugoid motion of this aircraft is stable.

Table 16-3: Eigenvalues of Phugoid motion

-0.9769	± 3.5109 i
-0.0034	± 0.0404 i

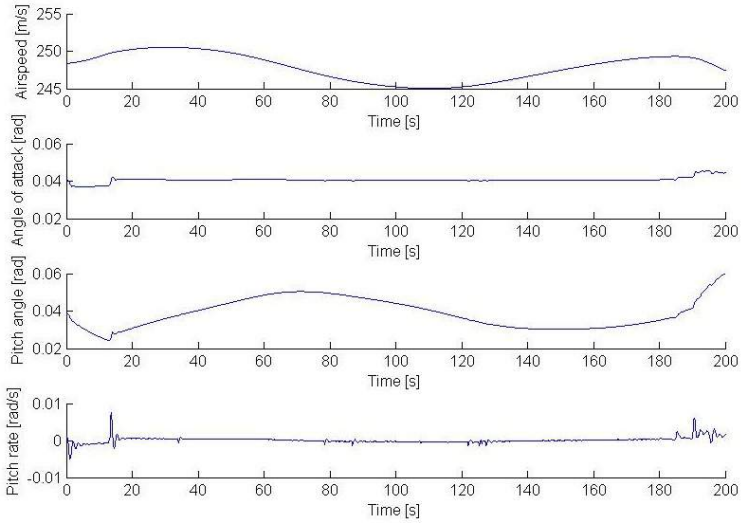

Figure 16-3: Simulated Phugoid motion

16-4 Asymmetric motion

Aperiodic roll Aperiodic roll is evaluated by implementing a step input to the ailerons. The plots in figure 16-4 show how the relevant aircraft parameters vary as the aircraft performs an aperiodic roll.

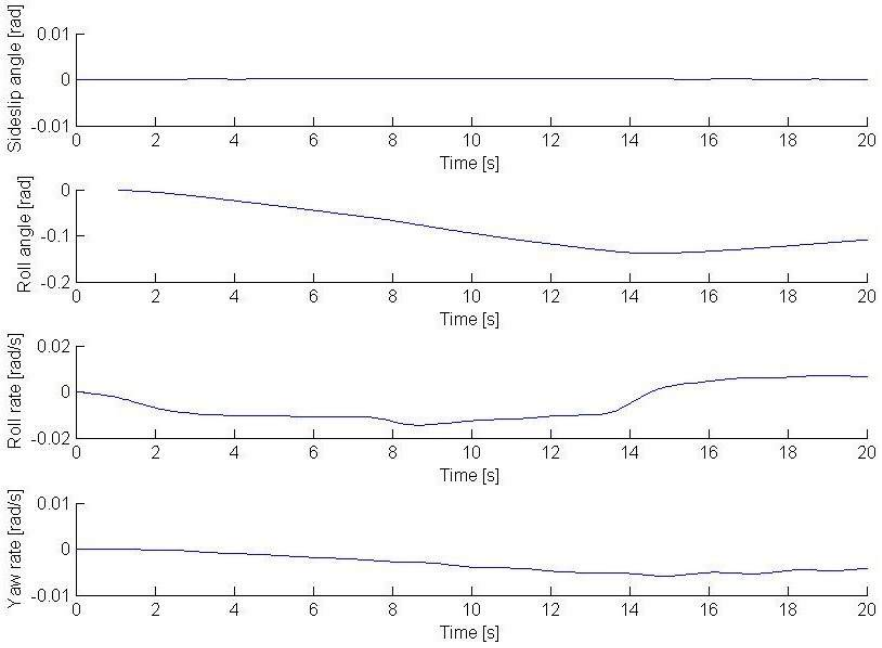

Figure 16-4: Simulated aperiodic roll motion

Because the aperiodic motion occurs within a small time frame, little to none sideslip and yaw can be seen, roll rate quickly converges to a constant value and the opposite direction seconds after. The eigenvalues are presented in table 16-4. One eigenvalue is slightly positive

but the others are negative, this aircraft is marginally stable in aperiodic roll.

Table 16-4: Eigenvalues of aperiodic roll motion

-0.0929	± 2.8605 i
-1.1952	
0.0244	

Spiral The spiral motion is created by putting the aircraft at an initial roll angle of 10◦. Lateral force contribution and reduction in lift cause the aircraft to perform spiral. The roll angle and yaw rate of the aircraft slowly increases.

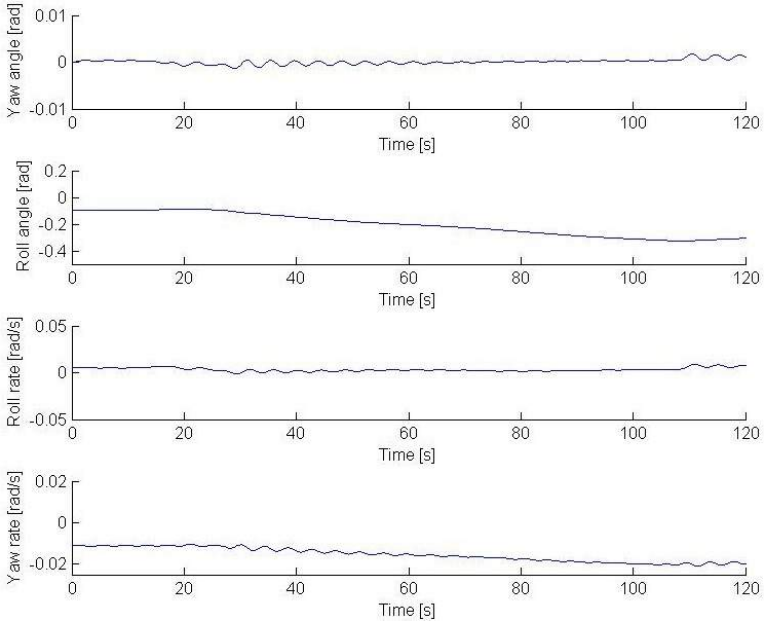

Figure 16-5: Simulated spiral motion

Table 16-5: Eigenvalues of spiral motion

-0.0354	± 1.4848 i
-1.2958	
-0.0002	

The eigenvalues of this motion is presented in table 16-5. Spiral stability is achieved because λ_{b_2} is negative and the spiral stability rule is satisfied:

$$C_{l_\beta} C_{n_r} - C_{n_\beta} C_{l_r} > 0 \tag{16-1}$$

However, stability is only marginal because convergence occurs really slowly.

Dutch roll The Dutch roll motion is initiated by applying an impulse input to the rudder, as a result the aircraft yaws. The difference in velocity between the two wings (induced by the yaw) leads to a difference in lift contribution from the two wings, causing the aircraft to roll. This roll, however, induces a yaw moment in the opposite direction, which is also known as adverse yaw. When roll rate is positive, the yaw rate is negative. Here, λ_{b_1} is slightly positive, the Dutch roll motion is marginally unstable.

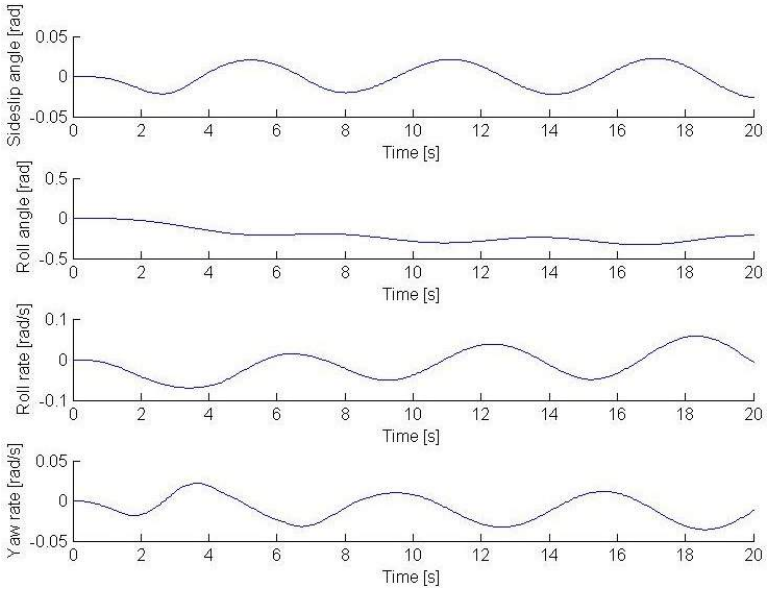

Figure 16-6: Simulated Dutch roll motion

Table 16-6: Eigenvalues of Dutch roll motion

0.0231	$\pm$ 1.0351 i
-0.3978	
-0.0045	

To conclude, the short period, Phugoid, aperiodic roll and spiral eigenmotions are stable for this aircraft. The Dutch roll motion is marginally unstable. By evaluating the eigenvalues, it can be said that the stability derivatives simulate results which are acceptable and can be used for further iterations. To verify and validate this system, the aircraft can be simulated in SIMONA for real performance data and compared with the design stability derivatives.

Chapter 17

Certification

Certification of aircraft in Europe has been unified under the European Aviation Safety Agency (EASA). Certification of any aircraft adheres to their regulations and therefore an innovative hybrid, c-tail mounted open-rotor configuration will be sufficiently different to require amendments to the legislation. Presently for large aircraft, CS-25 outlines all the requirements a twin-engine turbofan aircraft would have to be compliant with.

Even though no regulations exist as of now specifically addressing chosen aircraft configuration, fuel and propulsion system, a combination of requirements for propeller and turbine aircraft can be used to apply to unducted fan engines. Below are the requirements that could require alterations or special attention when applied to an open rotor c-tail aircraft on hybrid cryogenic kerosene-LNG fuel.

17-1 Powerplant

CS 25.903 - Engines
b) Engine isolation. Engines must be isolated from one another such that in case of failure or malfunction of any engine, it will not prevent continued safe operation of remaining engines or require immediate action by any crew member for continued safe operation. In the suggested design this problem is tackled by separating the engines by putting them on the opposite side of the fuselage. Redundancy in the horizontal and vertical control surfaces ensures operability of the aircraft even in the case of complete engine disintegration.

c) Control of engine rotation. There must exist means of stopping the rotation of the rotor in case that it may jeopardise the safety of the airplane. This regulation is more stringent for an open rotor system as there is no nacelle to contain any failures.

CS 25.905 - Propeller
Precautions must be taken in the event of the blade failure or release. Considered hazards must include damage to critical systems and aircraft structures as well as unbalance created by such a failure or release. This is applicable to open rotor engines, especially that due to a smaller diameter, open rotors have a larger possible rotational velocity, hence higher impact consequences. Shielding or reinforcement of the empennage and the aft part of the fuselage is required.

CS 25.907 - Propeller vibration
Determined vibration stresses for normal operating conditions must be determined by the actual measurement on the aircraft or by a comparison with a similar installation. These vibrations should not exceed the values determined safe for continuous operation. Since there are no open rotor systems currently in use, the vibrations caused by its operation can be determined experimentally and compared to the allowable vibrations of its support structure on the actual aircraft. Extensive field testing must be required as well.

CS 25.925 - Propeller clearance
All clearances are specified for the aircraft at maximum weight with the most adverse centre of gravity. Ground clearance must be at least 18cm for an aircraft with the nose landing gear. Ground clearance is not a large issue for the aft fuselage mounted engines. There must be at least 25cm radial clearance between the tips of the rotor and the aircraft structural components. Any further clearance could be used to reduce harmful vibrations of an open rotor system.

CS 25.929 - Propeller de-icing
For the airplanes expected to operate in the conditions where propeller icing might occur there must be means to prevent or remove hazardous ice accumulation if it has the chance to jeopardise safety or engine performance. This might incur additional countermeasures due to the use of cryogenic fuel that can accelerate icing process.

CS 25.933 - Reversing systems
It has to be demonstrated that either the aeroplane is capable of flight with thrust reverser systems active or that the deployment of the thrust reverser systems during flight is highly improbable. For propeller reversing a system has to be designed that will exclude the possibility of any pitch reversal in flight. In an open rotor a combination of thrust and propeller reversal is theoretically possible that will result in the strict requirements and compliance in both areas.

17-2 Fuel System

CS 25.951 - General Fuel System
Fuel system must be constructed to ensure the flow rate and pressure required for proper engine functioning under all operating conditions of the aircraft. In the case of cryogenic fuels the choice has to be made regarding the state in which the fuel is supplied to the engine. The fuel system must be constructed in such a way that a flame-out will not follow in case air is introduced into the system. This is an issue that will require careful consideration as the fuel system bleeding is usually required to avoid potential explosion dangers that can be a result of air trapped in the system.

CS 25.952 - Fuel system analysis and test
The failure of any heat exchanger using fuel as a coolant may not result in a hazardous condition. This is a crucial point for the cryoplane design and needs to be revised as cryogenic fuel is used as the main coolant due to its low temperature.

CS 25.953 - Fuel system independence
The use of wing pods enables the fuel to be cross fed to each engine independently, thus in case of tank or engine failure the other engine remains operational.

CS 25.993 - Fuel system lines and fittings
Where relative motion can exist between the parts of an aircraft, flexible hoses must be used, however use of cryogenic fuels causes materials to become very brittle, so the application of flexible fuel lines is very limited or not possible.

Chapter 18

Noise Evaluation

The target goal as set in chapter 2 of the A320 with respect to noise emissions is a 25% reduction. How this goal is achieved is explained in this chapter, by evaluating the main sources of noise. Furthermore, a distinction in analysis between ground noise and cabin noise is made, so that passenger comfort is also taken into consideration.

18-1 Ground Noise

Ground noise irritation levels caused by aircraft affect areas in high proximity of airports. This is induced mainly by the take-off of aircraft, however landing of large aircraft also add to the issue. At take-off configuration, aircraft are flying with high-lift devices deployed, high thrust settings and partly undercarriage employment (more so for landing). Thereby, the following affect the ground noise levels:

1. Engine acoustics and location
2. High-lift devices flow interaction
3. Undercarriage flow interaction
4. Airframe flow interaction

Engine Acoustics and Location

Open rotor engines produce more perceivable noise as the nacelle casing no longer encompasses the rotor blades, which are set up side by side, counter-rotating to each other. As a result, open-rotors are always louder than turbofan engines. However, by 2030, it is predicted that open-rotors entering service will not be louder than current turbofan engines (see chapter 12).

The noise level of open-rotors are mitigated by applying the following strategies.[3]

- Improve aeroacoustic blade design/geometry
- Increase blade count
- Reduce disk loading
- Aft rotor clipping
- Increase row spacing
- Decrease design tip speed & increase RPM
- Pitch setting
- Pylon Wake Mitigation
- Engine Location

Improve aeroacoustic blade design/geometry

In following section the aeroacoustic design for the open rotor engine is outlined. Information for this section was obtained from a document published from GE aviation and from carrying out interviews with relevant experts as well as from knowledge gathered thematic engineering courses. Improvements in the geometry of the blade design have led to significant improvements in aeroacoustic properties since the first rotor blades were conceived. Investigations done by the Federal Aviation Administration (FAA) into open rotor aeroacoustic technology have resulted in numerous stages of blade design improvement.

Historically, the first open-rotor blades had good aerodynamic properties, however at the expense of worse noise performance. The *Gen1A* that was later designed had two major features; a lower disk loading due to the larger blades and better interaction of airflow between blade row one and two, particularly tip vortices. *Gen2A* then further improved noise performance by including a geared drive architecture, which allows for torque ratios and tip speeds to have better settings. Figure 18-1 shows improvements made from *Gen1A* to *Gen2A* by depicting the reduction in surface pressure of blade row two. Clearly evident is the elimination of the high local tip surface pressure and the overall reduction in pressure.

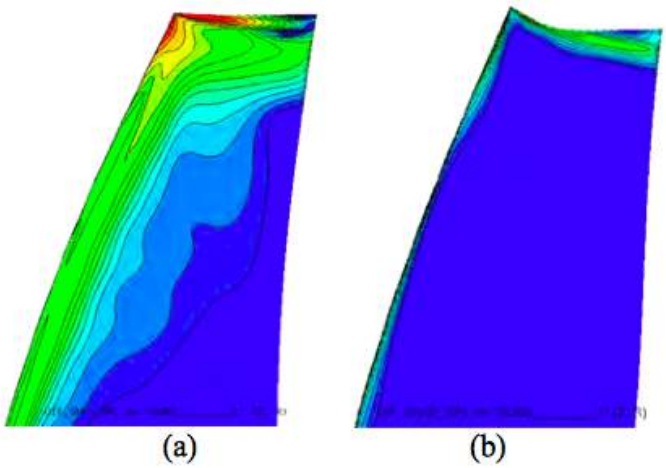

Figure 18-1: Blade row two surface pressure for (a) *Gen1A* and (b) Gen2A [3]

Increase blade count

By increasing the blade count, the loading per blade is decreased [3] as it distributes the power and thrust evenly in its wake. This reduces induced losses and the rotor-rotor interaction noise. Limiting to the maximum number of blades is the pitch change mechanism, blade solidity for reverse thrust and engine weight. The loading on blade B1 affects the strength of its vortices and wakes that it produces while the B2 blade loading affects the unsteady incoming flow from B1. Therefore, it is crucial to properly account for the number of blades for the forward and aft disks. However, the number of blades constrained by engine weight and blade pitch. Thereby, 12 blades will be used on the first set and 10 on the second set as these number are optimized with respect to noise and power carried out by [3] using finite element analysis techniques.[3]

Reduce disk loading

The disk loading can also be reduced by increasing the blade diameter, which results in a significant noise reduction. This also offers improved overall aerodynamic efficiency, at the expense of increased weight.

Aft rotor clipping

The vortex induced by the first row of the rotor blades produces large noise if interaction with the second row of blades occurs. Thereby by clipping the blades, as shown in figure 18-2, the noise can be reduced.

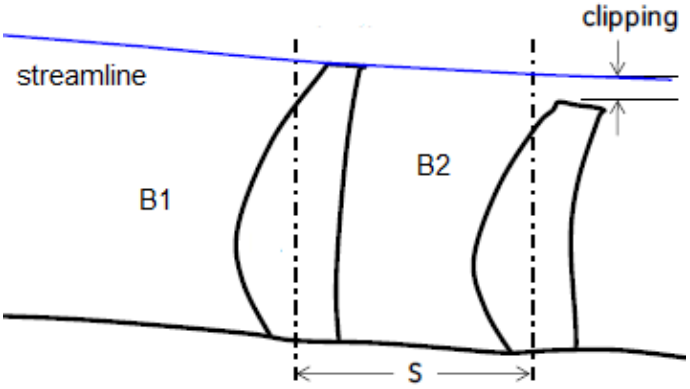

Figure 18-2: Aft clipping open-rotor

Increase row spacing

Increasing spacing reduces noise by having the airflow mix prior to the second rotor blade row. Thereby the wakes and vortices are lessened. Considerations though must be made in regards to the tip vortex from row one. As the spacing between the blade rows is increased, the tip vortex from row one moves inwards with respect to row two. Hence, aft clipping would have to be increased, and blade loading and net efficiency would change. Testing is required to attain an optimal setting.[3]

Decrease design tip speed & increase RPM

The blade tip speed can be adjusted for the various flight conditions due to the variable pitch mechanism. By having a lower design tip speed, at take-off this will reduce friction losses, whilst optimising the lift coefficient for an improved lift-to-drag ratio. [3] This happens as the blades have an increased camber, which increases aerodynamic loading of the blades. Contrary though, the induced losses increase due to stronger tip vortices and hence a balance has to be found.

Additionally, it has been shown that increasing the rotations of row one with respect to row two will lead to a noise reduction.[3] Hence, variable row rpm can be applied for improved acoustic performance.

Pitch Setting

The pitch correlates to the rotational speed of the blades. To achieve a required power and

thrust setting, the blades can either have increased pitch and lower rpm or vice versa. Hence, adjusting the pitch setting is tied into changing the rpm, and has the same influences as mentioned above. Figure 18-3 gives a graphical representation the variable pitch change of a blade. Moreover, designing the blades with variable pitch mechanism allows for optimization of the rotational speed with respect to thrust and the operating condition.

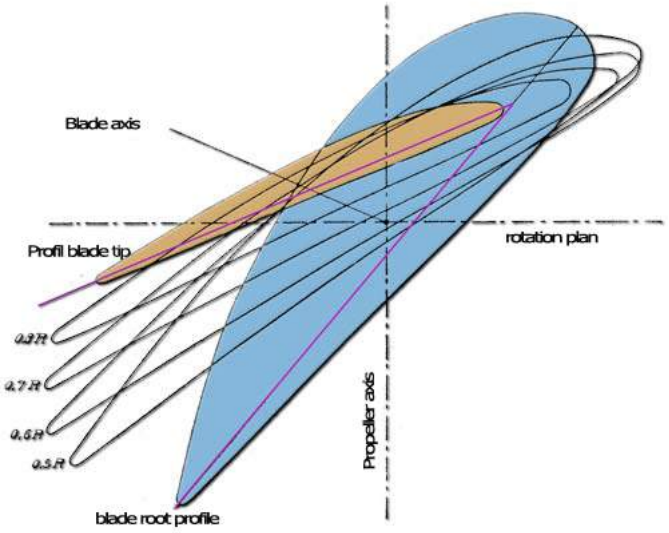

Figure 18-3: Variable pitch rotor blade

Blade design The rotor blades were designed using a CAE-systems empowering simulation software (CAESES). Figure 18-5 shows the designed blade. The blade surface was generated using a B-spline curve which was later manipulated to obtain the desired shape by varying its rake, pitch and skew properties. Furthermore, the blade has a length of 2.1m (from root to tip)with a NACA5514 airfoil cross-section. In addition, figures 18-4 and 18-5 clearly show a rendered view of the rear rotor stage containing 10 blades. The two figures also show the aerodynamic curvature of the blades.

Pylon Wake Mitigation

The installation of an open rotor onto an airframe increases the noise emitted by this engine as the airframe interferes with the airflow in front of the propellers and induces turbulence. These turbulences change the flow pattern at the propellers and thus increase the noise emission. However pylon trailing edge blowing has shown to remove these installation effects almost completely [98].

Engine Location

The engine location can offer vast improvement in noise levels. Figure 18-6 shows the gains by placing the engines 'above' the tail, where it is shielded. As can be seen, most of the noise is then directed upwards, reducing ground noise. In the presented design, the vertical and

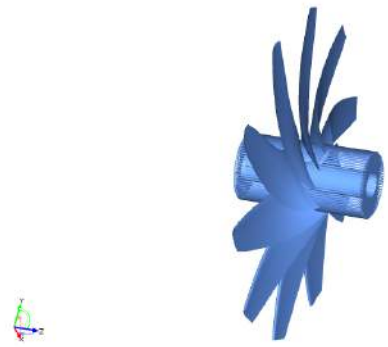

Figure 18-4: Side 3D view of the rear open rotor blade set designed using CAD software

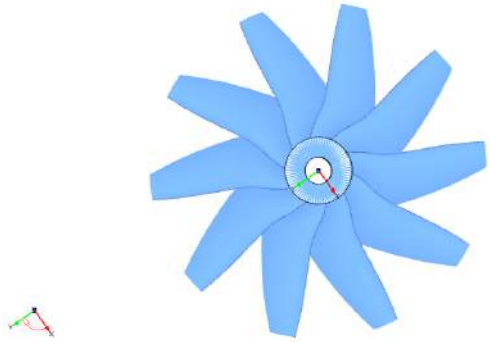

Figure 18-5: Front view of the rear open rotor blade set containing 10 blades designed using CAD software

horizontal stabilizer surfaces are positioned to shield the engine noise from spreading. Engine noise shielding can decrease the cumulative noise by up to 8 db [24].

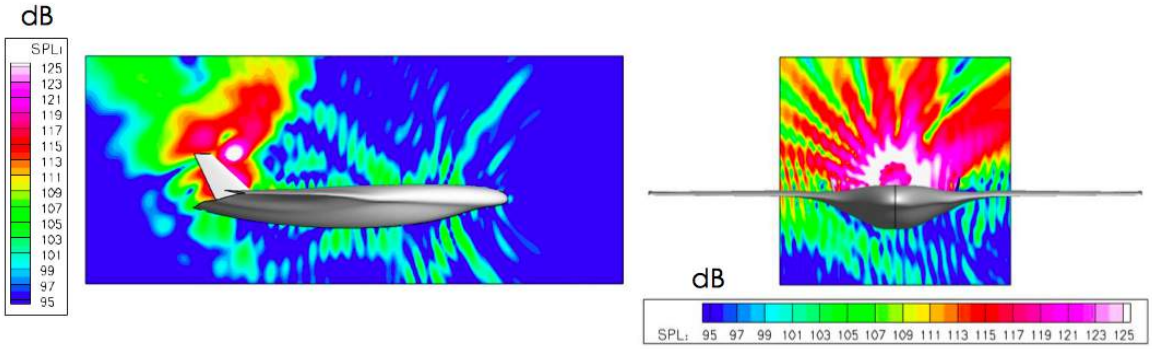

Figure 18-6: Sound [dB] scattering with engine placed above tail [52]

Airframe

The main sources of airframe noise are the landing gear and the high lift devices. Main sources of the noise of the high lift devices are the slat tracks, and the slat and flap side edges and vorticity in the slat flow. It was found that slat track noise is easily removable by a more aerodynamic form as acoustics are not considered in current slat track designs. Furthermore, the vorticity inside the slat flow can be decreased by the use of an cover in the cove of the slat. The use of a brush or porous element showed potential to reduce the slat side edge noise. Lastly, the flap edge noise can be reduced by applying trailing edge fences. The effects of these modification depend on the considered frequency but have shown to reduce the noise in the order of 3-8 db[122].

Next to the high lift devices, the landing gear is a major source of noise on an aircraft. The landing gear creates even more noise than the high lift devices. However the application of fairing around the noisy parts of the landing gear have shown to reduce the noise by 5db. The computation of the effective noise emission is very complex and depends on many factors. It

was shown that the aforementioned improvements can reduce the EPN by 2 db which equals a noise reduction of 37%[72]. This ensure that the airframe enables the goal noise reduction of a 25%.

18-2 Cabin Noise

While the previous explanations and the goals were focused on the external noise emissions, this subsection will explain the differences inside the cabin. The noise inside the cabin is mainly created by the noise and vibrations of the engines. As described earlier, the noise emission of an open rotor engine to enter service in 2030 is expected to be not higher than a current turbofan engine. Furthermore the vibration loads of a open rotor are comparable to the ones of a turbofan[90]. The position in the back of the reduces noise and vibration levels in the cabin is engine noise is mainly emitted to the back. The fuselage will be build from composite materials. These structures generally have a lower transmission loss and thus a less insulating effect compared to currently used aluminium structures. This means that the cabin noise level is expected to stay at the same level as compared to the current A320.

18-3 Conclusion

In this section, the acoustic modifications to the aircraft have been described and their impact has been assessed. It was found that by 2030 an open rotor engine will have the same or less noise emission as a current turbofan engine. The shielding by the stabilising surfaces has the potential to reduce the engine noise value by 8 db. Modifications to the high lift devices and landing gear can reduce the airframe noise by 2db. The noise level is expected to stay the same without the need for increased noise insulation. These numbers show that the noise goal of a 25% reduction is achievable and that the often quoted noise problem of open rotor engines is manageable. This fits the observation that a MD 91 demonstration aircraft equipped with an early prototype of an open rotor in the late 1980 years already met the requirements for a class 3 noise certification[90].

Chapter 19

Airport Operations

The objective of this chapter is to determine the necessary facilities, equipment and operating procedures for an airport terminal in order to enable the airport to serve LNG fuelled aircraft in 2030. This chapter considers the airport environment, transport, liquefaction and storage of LNG. After this ground handling, maintenance, turnaround procedures and changes to airport infrastructure are considered.

19-1 Airport Environment

Rising pressure from environmental bodies pose many design challenges for aircraft designers to design airframes and engines that aim towards cleaner skies in the future. Hence, this section discusses the importance of local air quality at the vicinity of airports and also the importance of local noise level is discussed. Finally, some crucial recommendations are stated in order to make the airport more sustainable.

Air Quality and Noise at Airport-Level

The most damaging emissions at airports are nitrogen oxides, sulfur oxides, carbon monoxide, smoke and unburned hydrocarbons [97]. These pollutants are emitted during the taxi, takeoff and approach phases of aircraft operating into and out of the airport. Airports can reduce their carbon footprint by implementing more efficient operational procedures, both for aircraft and ground vehicles, and setting emission charges to encourage the usage of cleaner aircraft.

The A320LNG aircraft will be fitted with an electric taxi system (ETS) (see section 20-2). The aircraft will takeoff and approach on LNG. This will greatly reduce air pollutant emissions during the taxi, takeoff and approach phases.

In the airport noise studies, three phases are studied: ground operations, climb-out and approach. The proposed ETS reduces noise at ground level substantially. The climb-out and approach are performed using LNG powered open rotors which are designed to minimize noise.

Possible Mitigation Measures

Airports cannot force airlines to invest in cleaner and more sustainable aircraft. However, airports can encourage carriers to do so and reduce their own carbon footprint by implementing any of the following mitigation measures [44].

- Set APU use limits

- Encourage electric taxiing solutions with reduced airport operation fees
- Improve taxiing efficiency to reduce aircraft idling time
- Enforce emission based landing fees
- Use green energy for ground equipment

19-2 LNG Airport Infrastructure

Depending on the location of the airport, different options exist to transport LNG to airports.

- **By sea** on large tanker ships would be a good option for large airports located near seaports such as Barcelona or Rotterdam. The advantage of this method includes it being the cheapest option and ability to transport a large quantity in one shipment.
- **By rail** on trains could be an option for remote airports with an existing rail connection. However the infrastructure requirements for rail transport make this option very expensive.
- **By road** on tanker trucks could be one of the simplest options, but given the large demands for fuel this would result in hundreds of trucks required daily.
- **By pipeline** is the most feasible option and is also being used currently for kerosene at large airports. To reduce investment costs and to be able to use current infrastructure, the pipes are used to transport natural gas. Subsequently, airports are required to invest in liquefaction plants at the airfield to convert the gas to LNG.

On site Liquefaction

Europe has a large existing network of natural gas piping (see figure 19-1). Major European airports are all located within this network. In case the airport has its own small-scale liquefaction plant, the transportation difficulties involved with cryogenic LNG can be avoided. The natural gas can first be supplied to the airport, liquefied and stored in cryogenic tanks on site.

Cryostar is a company which builds and sells small-scale liquefaction plants for natural gas [41]. Their plants have a capacity of up to 400 tpd (tonnes per day). This is consistent with a volume of about $890m^3$ per day, assuming a LNG density of $450kg/m^3$.

19-2-1 LNG Storage

Upon completion of the liquefaction process, the LNG fuel must be stored in an insulated cryogenic tank. There are already many kind of storage tanks available from companies such as Chart Ferox. LNG tanks have to be well insulated in order to minimize the amount of vapor generated and fuel lost, limiting boil off.

There are many different sizes for storage tanks available ranging from 3 [56] to $200,000m^3$.[69]. A reasonable volume for the storage of LNG could be $1000m^3$. Depending on the airport size and amount of LNG fueled aircraft operating on the airport, the tanks can be sized accordingly. The $1000m^3$ engineered LNG storage tank of Chart Ferox has a height of 48.8 m and outer diameter of 5.8 m [55].

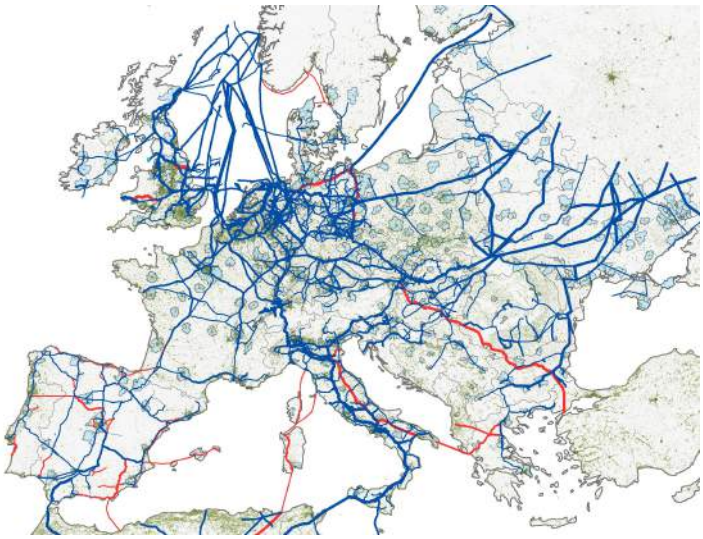

Figure 19-1: Natural gas piping network in Europe (blue = current, red = planned) [41]

Case Study: Barcelona Airport

As a case study, the international airport of Barcelona is taken. Barcelona airport is located near a major harbour and natural gas pipelines. It is also the home base of Vueling, the largest operator of A320 aircraft in Europe. Therefore, Barcelona airport is considered a good case study for implementing A320LNG aircraft and its required airside infrastructure. The air carrier operates 160 to 180 flights per day [119]. As a rough estimate, it is assumed that $10m^3$ of LNG is required per flight. The daily demand would be approximately $1600 - 1800m^3$. Hence, three Cryostar liquefaction plants (or one with threefold capacity) and two Chart Ferox cryogenic tanks would be sufficient if Vueling were to operate A320LNG aircraft.

From a sustainability point of view, it is found that a combination of the ETS and takeoff/landing on LNG reduce CO_2 emissions by two-thirds per flight and approximately 130 to 150 tpd for the entire Vueling A320 fleet. These values are calculated based on ETS emission reductions concluded in chapter 20-2 and takeoff/landing emission reductions due to the open rotor engines as specified in chapter 12. Furthermore, it is assumed that the aircraft meets the emission target of 50% less carbon dioxide.

19-3 Ground Handling of LNG

Handling of LNG can be dangerous and should not be underestimated. Spillage of LNG can result in vaporization of the fuel leading to plume formation. Contact with human skin will damage human tissue and can cause asphyxiation. Therefore, ground handling personnel will have to wear protective clothing and masks when handling LNG at all times [105].

Refuelling Operations

Due to the cryogenic nature of LNG, standard operating procedures for aircraft refuelling have to be adjusted. Before refuelling, the tanks must be purged with nitrogen to remove air

inside the system. Furthermore, if impurities are found inside the tanks, the tanks will have to be reheated. The necessity of removing impurities depends on the quality of the LNG fuel used and is estimated to be required every five to six turnarounds. For a short haul carrier operating as many flights per day, this procedure would be required once a day. During the refuelling process, the maximum flow rate cannot be achieved instantly. The LNG fuel must be eased in, sped up and slowed down upon completion of the refuelling process in order to avoid temperature shocks. Three risks have been identified during this process, shown below in order of importance.

1. Transfer of fuel to the tanks. Figure 19-2 shows the systematic procedure to prevent incidents during the refuelling procedure.
2. (Dis)connection of LNG transfer hose to the aircraft, risk of spillage and improper sealing in the process
3. Integrity of aircraft systems and its vulnerability to possible collisions with ground equipment

It is recommended to turn off all radar and high frequency equipment and also to disconnect electrical equipment during fuelling. A fuel zone barrier should be established during the fuelling process. Open flames should be kept out of the fuel zone barrier. The airport should have an up to date fire fighting system in case of a fire. Furthermore, vehicles used during the operation should be electrical or diesel powered in order to eliminate sparks [105].

Refuelling time is crucial as it is a major factor of turnaround time. Given the aircraft design under consideration is a hybrid configuration, further research into safety procedures are necessary to assess the feasibility of simultaneous refuelling of LNG and kerosene.

19-4 Safety of LNG Infrastructure

All LNG facilities are designed with many safety systems. These include gas, fire detection and suppression systems, pressure release systems and emergency shutdowns systems. In general, there are four layers of protection [49]: The primary and secondary containment (actual shells around the tank), Safeguard systems and separation distances between facilities and other objects. Methane gas detectors are mandatory in all LNG facilities to detect leakage given the odor and colorless nature of the gas [120]. Furthermore, similar to current facilities, fire detectors have to be installed. Safeguard systems are required to automatically shutoff LNG systems in case of leakage or fire.

Several LNG hazards [57] have been identified and are elaborated on below.

- **Explosion:** An explosion might happen in a pressurised vessel due to structural failures. An explosion might also occur if LNG is accidentally ignited. However, if LNG is stored at -162 degrees Celsius and atmospheric pressure, explosion due to structural failure is not a danger because there is no pressure difference. Furthermore, the tanks are designed in such a way that ignition sources should never be in contact with the LNG.
- **Vapor clouds:** When LNG is released, LNG evaporates into a gas as it warms up. As a result, it disperses into the air. Shortly after escape, a vapour cloud will form.

The vapour cloud ignites when put into contact with an ignition source. The facilities have to be designed in such a way that the probability of a vapour cloud outside of the facility is minimized.

- **Freezing Liquid:** Because LNG is at a cryogenic temperature, exposure of LNG to human body can be harmful and should be avoided. Airport personnel should wear protective clothing including gloves and a mask when handling LNG.

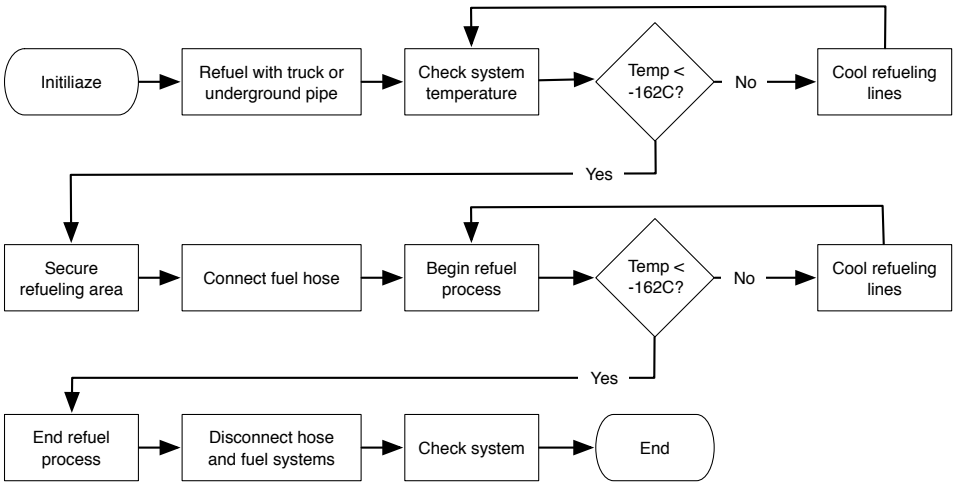

Figure 19-2: Flowchart describing the refueling process of the A320 with LNG fuel

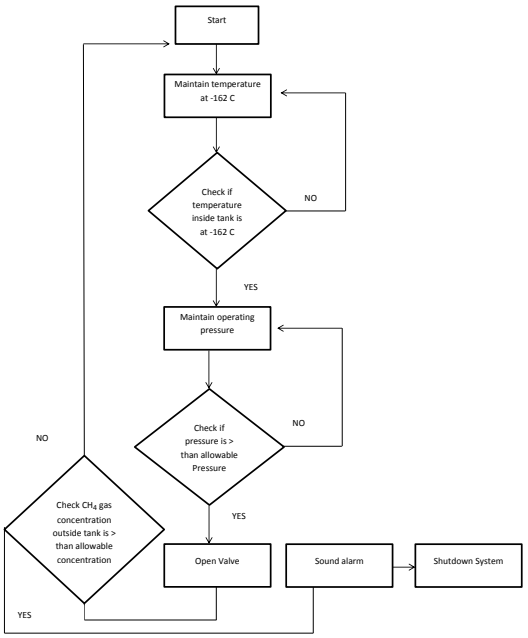

Figure 19-3: Flowchart describing the continuous monitoring process of LNG fuel tanks

Chapter 20

Aircraft Operations

This chapter focusses on the operation of the A320LNG aircraft. First two novel green taxi solutions are investigated for feasibility. Subsequently the standard operating procedures for the A320LNG are presented.

20-1 Green Taxi Solutions

To further reduce fuel consumption, noise and emissions an alternative taxiing solution is investigated. Currently engine thrust provides the necessary force to move an aircraft across an airport. Short haul aircraft typically spend twenty minutes per flight on the ground with engines running [123]. For an airline operating three to four flights per day this accumulates to more than an hour taxiing per day, with corresponds to nearly 1000 kilograms of fuel [123]. An electrically or pneumatically powered taxi system could save this amount of kerosene and subsequent emissions on a daily basis. The following requirements are given for any taxiing solution.

- **A320LNG-REQ-TAXI-01:** A maximum speed of 20 knots (10 m/s) and endurance of minimum 10 minutes must be achievable at maximum takeoff weight (MTOW).
- **A320LNG-REQ-TAXI-02:** The aircraft should accelerate from standstill to maximum speed in less than 90 seconds.

To meet these requirements a certain power and torque must be delivered by the system. The following requirements were obtained.

- **A320LNG-REQ-TAXI-03:** The system must deliver a minimum power of 143 kW.
- **A320LNG-REQ-TAXI-04:** The system must deliver a minimum torque of 369 Nm.

Both the electric and pneumatic taxi systems studied involve a motor that applies a direct torque to the wheels of the aircraft moving it forward. Therefore the engines will remain idle until the last part of the taxi phase during which an engine warmup period is required. The following benefits are expected from either system.

- Autonomous push back, reduces ground handling fees and saves valuable time.
- Less foreign object damage to the engines since they are not running during taxiing and reduced brake wear, saving maintenance costs.

20-2 Electric Taxi System

Currently there are two electrical taxi system (ETS) solutions available on the market: EGTS International, a joint venture of Honeywell and Safran, and WheelTug, a British company headquartered in Gibraltar. Literature on these two products and a master thesis on ETS [123] were reviewed.

An ETS in its most basic form is an electric motor installed directly on the main landing gear assembly. Electrical power is acquired from the auxiliary power unit (APU). The system can work in nearly all operating conditions, except for some severe cases of icing, snow and marginal visibility. Figures 20-1 and 20-2 show estimated fuel and cost savings as per a study preformed in collaboration with KLM [123].

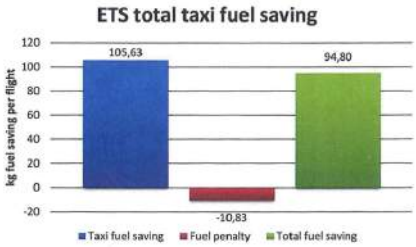

Figure 20-1: ETS fuel savings [123]

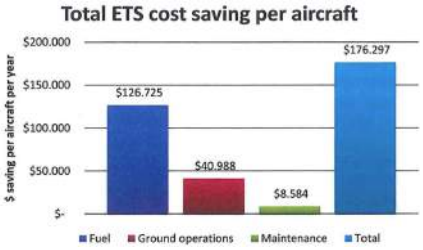

Figure 20-2: ETS cost savings [123]

Impact on Electrical System

The APU must deliver the necessary power to operate an ETS [123]. The AC generators in the APU of the current A320-200 deliver 90kVA of apparent power (see table 20-1). Since the power required of the ETS is much higher the APU will need to generate more power. As a result the voltage across the system must be increased to avoid very large wiring and system weight. A voltage similar to the Boeing 787, an example of a next generation all-electric aircraft, will be required for an A320 equipped with an ETS.

Table 20-1: Electrical System Comparison A320 and B787

Electrical System Parameter	A320-200	B787-8
Voltage AC system	115V	235V (secondary system on 115V)
Voltage DC system	28V	270V (secondary system on 28V)
Generators per APU	1	2
Power APU Generators	90kVA	225kVA
Current APU Generators	782A	957A

Concluding Remarks

The ETS will require a large APU, add weight to the aircraft and will demand a redesign of the electrical system. It is questionable whether the ETS will be profitable. Operating at small airports will render the ETS useless as the engines will require a minimum 5 minute warm-up period [123].

20-3 Pneumatic Taxi System

A pneumatic taxi system (PTS) is based on a compressed air engine, a type of motor that does mechanical work by expanding compressed air. Several concepts have been tried out in the automotive industry however have failed to succeed. A major advantage of PTS is that it only emits air and does not consume fuel, therefore not contributing to global warming. Limited literature is available on a PTS, therefore a numerical model was constructed in an effort to estimate the system's feasibility. The simulation is based on the following assumptions and is designed based on the previously mentioned requirements.

- The dead volume at the top of the cylinder is 5% of the total cylinder volume.
- Friction and pump losses during power generation are 5%.
- A small housing around the cylinder is sufficient since no cooling is required.

Two concepts were conceived of the which the last is more practical. In the first concept the air tank is charged with hot compressor bleed air during climb, which comes with several technical challenges and impracticalites. The second concept is designed for use during taxi-out towards the runway and the tanks are filled by ground service trucks. The airport will be equipped with a air compressor and storage facility. The compressor will run on green energy provided by wind energy farms on windy days when more energy is produced than consumed on a nation-wide energy grid. Storage facilities will be sized such that sufficient compressed air is always readily available.

System Design

The simulation model is split into two parts. The first part includes the charging of the air tank by ground service vehicles. The second phase is when the air motor is operational during taxi-out to the runway. A dynamic analysis of conditions in the air tank is done and the thermodynamics of the air motor are determined. Figures 20-3 and 20-4 show the results from a dynamic simulation of tank charging and discharging respectively. Within five minutes the air tank can be filled to maximum capacity of 460 liters at 30 bars. The air consumption of the motor is determined by piston and cylinder dimensions and is therefore constant during operation. Based on the mass flow the decrease in system pressure can be computed. Final tank pressure after taxi-out operation is found to be 15 bars.

Based on these simulations it was concluded that the air motor must be sized such that it meets the power requirements at an air pressure of 15 bars. An iterative process was used to determine the final dimensions. Air is expanded in the piston during an isobaric and isentropic process consecutively. Isentropic expansion starts at the cutoff volume (point 2), which mechanically is when the inflow valve closes. The average power during one stroke of the engine is determined by integrating over the piston displacement in one stroke.

The p-V diagram is shown in figure 20-5, where the expansion process is from point 1 to point 3. Figure 20-6 displays the air motor performance. As the system is designed for 15 bars and initial tank pressure is 30 bars the air motor delivers much more power than is required. As a result the power requirement of $143kW$ is still met after 10 minutes of taxiing.

A rough weight estimation (see table 20-2) concludes that total system weight (including air) will be just under 150 kg. Since the design is made such that all air is consumed during

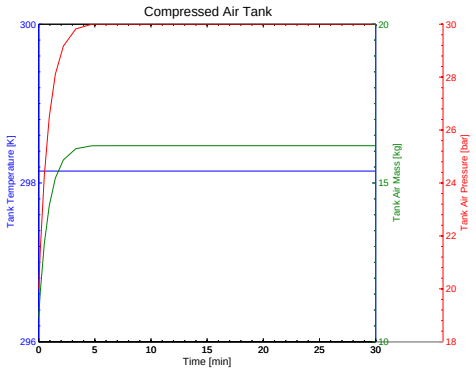

Figure 20-3: Dynamic simulation of tank charging

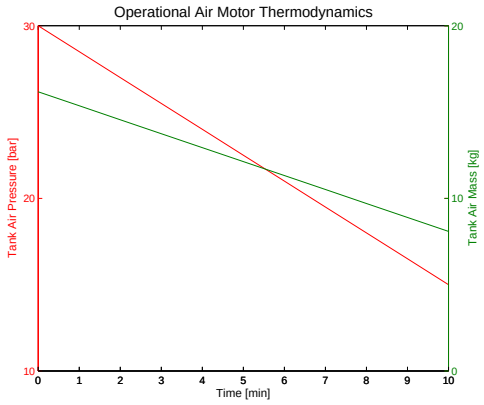

Figure 20-4: Dynamic simulation of tank discharging

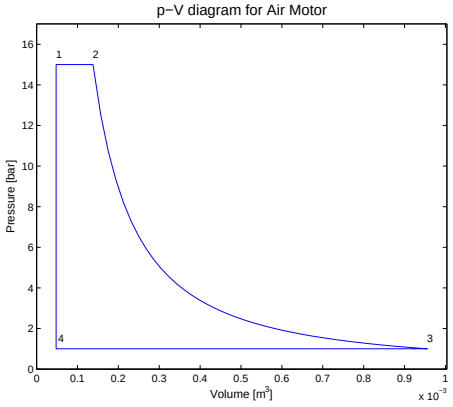

Figure 20-5: Thermodynamic p-V Diagram of Air Motor

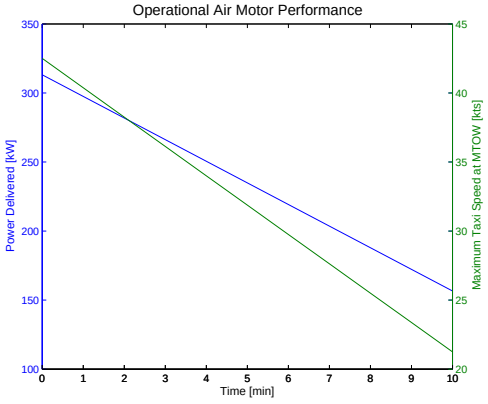

Figure 20-6: Air Motor Performance during 20-minute Taxi

taxi-out the system weight at takeoff will be the empty weight, roughly 130 kg. This is much lighter than the ETS, weighing nearly 400 kg [123].

Table 20-2: Initial Weight Estimation PTS

System Component	**Weight [kg]**
Motor (one for each main gear)	16.9
Tank	76.4
Piping	3.5
Additional (15% for elements unaccounted for)	17.0
Empty Mass	**130.7**
Compressed air	16.2
Total Mass	**146.9**

The different sections of the thermodynamic model have been verified. This was mostly done by adjusting input values such that the model becomes much simpler and an analytical

calculation is possible to verify results. For instance the pressure was lowered to lengthen the isobaric expansion and shorten the isothermal expansion. This makes the power calculation much easier and an analytical calculation could be used to verify.

Concluding Remarks

Figure 20-7 shows a schematic diagram of the final proposed system. Technically the PTS is feasible and will be able to meet requirements. An additional weight of 150 kg approximately corresponds to 6 kg higher fuel burn during flight [123]. During taxi the A320 aircraft burns roughly 12.5 kg/min [123]. For a fifteen minute taxi including a five minute engine warm-up potential fuel savings are estimated at 119 kg per taxi-out. Based on these estimations and the total system weight the PTS will save more and weigh less compared to the ETS.

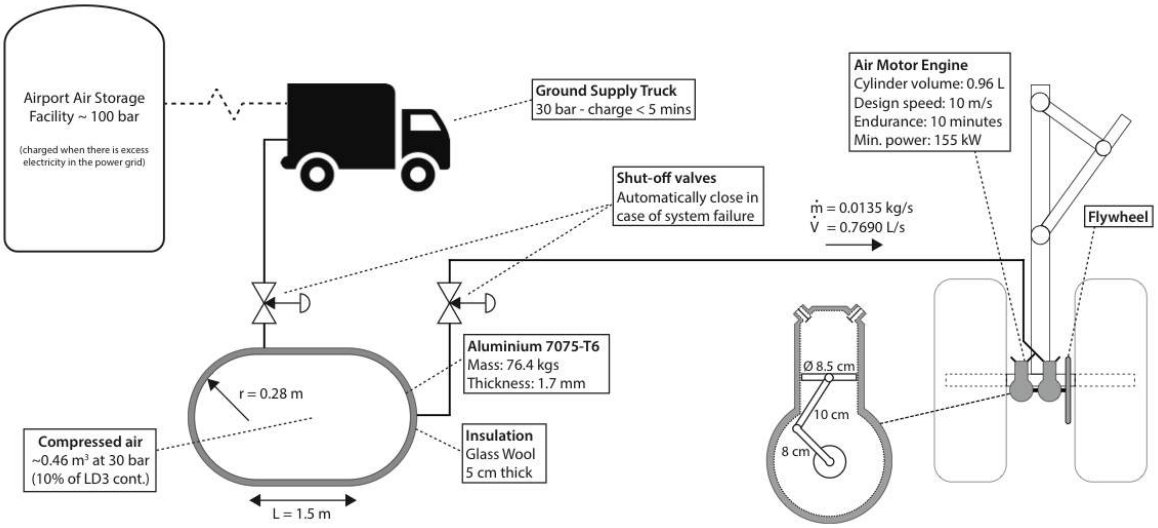

Figure 20-7: Pneumatic Taxi System

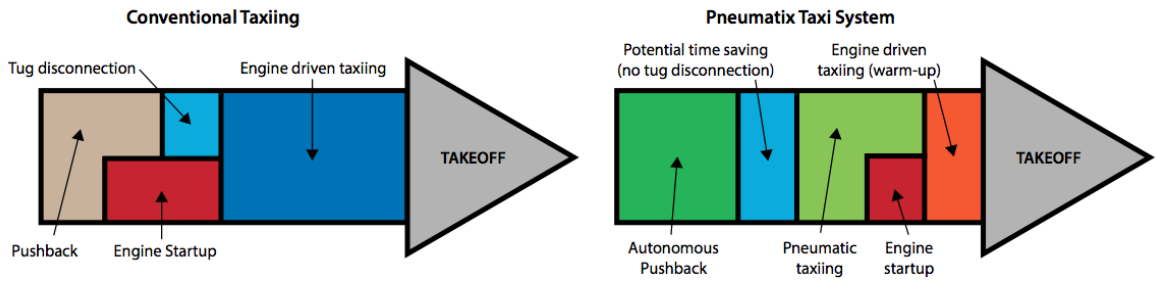

Figure 20-8: Potential PTS Time Savings

20-4 Cockpit Panel Changes

To accommodate subsystem changes the cockpit will have to be altered. To reduce training, certification and development costs a minimum change philosophy was used (see figure 20-9).

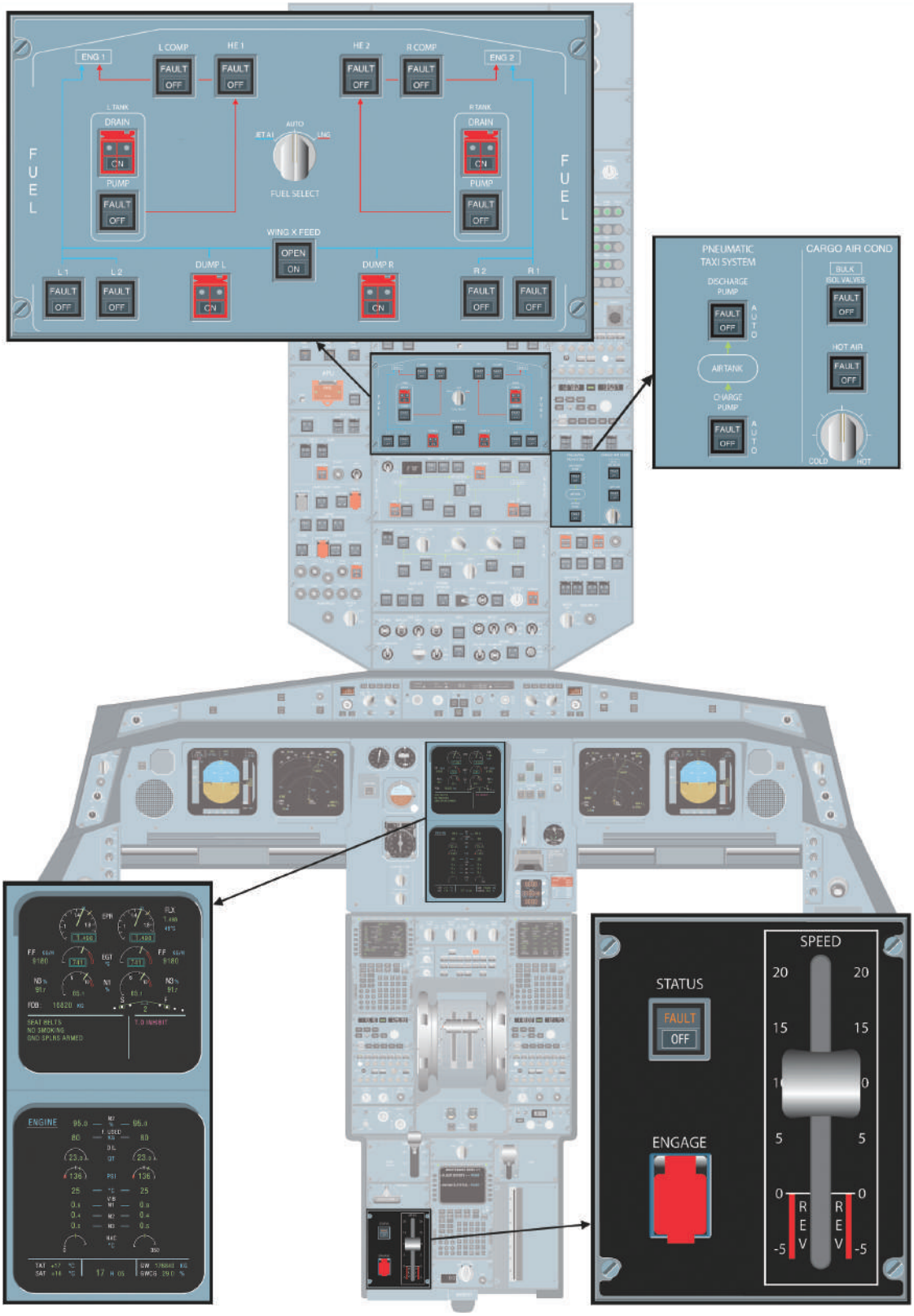

Figure 20-9: Changes required in A320 cockpit panels

20-5 Standard Operating Procedures

In this section the standard operating procedures (SOP) for the A320LNG are discussed. As a baseline the SOP of the current A320 are taken. This section focusses on the new LNG related procedures. Schematic drawings of the SOP are given in figures 20-10 through 20-14 and steps are labeled with a number.

During preflight preparations the flight crew will make decisions to determine the mission profile. The main change during cockpit preparation will be fuel system management and the pneumatic taxi system.

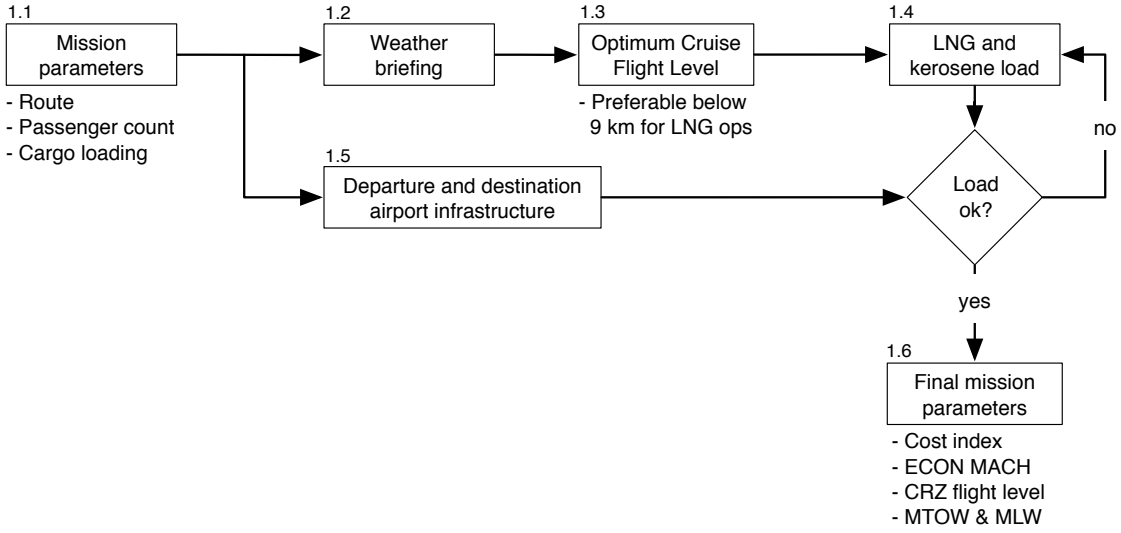

Figure 20-10: Preflight SOPs

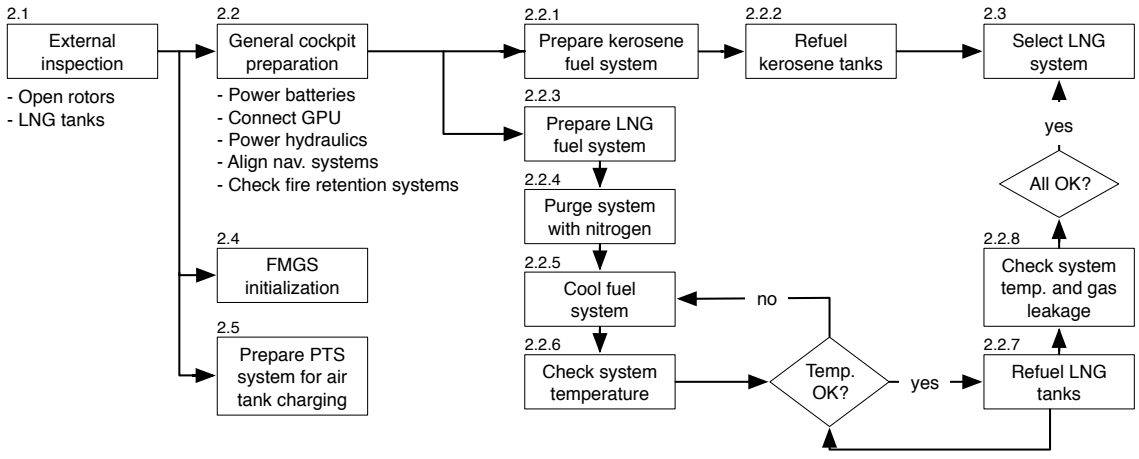

Figure 20-11: Cockpit Preparation SOPs

Upon completion of all preparatory procedures and passenger boarding the auxiliary power

unit (APU) will be started. Once electrical generation from the APU is confirmed the GPU can be disconnected. Subsequently the entire pushback and taxi is preformed on PTS.

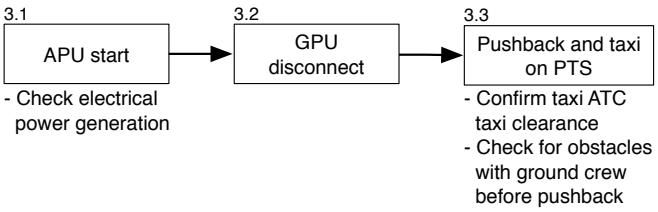

Figure 20-12: Pushback and Taxi SOPs

Five minutes prior to reaching the runway holding point the pilot will confirm that the fuel system computers have selected LNG and will subsequently initiate automatic engine start. Following successful engine start the APU will be disconnected as well as the PTS and proper functioning of flight controls and systems is verified.

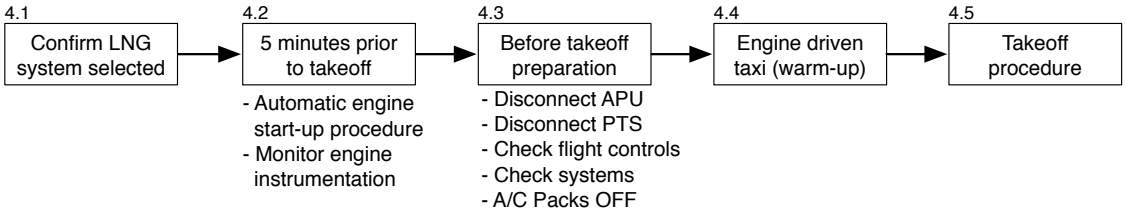

Figure 20-13: Engine Start and Takeoff SOPs

If during the preflight planning a hybrid operation was selected then a switch of energy source will occur during cruise. By default, to minimize GWP (see chapter 5), the transition flight level is set to FL300 (approx. 9000m). This altitude can be adjusted as required in the flight computers. The transition will be done automatically with a manual backup system. The engines will transfer separately to assure available thrust in case the transfer fails. Proper monitoring of both fuel systems must be preformed before and after the transition.

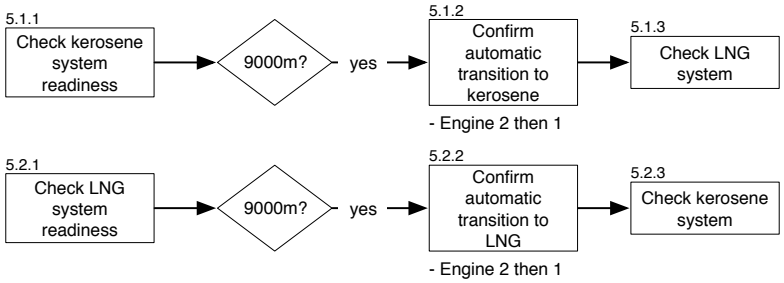

Figure 20-14: Cruise SOPs

Chapter 21

Reliability, Availability, Maintainability and Safety

In the preliminary design phase, the A320LNG has had key subsystems redesigned. These changes have an impact on the reliability, availability, maintainability and safety (RAMS) of the aircraft. This chapter investigates these areas, beginning by analysing the reliability of the adopted subsystems. From there, a better suited maintenance scheme can be implemented. Safety here pertains to negative impacts on the environment and has been covered in the chapter 2.

21-1 Reliability & Availability

The reliability (and consequently availability) of the changes in the A320LNG affect both maintenance and safety. To simplify the analysis of the reliability, first only the adopted subsystems will be investigated and secondly subsystems will be considered to be events independent of each other. The subsystems that have been redesigned can be split up into three groups,namely propulsion, fuel supply, structures % control and internal systems. By making this grouping, fault trees for each group can be made from which the possible causations of downtime can be deemed.

Fault Trees

Fault trees for the above groupings are given in this section to better understand the faults that can occur in the main redesigned subsystems. The fault trees are simplified and stop at top layer faults, not going into depth of minor faults as this is beyond the scope.

Propulsion

- The propulsion system is composed of multiple mechanical parts, namely the gearbox, turbine blade, cooler and combustion chamber. All of these components are prone to malfunctions as time used increases. Partial blade damage may be sustained from collision with small unidentified objects.
- Bird strike, volcanic ashes and icing are external factors which may contribute to engine failure.
- Weather conditions determines the rate of which the propulsion system requires maintenance. The poorer the weather conditions, the more friction the components experience and thus the higher the rate of maintenance.

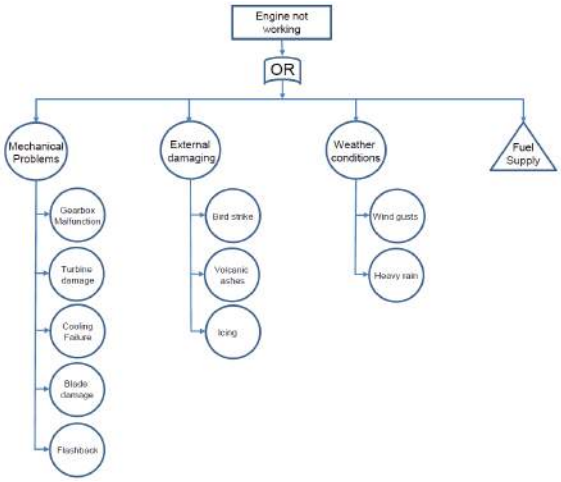

Figure 21-1: Propulsion system fault tree

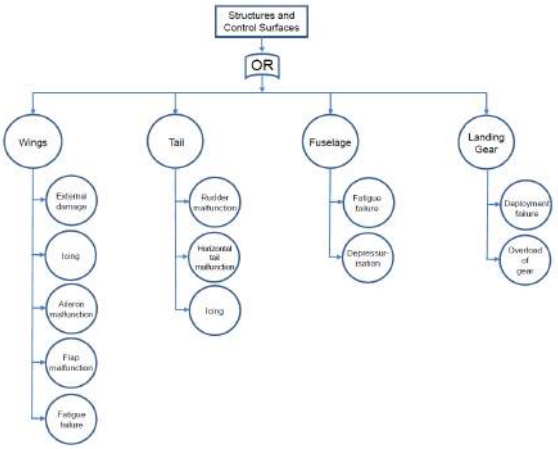

Figure 21-2: Structures and control fault tree

- Fuel systems and tanks are subsystems of the propulsion system and are to be investigated into more detail.

Fuel supply

- Fuel system distributes the fuel between the tanks and the engines. The fuel pumps, fuel gauge and engine feed tank are components which have a probability to fail over time. Fuel lines may be blocked due to impurities. If the heat exchanger is not working probably, there is also the possibility of frost formation when the aircraft is operating at low temperatures.

- Fuel tanks are facilities which accommodate fuel. Fuel contamination is one potential reason why the fuel supply is disrupted. Lack of pressure control and boil-off rate control from the fuel tank may also disrupt fuel supply. Cracks in the fuel tank can lead to fuel leakage.

Structures & Control

- Wings are exposed to air whilst operation, this increases the chances of collision with foreign objects, leading to stress fractures on the wing. At extreme temperatures, ice may form on the wing. Ailerons and flaps are mechanical components, both items have the potential of malfunction. The root of the wing experiences high bending loads during operation, this may lead to fatigue failure of the wing.
- Tail is composed of a horizontal stabilizer and a vertical stabilizer. Both control surfaces have the possibility of malfunctioning and icing.
- Fuselage experiences torsional and normal stress loads, both contribute to the potential of fatigue failure. Cracks or holes in the fuselage may also lead to de-pressurisation.
- If the landing gear door malfunctions, the landing gear cannot be deployed successfully. Also, if the distribution of payload and fuel weight is not managed correctly, the landing gear may carry too much load and structurally fail.

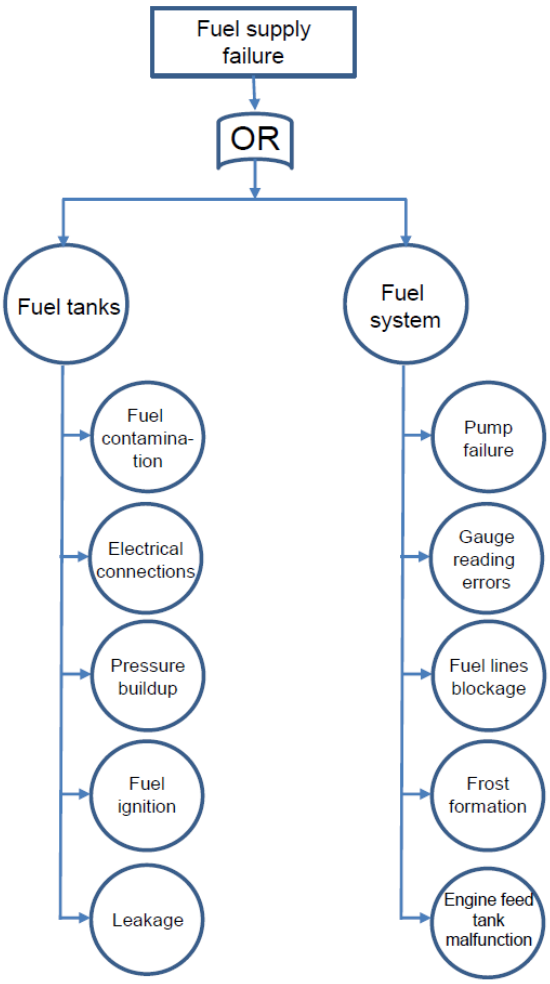

Figure 21-3: Fuel supply fault tree

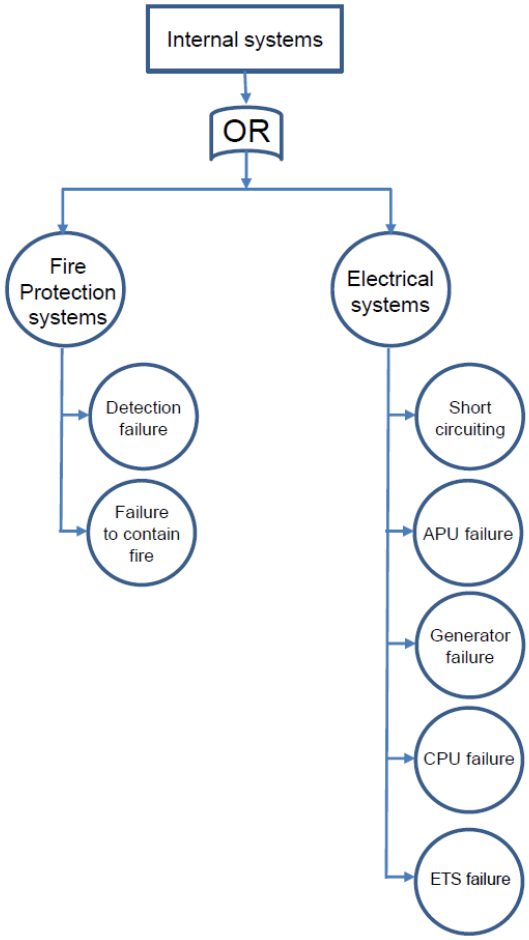

Figure 21-4: Internal systems fault tree

Internal Systems

- Short circuiting can occur if wire is not insulated properly or if a moving part is jammed. Similarly, the APU can be disrupted and fail due to abnormal current flows. There is a possibility in which the generator malfunctions and fails to provide electricity. The central processing unit controlling the electrical systems may fail if the circuit boards are damaged. This also applies to the electric taxi system.
- Fire protection system relies on the detection of fire from its detectors and the ability of walls to contain fire. Both components are important for a successful fire protection system.

Failure Rate Diagram

The components in the fault tree will have different modes of failure. However, given that they are novel in their use, they will mostly follow a bathtub failure mode, or otherwise known as a Weibull distribution [75] Thereby most failures will occur at the beginning or end

of a product life cycle (see figure 21-5). The maintenance scheme will have to be adjusted accordingly to accommodate for the increase in infant mortality rates.

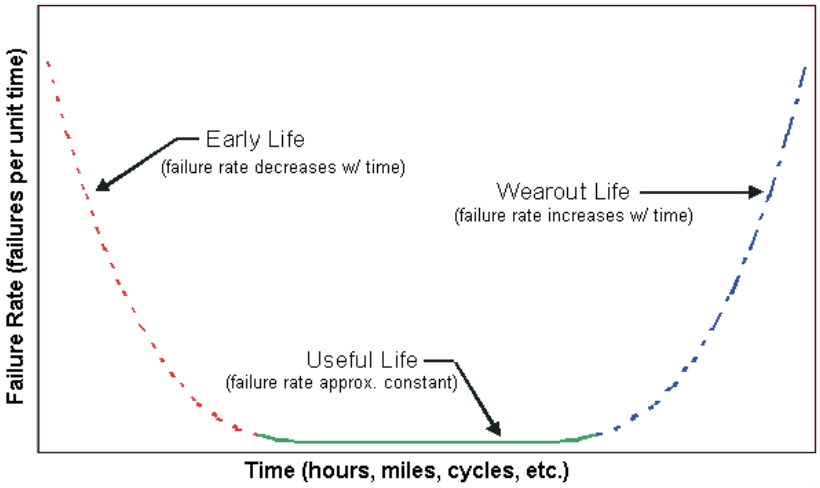

Figure 21-5: Bathtub curve failure rate [126]

21-2 Maintenance

Maintainability of the aircraft is defined by the workload imposed by scheduled or unscheduled maintenance [105]. By increasing the reliability of the LNG aircraft and ease of maintenance, the maintenance requirements can be reduced. This is an important feature for the aircraft since maintenance costs have an impact on the Direct Operating Cost (DOC). Increasing the maintenance intervals increases the aircraft utilisation since the downtime decreases. As a result, the revenue earning from the aircraft increases.

Maintenance and Inspection of the A320LNG

Maintenance steering group 3 (MSG3) schedule is implemented to ensure the safety of A320LNG. Instead of checking and maintaining the aircraft at specific time intervals, specific maintenance checks are now based on the number of flight hours. A320LNG is compared with the current A320 and measures are taken to keep maintenance time consistent. First, the key configuration differences between A320LNG and A320 are identified:

- Open rotors engines are used instead of geared turbofan engines
- A H-tail is used instead of a conventional tail
- Engines are mounted at the tail, no longer at the wing
- Wing pods are added to contain LNG fuel
- Centre kerosene fuel tank no longer contains kerosene
- LNG fuel system is implemented
- Cryogenic fuel feed and storage systems are installed

To compare maintenance time of the new aircraft, the different MSG3 checks are listed and evaluated against the A320LNG. There are four types of maintenance scheduled servicing

checks namely; A, B, C and D checks. The 'A' check is a visual inspection of specific components of the aircraft. Normally, for the A320 the time interval between an 'A' check is between 350 to 600 flight hours. The 'B' check is an intermediate check which inspects. the aircraft for assuring continued airworthiness [105]. The 'C' check is a heavy maintenance check that requires a thorough visual inspection to ensure continued airworthiness [105]. This check is done every 3500 flight hours on the A320. Furthermore, the 'D' check is not performed on newer generation aircraft instead multiple progressive 'C' checks are carried out [105]. Analysing the A320LNG case,

- 'A' check - The engines are now mounted at the tail of the aircraft, making it more difficult to inspect. Also, wing pods and cryogenic fuel system are added onto the checklist. The LNG fuel system check is particularly important because the system ensures that the fuel is under control. Additional training and special equipment to handle LNG are required for safety considerations.
- 'B' check - More in depth check on the control surfaces is performed, because there are two vertical control surfaces instead of one, more time is required to ensure that both operates acceptably.
- 'C' check - Detailed checkup on engine is required, since open rotor engines are more complex than a turbofan engine, more downtime is necessary. A larger number of fuel lines and pumps are required for checkup.

Inspection, Maintenance and Repair of Tank and Insulation Systems

It is assumed that frequent structural inspections of the A320LNG tanks will be required during the early operations of the aircraft. The inspection will also monitor the thermocycling of the cryogenic tank [27]. According to [27] it is recommended that the nominal inspection of the inside of the tanks should be performed every 4000 hours. The inspection of the tanks will be done using non-destructive testing methods. New service equipment and testing equipment will be required, which will need to be adapted to service LNG components [105].

In addition, the LNG fuel pipes and the insulation of the shroud material of the tank will be inspected during normal C-checks. Furthermore, mobile and fixed methane detection systems will be required during the operational procedure [105]. Strict requirements with regard to the operation of maintenance vehicles have to also be considered, in particular the prevention of spark ignition during fuel system checks. The airport will be required to build and develop LNG infrastructure to support the repairing and maintenance procedures.

Chapter 22

A320LNG Design Evaluation

In this chapter a sensitivity analysis is done in order to make a comparison between the designed A320LNG and other similar aircraft. A comparison is made between the A320neo, the next generation A320 turbofan and the newly designed A320LNG. Calculations are based on an average A320 mission of 800 nm at a cruising altitude of nine kilometers. Both aircraft are compared based on emissions and sustainability, acquisition cost, direct operating cost and safety. Finally the changes in configuration are presented.

22-1 Emissions

There are two main factors involved in reducing the emission: LNG and open rotor engines. In this section a comparison will be made between the A320LNG, the A320neo and the A320-200 turbofan aircraft. The aircraft will be compared based on their emissions. As baseline, the current A320-200 is chosen. The A320neo has an CO_2 reduction of 30.6% due to a more efficient engine, this has been calculated by determining the increase in range due to the fuel fraction method. The open rotor engines have an increase in efficiency of 25 %, see section 12-5. The reduction which can be achieved by using LNG as compared to kerosene has been calculated using analytic methods and is found to be 25% per MJ. Hence the total reductions for the A320LNG compared to the A320-200 is 43.7 %.

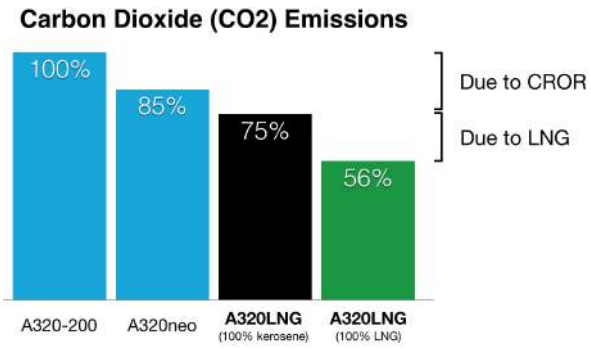

Figure 22-1: Expected carbon dioxide emission reductions

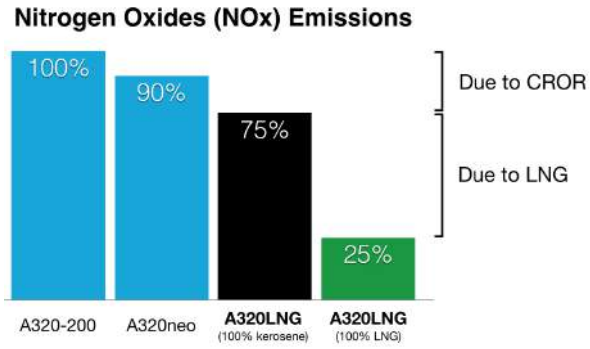

Figure 22-2: Expected nitrogen oxide emission reductions

NO_x will be decreased by at least 10% for the A320neo according to Airbus. The decrease for the A320LNG is calculated by accounting for the 25% increase in efficiency and the 66% decrease in NO_x emissions of LNG compared to kerosene, see chapter 2. The change in MTOW is taken into account as well. The total NO_x decrease is found to be 74.5 %.
The SO_x reduction due to the usage of LNG is 100% since no SO_x is produced during LNG combustion, see chapter 2. It has not been found by how much the A320neo reduces the SO_x

production but when assuming the same engine characteristics as for the A320-200 the value will be close the the CO_2 reduction value.

22-2 Unit Acquisition Cost and DOC

As has been determined in chapter 8, the unit acquisition cost will increase by 8 percent. In the same chapter it has been determined that the direct operating cost will decrease by 23 percent as compared to the A320-200. This is mainly achieved because of the lower price of the fuel as well as the decrease in expenses on CO_2 taxes. Overall, the money spend on both the acquisition and the operation of the aircraft will decrease since the direct operating cost are a larger part of the total cost. Hence, total cost will decrease for the A320-LNG. The A320neo has a decrease of 8% in operational cost compared to the A320-200 [13]. Hence, the A320LNG is cheaper to operate.

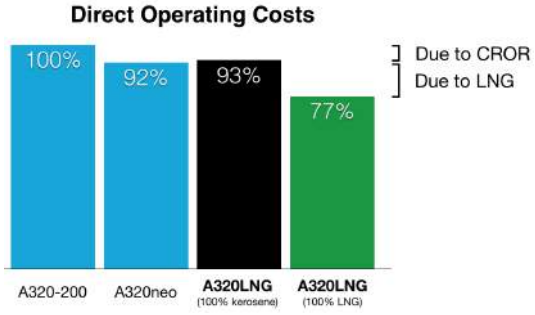

Figure 22-3: Expected reductions in direct operating costs

22-3 Safety

There are several changes made to the original A320 aircraft which influence the safety. The LNG fuel system introduces extra safety issues which have to be addressed. The LNG tanks are located outside of the fuselage which is beneficial for safety since possible leakages are kept away from the fuselage. However, the fuel lines run from the fuel tank to the engines at the back of the aircraft. Hence, the LNG has to be transported through the fuselage and in this case a possible leak can cause a dangerous situation to occur since an explosive mixture may avert. This is solved by having leakage detection devices. In case a blade flies off of the open rotor engine, the fuselage has been designed to be able to withstand the impact. An H-tail is used, so if the vertical tail is hit, the other vertical is still functional. With the A320LNG aircraft, safety will not be compromised and all certification regulations are met.

22-4 Weight

The OEW of the A320LNG has a 2 percent decrease compared to the A320-200, a 32 percent decrease in fuel weight which constitutes to a 5 percent decease in MTOW. The decrease in these weights enable an increase in payload weight capability which benefits the airline as it

increases revenue. For more information regarding weight the reader is advised to refer to chapter 13.

22-5 Payload-Range Diagram

The payload-range plot for the current A320-200 was plotted using data obtained from *Piano-X* aircraft analysis tool and is shown in figure 22-4. Furthermore, the payload-range plot for the A320LNG was plotted using the Breguet range equation for a 50/50 configuration. As seen in figure 22-4, the A320LNG has almost the same range as the A320-200 at maximum payload while carrying 32 percent less fuel compared to the A320-200. Moreover, the range at maximum fuel capacity is relatively less for the A320LNG. This decrease in range is constituted by the increase in drag caused by the fuel tanks. Furthermore, table 22-1 gives a breakdown of the range that could be achieved based on the type of fuel used and payload and fuel weights.

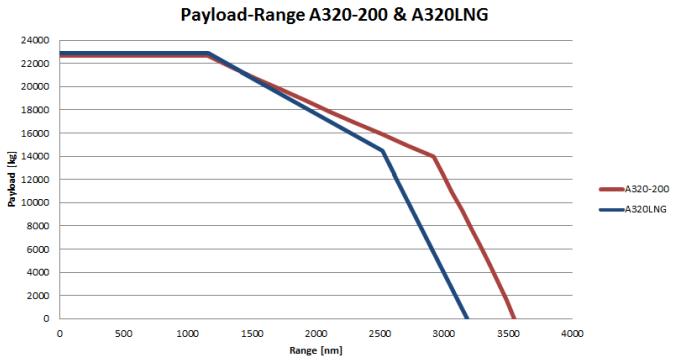

Figure 22-4: Payload vs range for the current A320 and the new A320LNG

Table 22-1: Payload versus range table

Mass [kg]	Range kerosene [nm]	Range LNG [nm]
Maximum payload capacity: 22853 Fuel: 7191.3 Kerosene: 3207 LNG: 3984	201.85	857.46
Maximum fuel capacity: 15600 Payload: 14444 Kerosene: 8100 LNG: 7500	1640.83	2973.49

22-6 Speed

The cruise Mach speed will decrease a little bit for the A320-LNG, from 0.78 Mach to 0.73 Mach. However, as has been determined in section 8, the time loss for a flight from Amsterdam to Istanbul is only increased by 10 minutes and direct operating costs are not affected.

22-7 Configuration

Figure 22-5 shows the changes in configuration between the current A320 and the A320-LNG. The major changes are the type of engines (open rotor instead of turbofan engines) and the positions of the engines (at the back of the fuselage instead of under the wing). Furthermore, there are two additional fuel pods underneath the wing used for the storage of LNG. The position of the nose and main landing gears is changed as well as the wing position in order to meet the control and stability requirements. The tail is changed from a conventional tail configuration to an H-tail. The H-tail provides redundancy in case of a rotor blade impact and noise shielding necessary because of the use of open rotor engines. The fuselage is made of carbon fibers which will cause a weight reduction. Three more seats are added due to a change in cabin layout. The back part of the fuselage is reinforced with kevlar and high modulus carbon fibers in order to be able to withstand a possible blade impact.

22-8 Overall Comparison

The A320LNG is superior in terms of emissions compared to the A320-200. Its CO_2 reduction is significant as compared to the current A320-200 at 43.7%. Furthermore, it reduces SO_x and NO_x by 100% and 74.5% respectively. Hence, the A320 is the most sustainable aircraft. The operating cost are less as well compared to the other A320 designs considered. This makes the A320LNG the most attractive for customers. Flight time is increased remains within reasonable limits. The A320LNG can achieve a larger range if both fuels, LNG and kerosene, are used during flight. The A320LNG is a cheaper, more sustainable and safe aircraft to fly compared to other A320 designs.

Figure 22-5: 3 views of the changes in configuration between the A320 and the A320-LNG

Chapter 23

Conclusion

To ensure sustainable air traffic in the future a new single aisle aircraft using alternative fuel for an entry into service in 2030 has been designed. The major alteration that is driving changes in the design is the transition to LNG, which will greatly impact subsystem design and aircraft operations. The goal of the task is to bring forward a design that will have significant reductions in greenhouse gas emissions and be compliant with noise regulations, as well as being attractive for airlines. A hybrid design is chosen which can fly on both LNG and kerosene, 50 percent of the total energy content of the fuel is kerosene and the other 50 percent is LNG. This has been chosen because LNG will not be available at all airports by 2030. Hence, a hybrid design increases operational flexibility. The design results in a significant emission reduction as presented in section 22-1.

There are several changes made to the A320 in order to adapt it to the A320LNG. Fuel tanks are added, engines are relocated and changed from turbofans to open rotors. Furthermore, the fuselage is made of carbon fibers resulting in a decrease in weight. All configuration changes were discussed in section 22-7. The locations and size of the wing, tail and landing gears are considered in order to make sure the aircraft meets all control and stability requirements.

Changes in airport operations are also necessary. The transportation of LNG to the airport is a major issue. As a solution the usage of existing natural gas pipelines is proposed after which the gas can be liquefied by small scale liquefaction plants on the airport itself. This reduces the complexity associated with the transportation of a cryogenic fuel.

Additionally, electrical and pneumatic taxiing systems are investigated. The electrical taxiing system is found questionable as to whether it will pay off in terms of direct operational cost. The pneumatic taxiing system is found to be technically feasible but more detailed studies are required to determine whether or not it is more cost effective to an electrical taxi system or a conventional one. Initial results from the pneumatic taxiing model show that the system weight and volume is acceptable and that the air motor can deliver the required power to meet taxi requirements.

The A320-LNG is an aircraft with a promising future. Not only will it significantly reduce the emissions associated with air traffic, it will also be attractive to operate for airlines. The total cost of the aircraft will decrease as compared to the current A320 meaning that an airline can make more profit. The A320LNG will be the aircraft of the future.

Bibliography

[1] 305 stainless steel. http://www.aksteel.com/pdf/markets_products/stainless/Stainless-%20Steel%20Price%20Book%2020140414.pdf. 2014-05-20.

[2] Titanium. http://www.matweb.com/search/DataSheet.aspx?MatGUID=66a15d609a3f4c829cb6ad08f0dafc01&ckck=1. 2014-05-20.

[3] Open rotor engine aeroacoustic technology final report. Technical report, 2013.

[4] Federal Aviation Administration. Fire-wall construction. http://www.flightsimaviation.com/data/-FARS/part_121-247.html. 2014-04-29.

[5] Federal Aviation Administration. Basic fuel system requirements. *Aircraft fuel system*, 2014.

[6] Federal Aviation Administration. Federal aviation regulations: Fuel system lines and fittings. http://www.risingup.com/fars/info/part121-231-FAR.shtml, 2014-05-22.

[7] U.S. Energy Information Administration. U.s. dry natural gas production projection. *Annual Energy Outlook 2013 Early Release*, 2013.

[8] Aerogels-Australia. Cryogel z. http://www.insulationindustries.com.au/SiteFiles/insulationindustries2010comau/Cryogel_z_ds.pdf. 2014-05-22.

[9] United States Environmental Protection Agency. Natural gas combustion. *EPA*.

[10] United States Environmental Protection Agency. Air and radition - sulfur dioxide. *EPA*, 2014.

[11] Airbus. A400m. http://www.airbusmilitary.com/Aircraft/A400M/A400MSpec.aspx. 2014-05-21.

[12] Airbus. All about the a320 family, technical appendices. http://www.aircraft24.com/images/aircraftpics/76/attach_115976_1.pdf. 2014-05-25.

[13] Airbus. Navigating the future. *Global Market Forecast*, 2012.

[14] Crosby Anderson Greenwood and Varec Products. Pentair pressure relief valve engineering handarticle. 2011.

[15] Hsuan-nien Chen Anupam Sharma. Prediction of tonal aerodynamic noise from operators. *AIAA*, 2012.

[16] ASM. Aluminum 7075-t6. http://asm.matweb.com/search/SpecificMaterial.asp?bassnum=MA7075T6. 2014-05-16.

[17] ASM. Aluminum and aluminum alloys. *The materials information society*.

[18] Aspen-Aerogels. Cryogel-z. http://www.aerogel.com/products-and-solutions/cryogel-z/. 2014-05-22.

[19] National Fire Protection Association. Liquefied natural gas (lng) vehicular fuel systems code. 2002.

[20] Autozone. Fuel fitting. http://www.autozone.com/autozone/accessories/Tools-Garage-and-Equipment/Fuel-Fitting/_/N-25no, 2014-05-22.

[21] AvioAero. Tp 400-d6. http://www.avioaero.com/en/catalog/military/engines/tp400_d6. 2014-05-21.

[22] Azom. Stainless steel - grade 316. http://www.azom.com/article.aspx?ArticleID=863. 2014-05-16.

[23] M. Bahrami. Forced convection heat transfer. http://www.sfu.ca/-mbahrami/ENSC%20388/Notes/Forced%20Convection.pdf. 2014-06-03.

[24] J.J. Berton. Empennage noise shielding benefits for an open rotor transport. *17th AIAA/CEAS Aeroacoustics conference*, 2011.

[25] Vincent Blandeau. Aerodynamic broadband noise from contra-rotating open rotors. 2011.

[26] Daniel Brewer. *Hydrogen Aircraft Technology*. CRC Press, Boca Raton, 1991.

[27] G.D. Brewer. Lh2 airport requirements study. Technical report, Langley Research Center, National Aeronautics and Space Administration, 1976.

[28] J Wayne Burns. Aircraft cost estimation methodology and value of a pound derivation for preliminary design development applications. *53rd Annual Conference of Society of Allied Weight Engineers*, 1994.

[29] Cabot. Particles. http://www.cabot-corp.com/wcm/download/en-us/ae/Particles_P100_200_300_DS_2013_v4_final%20lo%20res.pdf, 2014-05-18.

[30] The canadian pro. Environmental benefits. http://www.propane.ca/. 2014-05-10.

[31] Global Digital Central. Natural convection on cylinders and spheres. https://www.thermalfluidscentral.org/encyclopedia/index.php/Natural_convection_on_cylinders_and_spheres. 2014-06-02.

[32] CFM. Cfm56-5b. http://www.cfmaeroengines.com/engines/cfm56-5b. 2014-05-21.

[33] Cameo Chemicals. Liquefied natural gas. http://cameochemicals.noaa.gov/chris/LNG.pdf. 2014-05-24.

[34] Clariant. Aircraft de-/anti-icing fluids. http://www.aviation.clariant.com/C12576720021BF8F/vwWebPagesByID/E1C87CC572A4453BC12576FE002E0DFF. 2014-05-22.

[35] Combustion and Fuels. Nitrogen oxides formation in combustion processes. http://fluid.wme.pwr.wroc.pl/~spalanie/dydaktyka/combustion_en/NOx/NOx_formation.pdf. 2014-05-21.

[36] Parker Steel Company. Metric aluminum round tube. http://www.metricmetal.com/products/rdalum_tube.htm. 2014-05-22.

[37] JK Consulting. High reflectors. http://www.kruschwitz.com/HR%27s.htm. 2014-05-18.

[38] David C. Copley. Project xp-38n. http://www.kazoku.org/xp-38n/articles/p38info.htm. 2014-06-14.

[39] Eaton Corporation. Main fuel pump models. http://www.eaton.com/ecm/groups/public/@pub/@eaton/@aero/documents/content/ct196296.pdf. 2014-05-22.

[40] Pittsburgh Corning Corporation. Foamglass. http://www.industry.foamglas.com/__/frontend/handler/document.php?id=441&type=42. 2014-05-22.

[41] Cryostar. Small scale liquefaction & distribution.

[42] Dr. Neil Dickson. Aircraft noise technology and international noise standards. *ICAO Environment*, 2014.

[43] FAST Airbus Technical Digest. Hydraulic and fuel systems. http://www.airbus.com/support/publications/?eID=dam_frontend_push&docID=17435, note = 2014-05-20.

[44] Visser Dries. *Airport Planning, Design and Operations*. Delft University of Technology, Delft, 2013.

[45] Easa. Tcds a.064 annex-airbus a318,a319,a320,a321-special conditions. 2003.

[46] EASA. Compliance with cs-25 bird strike requirements. 2012.

[47] Engineers Edge. Pressure vessel, thin wall hoop and longitudinal stresses. http://www.engineersedge.com/material_science/hoop-stress.htm. 2014-05-16.

[48] General Electric. Open rotor engine aeroacoustic technology final report. *FAA*.

[49] Arrow Energy. The potential risks associated with lng.

[50] The Flying Engineer. Technically and operationally commerical aviation: Fuel systems. http://theflyingengineer.com/projects/airbus-tech/fuel-systems/, 2014-02-22.

[51] Engineersparadise.com. Cfrp, plastic with special properties. http://www.ingenieurparadies.de/en/ipar/188321. 2014-06-10.

[52] Ed Envia. Nasa open rotor noise research. In *14th CEAS-ASC Workshop & 5th Scientific Workshop of X3-Noise Aeroacoustics of High-Speed Aircraft Propellers and Open Rotors*, 2010.

[53] N Epstein. Cfm56-3 high by-pass technology for single aisle twins. *International Air Transportation Conference*, 1981.

[54] Dr. Reinhard Faab. Flugzeuge mit wasserstoffantrieb. *Airbus*, December 2001.

[55] Chart Ferox. Lng vehicle system. http://www.chart-ferox.com/LNG/Vehicle_Systems/Vehicle_Systems.aspx. 2014-05-21.

[56] Chart Ferox. Vts series. http://www.chart-ferox.com/LNG/Tanks_and_Cylinders/VTC_LNG.aspx. 2014-05-20.

[57] Michelle Michot Foss. Lng safety and security. *EEC*, 2006.

[58] NexGen Fueling. Vehicle fuel tank system operation manual. 2014.

[59] Grainger. Booster pumps. *Booster Pumps and Systems*, 2014.

[60] Robert Heffley. Aircraft handling qualities data. http://www.roberthefflley.com/docs/Data/NASA20CR-2144--Heffley--Aircraft20Handling20Qualities20Data.pdf. 2014-05-23.

[61] Andreas Hoevelmann. Aerodynamic investigations of noise-reducing high-lift systems for passenger transport aircraft. Technical report, DEPARTMENT OF AERONAUTICAL AND VEHICLE ENGINEERING ROYAL INSTITUTE OF TECHNOLOGY, 2011.

[62] ICAO. Environmental report 2010. *Aviation and Climate Change*, 2010.

[63] ICAO. Global aviation and our sustainable future. *ICAO*, 2012.

[64] Experimental Aircraft Info. Firewall preparation. http://www.experimentalaircraft.info/articles/aircraft-firewall-preparation.php, 2014-05-22.

[65] Airlines Inform. Airbus a320 specifications. http://www.airlines-inform.com/commercial-aircraft/Airbus-A320.html. 2014-05-18.

[66] Inc. Infrared Services. Emissivity values for common materials. 2014.

[67] Forecast International. The market for aviation apu engines. http://www.forecastinternational.com/samples/F644_CompleteSample.pdf. 2014-05-21.

[68] Louis S. Stivers Jr. Ira H. Abbott, Albert E. von Doenhoff. Report number 824, summary of airfoil data. Technical report, 1945.

[69] Kangwon Lee Ihn-soo Yoon Ji-hoon Kim, Heung-seok Seo. Development of the world's largest above-ground full containment lng storage tank. In *23rd World Gas Conference*, 2006.

[70] R.Henne K.A. Friedrich. Auxiliary power unit applications. *DLR*, 2006.

[71] Michael J. Kingan. Open rotor broadband interaction noise. *AIAA*, 2012.

[72] L.C.Chow. Landing gear and high lift devices airframe noise research. *8th AIAA/CEAS Aeroacoustics conference*, 2002.

[73] Jan Eiof Jonson Leonor Tarrason. Study on air quality impacts of non-lto emissions from aviation. *Norwegian Meteorological Institute*, 2004.

[74] Konstantinos G. Kyprianidis Linda Larsson, Tomas Gronstedt. Conceptual design and mission analysis for a geared turbofan and an open rotor configuration. 2011.

[75] M.Achternbosch. Material flow analysis - a comparison of manufacturing, use and fate of cfrp-fuselage components versus aluminium-components for commercial airliners.

[76] Bruce MacKinnon. An aviation industry guide to the management of wildlife hazards. *TP 13549 Sharing the skies*, 2005.

[77] Air & Space Magazine. Why the fire in a perfectly healthy jet engine can die. *Airspacemag*, 23 May 2014.

[78] Matweb. Titanium. http://www.crptechnology.com/sito/images/PDF/Titanio_da_lavorazione.pdf. 2014-05-20.

[79] T.H.G. Megson. Aircraft structures for engineering students. 2010.

[80] Roel H. Self Michael J. Kingan. Open rotor tone scattering. *AIAA*, 2011.

[81] LTD. Mitsubishi Heavy Industries. Press information - mhi ships composite-material wing box for 100th boeing 787. http://www.mhi-global.com/news/story/1212191607.html. 2014-06-13.

[82] Freddy Moriniere. Low velocity impact on fibre-metal laminates. 2014.

[83] NASA. Composite cryotank technologies and demonstration (cctd). http://gcd.larc.nasa.gov/projects/composite-cryogenic-propellant-tank/#.U33oHvmSzh5. 2014-05-22.

[84] NASA. Conservation of energy. https://www.grc.nasa.gov/www/k-12/airplane/thermo1f.html. 2014-06-04.

[85] Jon Drapkin Paul Workman Ryutaro Nambu David Zanussi Lasantha Subasinghe Nikolaos Kontaxis, Kyriakos Gennadis. Iata guidance on airport fuel storage capacity. *IATA*, May 2008.

[86] University of Delaware. Lecture notes. https://www.ccm.udel.edu/Tech/Lam3D/FailureCriteria.pdf. 2014-05-16.

[87] Federation of European Rigid Polyurethane Foam Associations. Thermal insulation materials made of rigid polyurethane foam. http://www.excellence-in-insulation.eu/site/fileadmin/user_upload/PDF/Thermal_insulation_materials_made_of_rigid_polyurethane_foam.pdf. 2014-05-22.

[88] Openflights.org. Open flights. http://www.openflights.org. 2014-05-26.

[89] The World Corrosion Organization. Materials - effects and economic impact of corrosion. http://www.wermac.org/materials/corrosion_allowance.html. 2014-06-11.

[90] P.A.Henne. Md-90 transport aircraft design. 1989.

[91] Joyce Penner. Intergovernal panel on climate change (s) special report, aviation and the global atmosphere. *Cambridge University Press*, 1999.

[92] Australia Pertiles. Cryogenic insulation. http://australianperlite.com/perlite-cryogenic-insulation.htm. 2014-05-26.

[93] Pratt and Whitney. V2500 engine. https://www.pw.utc.com/V2500_Engine. 2014-05-21.

[94] Technifab Products. Cryogenic liquid flow. http://www.technifab.com/cryogenic-resource-library/cryogenic-liquid-flow.html, 2014-05-21.

[95] PvEducation. Calculation of solar insolation. http://www.pveducation.org/pvcdrom/properties-of-sunlight/calculation-of-solar-insolation. 2014-06-02.

[96] Tom De Vuyst James C. Campbell Rade Vigejevic, Michal Orlowshki. A parametric study of bird strike on engine blades. *International Journal of Impact Engineering, Elsevier*, 2012.

[97] Amedeo R. Odoni Richard de Neufville. *Airport Systems*. Mc Graw Hill Education, 2003.

[98] J. Ricouard. Installation effects on contra.rotating open rotor noise. In *16th AIAA/CEAS Aeroacoustics conference*, 2010.

[99] Rolls-Royce. Low density materials. http://www.rolls-royce.com/about/technology/material_tech/low_density_materials.jsp. 2014-06-06.

[100] Jan Roskam. *Part II: Preliminary configuration design and integration of the propulsion system*. Lawrence, Kansas, 1989.

[101] Mitch R.Withers. Progress in aerospace sciences. *Elsevier*, 2014.

[102] Mohammad Sadraey. *Aircraft Design : A System Engineering Approach*. Wiley, 2012.

[103] Peter Schimming. Counter rotating fans - an aircraft propulsion for the future? *Thermal Science Vol.12 No. 2*, 2003.

[104] Jeff Scott. Drag of cylinders and cones. *Aerospaceweb*, 2005.

[105] Michael J Sefain. Hydrogen aircraft concepts and ground support. 2005.

[106] Dr. Carlo De Servi. Conduction. 2014.

[107] Online Electrical Engineering Study Site. Servo motor, theory and working principle. http://www.electrical4u.com/servo-motor-servo-mechanism-theory-and-working-principle. 2014-05-28.

[108] R Slingerland. Innovative configurations and advanced concepts for future civil aircraft. *von Karman Institute for Fluid Dynamics*, 2005.

[109] SmartCockpit.com. A319/a320/a321 fuel system. http://www.smartcockpit.com/aircraft-ressources/A319-320-321-Fuel.html. 2014-05-25.

[110] Flight Operations Support and Line Assitance. Getting to grips with cost index. *Airbus*, May 1998.

[111] Mechanic support. Understanding aircraft hose dash size. http://www.mechanicsupport.com/Aircraft_Hose_Size.html. 2014-05-17.

[112] M. Taylor. Open rotor engine design and validation. *Rolls-Royce*, 2013.

[113] Gary L. Teper. Aircraft stability and control data for nasa. http://jsbsim.sourceforge.net/NASA_CR-96008.pdf. 2014-05-22.

[114] Scott K. Thomas and Robert P. Cassoni. Aircraft anti-icing and de-icing techniques and modeling. 1996.

[115] The Engineering Toolbox. Radiation heat transfer. http://www.engineeringtoolbox.com/radiation-heat-transfer-d_431.html. 2014-06-02.

[116] The Engineering Toolbox. U.s. standard atmosphere. http://www.engineeringtoolbox.com/standard-atmosphere-d_604.html. 2014-06-10.

[117] Egbert Torenbeek. *Advanced Aircraft Design*. Wiley, 2013.

[118] Egbert Torenbeek. *Torenbeek - AE3211-I Lecture Notes*. TU Delft, 2014.

[119] Gabriel Trindade. Vueling aims to control half of barcelona-el prat air traffic. *02B*, 2013.

[120] Unknown. Clean air program from the federal transit administration. *Chebeague*, 2014.

[121] Graham Warwick. Airbus, snecma tackle open rotor integration. *Aviationweek*, 2014.

[122] W.Dobrzynski. Airframe noise studies on wings with deployed high lift devices. 1998.

[123] Chris Wijnterp. Electric taxi systems. a value model and operations estimation. *TUDelft Master Thesis*, 2014.

[124] Wikibooks. Jet propulsion/jet engine types. http://en.wikibooks.org/wiki/Jet_Propul-sion/Jet_engine_types. 2014–05-21.

[125] Wikipedia. Nose cone design. http://en.wikipedia.org/wiki/Nose_cone_design. 2014-06-17.

[126] Dennis J. Wilkins. The bathtub curve and product failure behavior. http://www.weibull.com/hotwire/issue21/hottopics21.htm. 2014-06-10.

[127] Wolfbend. A lightweight system that makes tube-in-a-tube practical and easy. http://www.wolfbend.com/Wolfbend%20Brochure.pdf. 2014-05-21.

Appendix A

Requirements

Throughout the report targets, goals and requirements are presented for the general design and for the various subsystems. For easier reference a summary is presented here with an overview of all requirements.

Top level & Emission Requirements

- **A320LNG-REQ-TOPLEVEL-01:** Can take-off and land at all current A320 airport destinations
- **A320LNG-REQ-TOPLEVEL-02:** Has the same minimum speed stall characteristics
- **A320LNG-REQ-TOPLEVEL-03:** Has a similar mission profile, i.e. flight time and range
- **A320LNG-REQ-TOPLEVEL-04:** Seats the same amount of passengers

- **A320LNG-REQ-EMISSION-01:** 50% CO_2 reduction
- **A320LNG-REQ-EMISSION-02:** 65% NO_x reduction
- **A320LNG-REQ-EMISSION-03:** 80% SO_x reduction
- **A320LNG-REQ-EMISSION-04:** 25% noise reduction
- **A320LNG-REQ-EMISSION-05:** No increase in the effect of water vapour on Global Warming Potential (GWP)

Powerplant-ATA26

- **A320LNG-REQ-ATA26-01:** The CROR engine shall be ready for service by 2025.
- **A320LNG-REQ-ATA26-02:** The open rotor shall be designed such that it has a probability of a blade being released occurs for one failure per 1×10^8 flying hours.
- **A320LNG-REQ-ATA26-03:** The ingestion system of the open rotor engine shall be capable of within standing the same amount of water ingestion as the IAE V2500-A5 and CFM56-5B turbofan engines.
- **A320LNG-REQ-ATA26-04:** The open rotor combustion chamber shall have the same or better relighting capability than the current combustion chambers on the V2500-A5 and CFM56-5B.
- **A320LNG-REQ-ATA26-05:** The engine inlet shall be be able to function nominally after ingestion of a bird of 1.8kg.
- **A320LNG-REQ-ATA26-06:** The CROR engine shall be engineered such that it meets the cumulative noise margin limit of 15-17 EPNdB.

ATA57 - Wing

- **A320LNG-REQ-ATA57-01:** The wing shall be designed for optimal cruise speed
- **A320LNG-REQ-ATA57-02:** The wing root shall stall before the wing tip
- **A320LNG-REQ-ATA57-03:** The wing shall perform take-off and landing at current take-off and landing speeds
- **A320LNG-REQ-ATA57-04:** The wing shall utilise both leading edge and trailing edge high-lift devices

Green Taxi Solutions

- **A320LNG-REQ-TAXI-01:** A maximum speed of 20 knots (10 m/s) and endurance of minimum 10 minutes must be achievable at maximum takeoff weight (MTOW).
- **A320LNG-REQ-TAXI-02:** The aircraft should accelerate from standstill to maximum speed in less than 90 seconds.
- **A320LNG-REQ-TAXI-03:** The system must deliver a minimum power of 143 kW.
- **A320LNG-REQ-TAXI-04:** The system must deliver a minimum torque of 369 Nm.

Appendix B

Assumptions

Project Assumptions

- Air traffic demand will have positive growth
- Kerosene prices will continue to rise
- Natural gas will be cheaper than kerosene
- Shale gas will further decrease the price of natural gas compared to kerosene
- Emission taxes will be implemented/increase

Assumptions Powerplant

The following assumptions were used to arrive at the chosen final design for the propulsion subsystem:

1. **Rotor Blade:** The blades are modeled as a rigid, rectangular, homogeneous beam of mass 5 kg, in order to calculate the moment of inertia. In reality the moment of inertia will be higher.
2. **Bird Strike:** The bird is modeled as a homogeneous sphere of mass 1.8 kg, permissible by FAA. In reality the mass of the bird may vary depending on the species.
3. **Emissions:** All emissions, i.e. CO_2, NO_x and SO_x behave proportional to the fuel flow, in order to reduce the amount of combustion calculations.
4. **Efficiency:** All assumptions about efficiency are listed in table 12-6.
5. **Open Rotor:** Turboprop engines are assumed to be a good approximation for Open Rotor engines.
6. **Engine air bleed:** Any kind of air bleed (e.g. for cabin) is assumed to be negligible.
7. **Engine exit velocity V_8:** $V_8 = V_0$ (freestream velocity). (Matlab)
8. **Heat capacity C_p:** C_p is a step function, dependent on temperature. (Matlab)
9. **Engine exit pressure P_8:** P_8 is assumed to always be 1.1 times ambient pressure. (Matlab)
10. **Heat exchanger:** The HE (at exhaust nozzle) is neglected. (Matlab)
11. **Certification:** Further detailed design requirements treated after subsection 12-5, such as water ingestion, are recognized as important. However, the influence and impact on the design vary due to project constraints.

Appendix C

Fuel Tank Heat Transfer Equations and Technical Drawing

The equations C-1-C-21 are used to calculate the heat transfer to the LNG and the physical conditions inside the fuel tank.

The heat transferred into the tank increases the internal energy of the LNG which is represented by equation C-1.

$$M \cdot \frac{du}{dt} = Q_{tank} \tag{C-1}$$

where M is the mass of LNG, $\frac{du}{dt}$ is the change in specific internal energy over time and $Q_{\tan k}$ is the rate of heat transfer to the LNG.

The temperature of the inner tank skin is assumed to be equal to the temperature of the LNG by using equation

The equation C-2 is taken from [106] and calculates the heat transferred to the LNG based on the thermal conductivities of the aluminium wall and insulation.

$$Q_{tank} = A_{ins} \cdot \frac{(T_{ins} - T_{inner})}{\left(\frac{t_{inner}}{2 \cdot \lambda_{Al}} + \frac{t_{ins}}{2 \cdot \lambda_{Cr}}\right)} \tag{C-2}$$

where A_{ins} is surface area of the tank without insulation and outer skin, T_{ins} is temperature of the insulating material, t_{inner} is the thickness of the inner tank, t_{ins} is the thickness of insulation, λ_{inner} is the thermal conductivity of inner skin and λ_{ins} is the thermal conductivity of insulation.

To calculate the amount of heat taken by the insulating material equation C-3 is used.

$$M_{ins} \cdot C_{ins} \cdot \frac{dT_{ins}}{dt} = Q_{surf} - Q_{tank} \tag{C-3}$$

where M_{ins} is the mass of insulating material, C_{ins} is the specific heat capacity of the insulation, Q_{surf} is the rate of heat transfer to the surface.

The total amount of heat entering the tank consists of radiation and convection, see equation C-4.

$$Q_{surf} = Q_{sun} - Q_{radtank} + Q_{conv} \tag{C-4}$$

wher Q_{sun} is heat transfer due to radiation from sun and $Q_{radtank}$ is heat transfer due to radiation from tank and Q_{conv} is heat transfer due to convection.

The equation C-5 is taken from [95].

The heat from the sun can be represented by equation C-5.

$$Q_{sun} = \alpha I_{sun} \frac{A_{ext}}{2} \tag{C-5}$$

where α is the absorptivity of the outer surface, I_{sun} is the solar intensity and A_{ext} is the outer area of the tank.

The equation C-6 is taken from [115] and represents the outward heat flow due to the radiation from the body (the tank).

$$Q_{radtank} = \varepsilon A_{ext} \sigma {T_{surface}}^4 \tag{C-6}$$

where $Q_{radtank}$ is the radiation from tank, ε is the emissivity of the surface, σ is the Stephan-Boltzmann constant and $T_{surface}$ is the temperature of the surface of the tank.

The equations C-7-C-12 are taken from [31]. The heat transfer due to convection is calculated using C-7-C-15

$$Q_{conv} = (h_{natural} + h_{forced}) * A_{ext}(T_{air} - T_{surface}) \tag{C-7}$$

where $h_{natural}$ is the heat transfer coefficient due to natural convection, h_{forced} is the heat transfer coefficient due to forced convection, A_{ext} is the external surface area, T_{air} is the temperature of air and $T_{surface}$ is the surface temperature of the tank.

$$Gr = {D_{ext}}^3 {\rho_{air}}^2 gabs(T_{air} - T_{surface}) \frac{\beta}{{\mu_{air}}^2} \tag{C-8}$$

where Gr is the Grashof number, D_{ext} is the diameter of the outer tank, ρ_{air} is the density of air, β is the thermal expansion coefficient of air and μ_{air} is the viscosity of air.

$$Pr = \frac{\mu_{air} C_p}{\lambda_{air}} \tag{C-9}$$

where Pr is the Prandtl number , C_p is the specific heat capacity of air and λ_{air} is the thermal conductivity of air.

$$Ra = Gr \cdot \Pr \tag{C-10}$$

where Ra is the Rayleigh number.

$$Nu_{natural} = \left(0.6 + \frac{0.387 * Ra^{(1/6)}}{\left[1 + \left(\frac{0.559}{\Pr} \right)^{(9/16)} \right]^{(8/27)}} \right)^2 \tag{C-11}$$

where $Nu_{natural}$

$$h_{natural} = \frac{Nu_{natural} \cdot \lambda_{air}}{D_{ext}} \tag{C-12}$$

The equations C-13-C-15 are taken from [23].

$$Re = \rho_{air} V_{wind} \frac{D_{ext}}{\mu_{air}} \tag{C-13}$$

where Re and V_{wind} is the velocity of the wind.

$$Nu_{forced} = 0.3 + \left(\frac{0.62 Re^{1/2} Pr^{1/3}}{1 + (0.4Pr)^{2/3}} \right)^{1/4} \left(1 + \left(\frac{Re}{282000} \right)^{5/8} \right)^{4/5} \tag{C-14}$$

where Nu_{forced}

$$h_{forced} = \frac{Nu_{natural} \cdot \lambda_{air}}{D_{ext}} \tag{C-15}$$

The equation C-16 is taken from [106] and represents the heat transfer through the surface to the LNG.

$$T_{surface} = T_{ins} + \frac{Q_{surf}}{A_{ext} \lambda_{ins}} \frac{t_{ins}}{2} \tag{C-16}$$

The equation of state, equation C-17, is taken from [84].

$$Mu = M_{liq} hl_{sat} + M_{vap} hv_{sat} - PV + M_{inner} C_{inner} (T_{inner} - 298.15) \tag{C-17}$$

where u is the specific internal energy in LNG, M_{liq} is the mass of LNG in liquid state, M_{vap} is the mass of LNG is gaseous state, hv_{sat} is the specific internal energy of LNG in liquid state, h_{sat} is specific internal energy of LNG in gaseous state, P is the pressure inside the tank, V is the volume of the tank, M_{inner} is the mass of the inner tank and C_{inner} is the specific heat capacity of inner tank material.

From the conservation of mass it follows that:

$$M_{vap} = M - M_{liq} \tag{C-18}$$

Since the volume remains constant equation C-19 is valid.

$$V_{liq} + V_{vap} = V \tag{C-19}$$

where V_{liq} is the volume of LNG in liquid state, V_{vap} is the volume of LNG in gaseous state. Furthermore, use is made of equations C-20 and C-21.

$$V_{liq} = \frac{M_{liq}}{\rho_{liq}} \tag{C-20}$$

where ρ_{liq} is the density of LNG in liquid state.

$$V_{vap} = \frac{M_{vap}}{\rho_{vap}} \tag{C-21}$$

where ρ_{vap} is the density of LNG in gaseous state.

Pressure and density of LNG in liquid and gaseous state at saturation point are calculated using an external program called Fluidprop.

In figure C-1 the technical drawing of the fuel tank can be found.

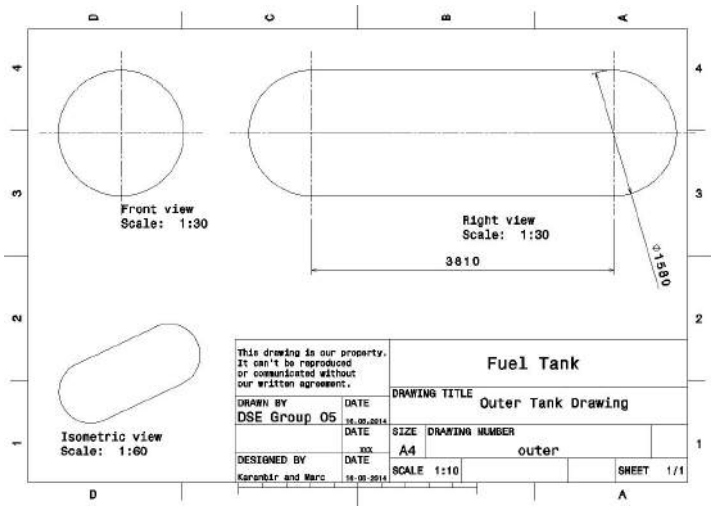

Figure C-1: Technical drawing of the fuel tank

Appendix D

Wing A320LNG Geometry

From the case study presented in section 8 it was found that the A320LNG cruise speed for minimum DOC is Mach 0.78.

With a decrease in cruise Mach number the wing sweep can be reduced which provides significant improvements in terms of high lift devices and low speed performance characteristics as well as a more optimal lift distribution. To calculate the new wing sweep the critical Mach number is computed based on the current maximum operating mach (MMO) of the A320 and wing sweep. The equation is then inverted to solve for wing sweep with the new MMO of 0.77 (see equation D-1).

$$M_{cr} = 0.82cos(25°) = 0.743 \rightarrow \Lambda = cos^{-1}\left(\frac{0.743}{0.73 + 0.04}\right) = 16.05° \tag{D-1}$$

A safety margin is added to avoid transonic drag conditions during cruise and subsequently the new quarter-chord sweep is set at 20°. In order to achieve an optimal lift distribution in order to decrease drag, the Oswald efficiency factor (e) must be maximized. Raymer presents a relationship between taper ratio and wing sweep to achieve this, see figure D-1. From this chart a taper ratio between 0.25 and 0.30 is required. A ratio of 0.277 has been selected.

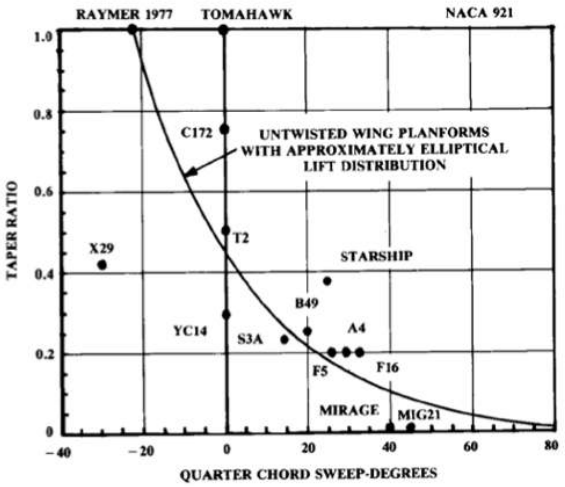

Figure D-1: Optimal Taper Ratio and Wing Sweep Combination [100]

The wing-tip chord is kept constant to avoid the necessity to redesign the A320 sharklets and as a result given the wing area, taper ratio and quarter-chord wing sweep, the root-chord and wing span were geometrically calculated. The results are:

$$S = 122.8\ m^2,\ \lambda = 0.277,\ c_r = 6\ m,\ c_t = 1.66\ m,\ b = 33.97\ m$$

Appendix E

Glossary

α	Absorptivity of the surface
α_t	Wing twist angle [°]
α_c	The take-off rotation clearance angle
α_{tb}	The tip-back angle
$\alpha_{TO,fus}$	Take-off angle of attack fuselage
α_{TO}	Take-off angle of attack wing [°]
$\bar{x_{ac}}$	Location of aerodynamic centre
β	Thermal expansion coefficient of air [1/K]
η_{net}	Overall propulsive efficiency
$\eta_{propulsive}$	Propulsive efficiency
η_{prop}	Propulsive efficiency
η_{th}	Thermodynamic efficiency
$\frac{d\eta}{d\alpha}$	Change in downwash angle
$\frac{du}{dt}$	Change in specific internal energy over time $[J/(kgs]$
γ	Swirl angle
λ	Taper ratio [-]
λ_{inner}	Thermal conductivity of inner skin [W/(mK)]
λ_{ins}	Thermal conductivity of insulation [W/(mK)]
λ_{air}	Thermal Conductivity of air [W/(m K)]
μ_{air}	Dynamic viscosity of air $[N-s/m^2]$
ρ_{liq}	Density of LNG in liquid state $[kg/m^3]$
ρ_{vap}	Density of LNG in gaseous state $[kg/m^3]$
σ	Stephan-Boltzmann constant $[W/(m^2K^4)]$
ε	Emissivity of the surface
A_{ext}	External area [m^2]
A_{ext}	Surface area of outer tank $[m^2]$
A_{ins}	Surface area of the tank without insulation and outer skin $[m^2]$
C_p	Specific Heat [J/(kg K)]
C_{inner}	Specific heat capacity of inner tank material [J/(kg K)]
C_{ins}	Specific heat capacity of insulation[J/K]
C_{L_h}	Lift coefficient to horizontal stabilizer
Cm_{ac_0}	Moment coefficient at aerodynamic centre
e	Oswald efficiency factor
H_c	Clearance height during take-off at maximum angle of attack
h_{forced}	Heat transfer coefficient due to forced convection $[W/(m^2K)]$
H_f	Distance of the lowest part of the fuselage to the ground
$h_{natural}$	Heat transfer coefficient due to natural convection $[W/(m^2K)]$
h_{sat}	Specific internal energy of LNG in liquid state [J/kg]
hv_{sat}	Specific internal energy of LNG in gaseous state [J/kg]
I_{sun}	Solar intensity $[W/m^2]$
l	Length of cylindrical section of the tank
M_{inner}	Mass of the inner tank [kg]
M_{ins}	Mass of insulating material [kg]
M_{liq}	Mass of the LNG in liquid state [kg]
M_{vap}	Mass of the LNG in gaseous state [kg]
Nu_{forced}	Nusselt number for forced convection [-]
$Nu_{natural}$	Nusselt number for natural convection [-]
Q_{conv}	Heat transfer due to convection [J/s]
$Q_{radtank}$	Heat transfer due to radiation from tank [J/s]
$Q_{radtank}$	Radiation from the tank [J/s]
Q_{rad}	Heat transfer due to radiation [J/s]
Q_{sun}	Heat transfer due to radiation of sun[J/s]
Q_{surf}	Rate of heat transfer at surface [J/s]
r_i	Radius of tank inner skin
T_{air}	Temperature of air [K]
T_{inner}	Temperature of the inner tank skin [K]
t_{inner}	Thickness of the inner tank
T_{ins}	Temperature of the insulating material [K]
t_{ins}	Thickness of the insulation
T_{LNG}	Temperature of LNG [K]
$T_{surface}$	Surface temperature of the tank
$T_{surface}$	Temperature of surface of the tank [K]
V_0	Free stream velocity
V_e	Engine exit velocity
V_{liq}	Volume of LNG in liquid state $[m^3]$
V_{tank}	Tank volume
V_{vap}	Volume of LNG in gaseous state $[m^3]$
V_{wind}	Velocity of wind [m/s]
Vh/V	Ratio stream velocity horizontal tail to wing
x_{LEMAC}	Location as x-coordinate of LEMAC
x_{LEMAC}	The leading edge mean aerodynamic distance from the nose
ρ_{air}	Density of air [kg/m^3

C_{L_α}	Lift coefficient vs angle of attack curve gradient
$Q_{\tan k}$	Rate of heat transfer for LNG [J/s]
D_{ext}	Diameter of outer tank [m]
a_s	Stall angle of attack
AR	Aspect ratio [-]
b_f	High lift device span
c_f	High lift device chord
C_L	Wing lift coefficient [-]
$C_{d_{min}}$	Minimum drag coefficient [-]
$C_{L_{req}}$	Required wing lift coefficient [-]
$C_{L_{TO,req}}$	Lift coefficient take-off
$C_{L_{TO}}$	Take-off lift coefficient
C_{m_0}	Moment coefficient at α_0 [-]
CCPR	Combustion chamber pressure ratio
CO_2	Carbon Dioxide
CPR	Compressor pressure ratio
dCL	HLD contribution to C_l [-]
Gr	Grashof Number [-]
i_w	Wing incidence angle [°]
L/D	Lift over drag ratio
LH_2	Liquid Hydrogen
M	Mass of LNGS [kg]
m	Mass [kg]
M_{cr}	Mach critical
NO	Nitric Oxide
NO_x	Nitrogen Oxides
NO_2	Nitrogen Dioxide
P	Pressure inside the tank [Pa]
Pr	Prandtl number [-]
Ra	Rayleigh numbner [-]
Re	Reynolds number [-]
S	Wing planform area [m^2]
SO_x	Sulphur Oxides
T/W	Thrust to weight ratio
u	Specific internal energy [J/kg]
V	Volume of the tank [m^3]
V_c	Cruise speed sea level [m/s]
V_s	Stall speed sea level [m/s]
V_s	Stall velocity
RAMS	Reliability, Availability, Maintainability, Safety
RPM	Rotations per minute
SOP	Standard Operating Procedures
V_{TO}	Take-off velocity
W/S	Wing loading (weight over wing area ratio)
ACARE	Advisory Council for Aeronautics Research
APU	Auxiliary power unit
BPR	Bypass ratio
CCET	Combustion chamber exit temperature
CFR	Carbon Fibre Reinforced Plastic
CFRP	Carbon-fibre-reinforced polymer
CROR	Contra-rotating open rotor
CS	Certification Specification
EI	Emission Index
EPNdB	Effective Perceived Noise in Decibels
EPNL	Effective Perceived Noise Level
ETS	Electric taxi system
FAA	Federal Aviation Administration
FL	Flight level
GE	General Electric
GE	General Electrics
GWP	Global Warming Potential
HE	Heat Exchanger
HLD	High lift device
HPT	High pressure turbine
ICAO	International Civil Aviation Organisation
IPC	Intermediate pressure compressor
IPT	Intermediate pressure turbine
LEMAC	Leading edge mean aerodynamic chord
LHV	Lower heating value
LNG	Liquefied Natural Gas
LPT	Low pressure turbine
M_{cr}	Mach critical
MCC	Minimum cost cruise mach number
MMO	Maximum operating mach
MRC	Maximum range cruise mach number
MSG3	Maintenance steering group 3
MTOW	Maximum take-off weight
NEO	New engine option
NFPA	National Fire Protection Association
NPSH	Net Positive Suction Head
OEW	Operational empty weight
PTS	Pneumatic Taxi System
tpd	Tonnes per day